18442.EG

Division of Engineering
BROWN UNIVERSITY
PROVIDENCE, R. I.

ANALYSIS OF SHEAR STRAIN LOCALIZATION IN THERMAL VISCO-PLASTIC MATERIALS

T. G. Shawki, R. J. Clifton, G. Majda

U.S. Army Research Office
Technical Report No. 3
Grant DAAG29-81-K-0121

ARO DAAG29-81-K-0121/3 *October 1983*

Approved for Public Release; Distribution Unlimited

The view, opinions and/or findings contained in this report are those of the authors and should not be construed as an official Department of the Army position, policy, or decision unless so designated by other documentation.

SECURITY CLASSIFICATION OF THIS PAGE (When Data Entered)

REPORT DOCUMENTATION PAGE		READ INSTRUCTIONS BEFORE COMPLETING FORM
1. REPORT NUMBER Technical Report No. 3	2. GOVT ACCESSION NO. AD-A138 180	3. RECIPIENT'S CATALOG NUMBER
4. TITLE (and Subtitle) "Analysis of Shear Strain Localization in Thermal Visco-Plastic Materials"		5. TYPE OF REPORT & PERIOD COVERED Technical 6. PERFORMING ORG. REPORT NUMBER
7. AUTHOR(s) T.G. Shawki, R.J. Clifton and G. Majda		8. CONTRACT OR GRANT NUMBER(s) Grant No. DAAG 29-81-K-0121
9. PERFORMING ORGANIZATION NAME AND ADDRESS Division of Engineering, Brown University Box D, Providence, RI 02912		10. PROGRAM ELEMENT, PROJECT, TASK AREA & WORK UNIT NUMBERS
11. CONTROLLING OFFICE NAME AND ADDRESS U.S. Army Research Office Post Office Box 12211 Research Triangle Park, NC 27709		12. REPORT DATE October 1983 13. NUMBER OF PAGES
14. MONITORING AGENCY NAME & ADDRESS(if different from Controlling Office)		15. SECURITY CLASS. (of this report) Unclassified 15a. DECLASSIFICATION/DOWNGRADING SCHEDULE

16. DISTRIBUTION STATEMENT (of this Report)

Approved for public release; distribution unlimited.

17. DISTRIBUTION STATEMENT (of the abstract entered in Block 20, if different from Report)

18. SUPPLEMENTARY NOTES

The view, opinions, and/or findings contained in this report are those of the author(s) and should not be construed as an official Department of the Army position, policy, or decision, unless so designated by other documentation

19. KEY WORDS (Continue on reverse side if necessary and identify by block number)

Shear bands, adiabatic shear, strain localization, thermo-plastic instability

20. ABSTRACT (Continue on reverse side if necessary and identify by block number)

Simple shearing deformations are analyzed as a means of investigating the effects of strain hardening, thermal softening, and strain-rate sensitivity on the formation of shear bands. Linear stability analysis is conducted for perturbations from homogeneous, time varying deformations. Finite difference solutions are obtained for the fully nonlinear system of governing equations. Velocity boundary conditions are emphasized although

DD FORM 1 JAN 73 1473 EDITION OF 1 NOV 65 IS OBSOLETE
S/N 0102-014-6601

Unclassified
SECURITY CLASSIFICATION OF THIS PAGE (When Data Entered)

20. solutions for the case of stress conditions are also presented. Three types of constitutive models are considered: the power law model, the Arrhenius law, and the Bodner-Merzer model. Inertia and heat conductio are included. Qualitative features of plastic response for the class of problems considered are illustrated by eighteen numerical solutions. General conclusions on the critical conditions for the stability of the solutions are difficult to draw in view of the many features of the problem that influence the formation of shear bands. Low strain harden high thermal softening, and weak strain-rate sensitivity all contribute to shear strain localization. The size of an initial perturbation is important in the stability of solutions for the case of velocity bounda conditions, but it is less important for stress boundary conditions because of the inherent inhomogeneity of dynamic solutions in the latte case.

Analysis of Shear Strain Localization In Thermal Visco-Plastic Materials

by

T.G. Shawki[1]

R.J. Clifton[2]

and

G. Majda[3]

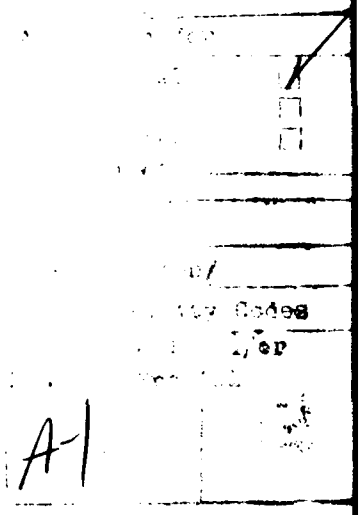

[1]Research Assistant, Division of Engineering
Brown University, Providence, RI 02912

[2]Professor of Engineering, Division of Engineering
Brown University, Providence, RI 02912

[3]Assistant Professor, Division of Applied Mathematics
Brown University, Providence, RI 02912

U.S. Army Research Office
Technical Report No. 3
Grant DAAG 29-81-K-0121/3

Division of Engineering
Brown University
Providence, R.I. 02912

October 1983

Abstract

Simple shearing deformations are analyzed as a means of investigating the effects of strain hardening, thermal softening, and strain-rate sensitivity on the formation of shear bands. Linear stability analysis is conducted for perturbations from homogeneous, time varying deformations. Finite difference solutions are obtained for the fully nonlinear system of governing equations. Velocity boundary conditions are emphasized although solutions for the case of stress conditions are also presented. Three types of constitutive models are considered: the power law model, the Arrhenius law, and the Bodner-Merzer model. Inertia and heat conduction are included. Qualitative features of plastic response for the class of problems considered are illustrated by eighteen numerical solutions. General conclusions on the critical conditions for the stability of the solutions are difficult to draw in view of the many features of the problem that influence the formation of shear bands. Low strain hardening, high thermal softening, and weak strain-rate sensitivity all contribute to shear strain localization. The size of an initial perturbation is important in the stability of solutions for the case of velocity boundary conditions, but it is less important for stress boundary conditions because of the inherent inhomogeneity of dynamic solutions in the latter case.

TABLE OF CONTENTS

I. INTRODUCTION

Localization of plastic deformation in the form of shear bands is observed frequently during tensile, compressive and shearing deformation tests. Shear bands occur in a wide range of applications such as ballistic impact, dynamic fracture, cryogenic behavior of materials, high velocity forming, machining and grinding.

Current understanding of the phenomenon is not fully established; however a common view is that at high strain rates the occurence of shear bands is related to thermal softening features of material behavior. That is, shear bands are thought to initiate under conditions of nearly adiabatic deformation when thermal softening overcomes strain-hardening so that the rate of change of the flow stress becomes equal to zero [1]. At this stage of deformation the flow stress decreases as temperature increases, resulting in inhomogeneous deformation. This inhomogeneous deformation results because the heat generated by plastic working is greatest in regions of highest strain rate. This leads to further softening of the material in these regions, and the cycle is repeated until the deformation is localized in the form of shear bands. The existence of material or geometric inhomogenieties appears to be necessary for triggering this mechanism. The exact nature and size of such inhomogeneities are not fully understood; however, it is believed that these defects play a major role in shear band formation.

Early observations and discussions of shear bands are attributed to Zener and Holloman [2], who observed a white etching band in an 0.25 C, low alloy steel subjected to a rapid punching test. They showed that a local temperature of 1000^{o}C is reached with a total

shear strain of (5.0). A large number of similar experiments are cited in a survey by Rogers [3]. Strain rate sensitive materials are viewed as being less sensitive to localization [4]. Some metals show very stable behavior in their superplastic ranges where they are well characterized as nearly Newtonian fluids. Rate independent models of plastic response, without thermal softening, exhibit shear strain localization when the effects of geometric softening due to lattice rotations and/or non-normality of the plastic strain-rate to the yield surface are included. These effects have been presented fully in a recent review by Asaro [5].

Experimental investigations of shear bands often are concerned with metallurgical effects on the onset of localization [6], and with measuring the strain, strain-rate and temperature at which bands are formed [7],[12]. Analytical discussions of shear bands seek, for assumed constitutive models, the critical conditions which characterize the instabilities reported experimentally. Most of the assumed constitutive models are based on a macroscopic point of view due to the associated complexity of plastic deformation at the microscopic level. Moreover, the pre-localization constitutive equations are assumed to hold when localization occurs. Several authors attempted to obtain a simple stability criterion for adiabatic plastic deformation by means of a linear perturbation analysis [8], [9], [10], [11]. However, the use of constant coefficients, evaluated from the homogeneous solution at the time the perturbation occurred, imposes a severe restriction on the validity of such results. In other analyses, computer simulations have been presented for the fully non-linear system [12], [13].

This work presents a general analysis of shear-strain localization in simple shearing deformations of thermal-visco/plastic materials. The system of governing equations for a one-dimensional simple-shearing deformation is formulated in Chapter II. An exact solution for quasi-static deformation with no heat conduction is presented in Chapter III for materials with temperature-dependent viscosity and no strain-hardening. In Chapter IV a linear stability analysis is presented in which the time-dependence of the coefficients in the linearized equations is retained. A stability criterion motivated by a bifurcation type of instability is also presented.

In Chapter V, a numerical simulation of the fully nonlinear system of equations is presented for a number of constitutive equations. These constitutive equations exhibit strain-rate sensitivity, strain-hardening (softening) and thermal softening (hardening) that are representative of the response of metals. The major objective underlying such numerical simulations is to study the material response to small initial perturbations of the homogeneous solution. This work serves as a means to obtain a better insight into the phenomenon of shear-strain localization, and to reconsider some of the common ideas concerning shear band formation.

II. PROBLEM FORMULATION

Consider a simple shearing deformation of an infinite plate at constant strain rate. The plate has thickness H in the y-direction as shown in Fig. II.1. The lower edge (y = O) is fixed, while the upper edge (y = H) has a velocity ($v = v_o$) in the x-direction. Assume that all physical quantities are uniform along the x and z directions so that the deformation depends only on one space coordinate. Under these conditions, the only non-zero displacement component is in the x-direction, and the only non-vanishing stress components are σ_{xy}, σ_{xx}, σ_{yy}, σ_{zz}. The equations of momentum balance reduce to:

$$\frac{\partial \sigma_{xy}}{\partial y} = \rho_o \frac{\partial v}{\partial t} \qquad \text{(II.1.a)}$$

$$\frac{\partial \sigma_{yy}}{\partial y} = O \qquad \text{(II.1.b)}$$

where σ_{xy} and σ_{yy} are the components of the Cauchy stress tensor, v is the particle velocity in the x-direction; and ρ_o is the mass density. Hereafter the shear stress σ_{xy} will be denoted by τ. The total strain is assumed to be composed of an elastic plus a visco-plastic part, i.e.

$$\gamma = \gamma^e + \gamma^p \qquad \text{(II.2)}$$

where the elastic part of this decomposition is given by

$$\gamma^e = \frac{\tau}{G} \qquad \text{(II.3)}$$

in which G is the elastic shear modulus. Differentiating (II.2) and (II.3) w.r.t. time and replacing the total strain rate by the velocity gradient one obtains

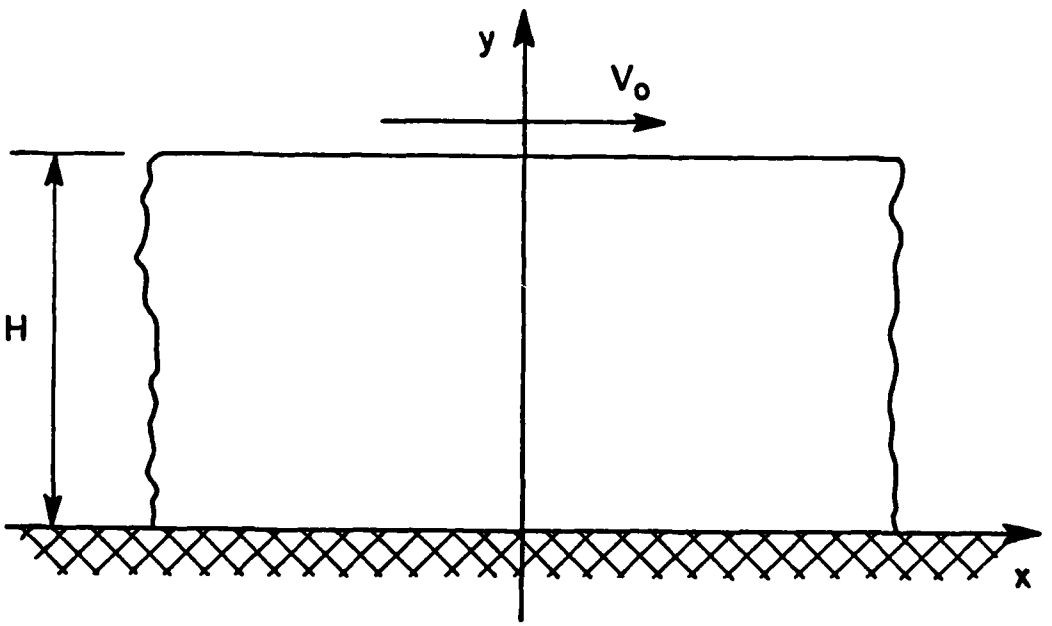

Figure (II.1) - Geometry of the problem

$$\frac{\partial v}{\partial y} = \frac{1}{G} \frac{\partial \tau}{\partial t} + \frac{\partial \gamma^p}{\partial t} \qquad \text{(II.4)}$$

The heat Q generated by plastic deformation is assumed to be related to the plastic work W^p by

$$\frac{\partial Q}{\partial t} = \beta \frac{\partial W^p}{\partial t} \equiv \beta\tau \frac{\partial \gamma^p}{\partial t} \qquad \text{(II.5)}$$

where the factor β is taken to be approximately 0.9. Heat transfer in the material is assumed to satisfy Fourier's law of heat conduction

$$h_y = - k \frac{\partial \theta}{\partial y} \qquad \text{(II.6)}$$

where h_y is the heat flux in the y-direction, k is the thermal conductivity and θ is the temperature. From (II.5) and (II.6) the energy balance equation can be written as

$$\rho_o c \frac{\partial \theta}{\partial t} = k \frac{\partial^2 \theta}{\partial y 2} + \beta\tau \frac{\partial \gamma^p}{\partial t} \qquad \text{(II.7)}$$

where c is the specific heat per unit mass.

The remaining equation is the constitutive equation that characterizes the material response to the given loading. We consider materials which exhibit strain-rate sensitivity, strain hardening, and thermal softening or hardening. Thus, in simple shear the flow stress is assumed to be given by a relation of the form

$$\tau = \psi \quad (\theta, \gamma^p, \dot{\gamma}^p) \qquad (\dot{\gamma}^p \equiv \frac{\partial \gamma^p}{\partial t}) \qquad \text{(II.8)}$$

The governing system of equations used for modelling the features of shear strain localization in thermal visco-plastic materials can be summarized as follows:

$$\rho_o \frac{\partial v}{\partial t} = \frac{\partial \tau}{\partial y} \tag{II.9}$$

$$\frac{\partial \gamma^p}{\partial t} = \frac{\partial v}{\partial y} - \frac{1}{G} \frac{\partial \tau}{\partial t} \tag{II.10}$$

$$\frac{\partial \theta}{\partial t} = \frac{k}{\rho_o c} \frac{\partial^2 \theta}{\partial y^2} + \frac{\beta}{\rho_o c} \tau \frac{\partial \gamma^p}{\partial t} \tag{II.11}$$

$$\tau = \psi(\theta, \gamma^p, \dot{\gamma}^p) \tag{II.12}$$

or

$$\dot{\gamma}^p = \phi(\tau, \gamma^p, \theta) \ . \tag{II.12a}$$

The complete initial-boundary value problem is defined once initial and boundary conditions are prescribed. These conditions will be given when numerical solutions are discussed (Chapter V).

Dimensionless Form

It is useful to rewrite the system of governing equations (II.9, 12) in a dimensionless form. The dimensional quantities in the system (II.9,12) will be relabeled by a superposed $\hat{}$, and then the unlabeled quantities will denote the corresponding dimensionless quantities.

The dimensionless quantities are defined by

$$t = \frac{\hat{t}}{\hat{t}_o} \ , \quad y = \hat{y}/H \ , \quad \tau = \hat{\tau}/\hat{\tau}_o \ ,$$

$$v = \hat{v}/(H/\hat{t}_o) \ , \quad k = \frac{\hat{k}\,\hat{\theta}_o\,\hat{t}_o}{\hat{\tau}_o H^2} \ , \quad \xi = \frac{\hat{\xi}\hat{\theta}_o}{\hat{\tau}_o}$$

$$\gamma^p = \hat{\gamma}^p/\hat{\gamma}_o^p \ , \quad \rho_o = \frac{\hat{\rho}_o H^2}{\hat{\tau}_o \hat{t}_o^2} \ , \quad c = \frac{\hat{c}\hat{\theta}_o \hat{t}_o^2}{H^2}$$

$$\frac{1}{G} = \frac{\hat{\tau}_o}{\hat{G}} \ , \quad \theta = \frac{\hat{\theta}}{\hat{\theta}_o} \ , \quad s^o = \frac{\hat{s}^o}{\hat{\gamma}_o^p}$$

$$V^o = \hat{V}^o \hat{\tau}_o / \hat{\dot{\gamma}}_o^p \quad , \quad T^o = \hat{T}^o \hat{\theta}_o / \hat{\dot{\gamma}}_o^p$$

where the subscript "o" refers to quantities evaluated for the homogeneous solution at the time a perturbation is introduced, while the superscript "o" refers to evaluation for the homogeneous solution. The characteristic time $\hat{t}_o = 1/\hat{\dot{\gamma}}_o^p$ is the time required to obtain a unit shear strain at the strain rate $\hat{\dot{\gamma}}_o^p$. The coefficients V,S and T are defined by

$$V = \frac{\partial \phi}{\partial \tau} \quad , \quad S = \frac{\partial \phi}{\partial \dot{\gamma}^p} \quad , \quad T = \frac{\partial \phi}{\partial \theta}$$

They are measures, respectively, of the strain rate sensitivity, strain hardening ($S < 0$), and thermal softening (or hardening). The dimensionless quantities defined earlier are chosen such that once introduced in the system of governing equations (II.9.12) , the resulting system will be exactly the same except that all quantities are dimensionless. The dimensionless form will be used in the remainder of this work.

III. ANALYTICAL SOLUTION FOR A SPECIAL CASE

Analytical solutions for the nonlinear system (II.9-II.12) are difficult to obtain due to nonlinearities associated with the constitutive equation (II.12). Examples of the nonlinear constitutive equation are the empirical relation,

$$\tau = \mu_o \theta^{\nu} (\gamma^p)^m \left(\frac{\partial \gamma^p}{\partial t} \right)^n \qquad \text{(III.1)}$$

where μ_o, ν, m, n are material parameters. and the Arrhenius law

$$\phi = \omega_o \exp \left\{ -\left[\tau_B(\gamma^p) - \tau \right] \frac{W^*}{K_b \theta} \right\} \qquad \text{(III.2)}$$

where ω_o is the frequency of vibration of dislocations as they attempt to overcome obstacles, $\tau_B(\gamma^p)$ is the stress barrier amplitude - which is a function of the plastic strain in case of a strain hardening material; W^* is the Activation volume; K_b is Boltzmann's Constant. For physically reasonable models these quantities satisfy,

$$\omega_o >> 1 , \quad \tau < \tau_B(\gamma^p) ,$$
$$\tau_B(\gamma^p) \frac{W^*}{K_b \theta} >> 1 . \qquad \text{(III.3)}$$

The function $\tau_B(\gamma^p)$ is assumed to be positive, monotonic and to have a saturation limit τ_B^{∞} as $\gamma^p \to \infty$; furthermore, its derivatives are assumed to vanish as $\gamma^p \to \infty$.

In order to be able to obtain an exact solution that exhibits some features of the solutions of (II.9-II.12), consider the following special case:

- quasi-static deformation, i.e. $\rho_o \frac{\partial v}{\partial t} = 0$
- no heat conduction, i.e. $k = 0$
- no elastic effects, i.e. $G \to \infty$
- constant shear stress boundary conditions, i.e.

$$\tau(0,t) = \tau(H, t) = \tau_1$$

- Non-Newtonian fluid with temperature dependent viscosity, i.e.

$$\tau = \mu_o(\theta)^{\nu}(\frac{\partial v}{\partial y})^n \quad ; \quad n > o \tag{III.4}$$

The effects of thermal - softening (hardening) are obtained for negative (positive) values of the power ν. Although this model does not represent solids of engineering interest, it is attractive because it allows an analytical solution that gives insight into instabilities of solutions of the system (II.9-II.12) as well as providing a reference for checking the validity of the solutions obtained by a linear perturbation technique and by a finite difference method. Under these assumptions the system of equations (II.9-II.12) reduces to

$$\frac{\partial \tau}{\partial y} = 0 \tag{III.5}$$

$$\frac{\partial \gamma^p}{\partial t} = \frac{\partial v}{\partial y} \tag{III.6}$$

$$\frac{\partial \theta}{\partial t} = r_1 \tau \frac{\partial v}{\partial y} \tag{III.7}$$

$$\tau = \mu_o(\theta)^{\nu}(\frac{\partial v}{\partial y})^n \tag{III.8}$$

where $r_1 = \beta/\rho_o c$. From (III.5) and the stress boundary conditions the shear stress is given by

$$\tau(y,t) = \tau_1 \qquad \text{(III.9)}$$

which is kept constant throughout the deformation. Eliminating $(\frac{\partial v}{\partial y})$ between equations (III.7) and (III.8) one obtains

$$\frac{\partial \theta}{\partial t} = \eta \theta^{-\tilde{\nu}} \qquad \text{(III.10)}$$

where $\eta = r_1 \tau_1 (\frac{\tau_1}{\mu_o})^{\frac{1}{n}}$ is a positive constant and $\tilde{\nu} = \frac{\nu}{n}$. Integration of equation (III.10) gives

$$\theta(y,t) = \{f(y,t,\tilde{\nu})\}^{\frac{1}{1+\tilde{\nu}}} \qquad \text{(III.11)}$$

where $f(y,t,\tilde{\nu}) \equiv \theta_o(y)^{\tilde{\nu}+1} + \eta(\tilde{\nu}+1)t.$ (III.12)

This expression for the temperature $\theta(y,t)$ can be used to obtain the following expressions for other quantities of physical interest

$$\frac{\partial \theta}{\partial t}(y,t) = \eta \left\{ f(y,t,\tilde{\nu}) \right\}^{\phi(\tilde{\nu})} \qquad \text{(III.13)}$$

$$\frac{\partial \theta}{\partial y}(y,t) = \left[\theta_o(y)^{\tilde{\nu}} \cdot \frac{d\theta_o(y)}{dy}\right] \cdot \left\{ f(y,t,\tilde{\nu}) \right\}^{\phi(\tilde{\nu})} \qquad \text{(III.14)}$$

$$\dot{\gamma}^p(y,t) = \left(\frac{\tau_1}{\mu_o}\right)^{\frac{1}{n}} \cdot \left\{ f(y,t,\tilde{\nu}) \right\}^{\phi(\tilde{\nu})} \qquad \text{(III.15)}$$

where

$$\phi(\tilde{\nu}) = \frac{-\tilde{\nu}}{\tilde{\nu}+1} \; . \qquad \text{(III.16)}$$

Analysis of the exact solution:

The functions $f(y,t,\tilde{\nu})$ and $\phi(\tilde{\nu})$ characterize all the features of the solution to the problem. The function $\phi(\tilde{\nu})$ is negative for $\tilde{\nu} > 0$ and $\tilde{\nu} < -1$, while it has positive values for $-1 < \tilde{\nu} < 0$. The function $f(y,t,\tilde{\nu})$ is always positive for $\tilde{\nu} > -1$. For $\tilde{\nu} < -1$ there

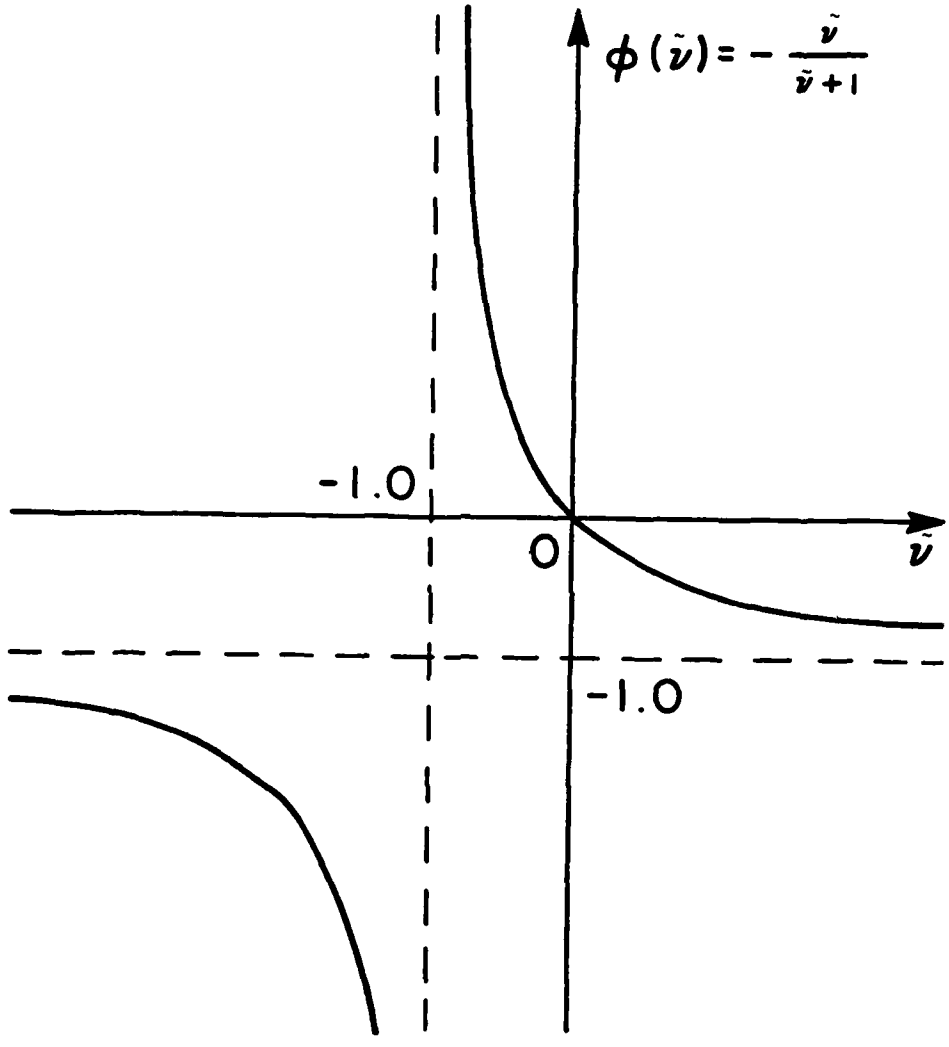

Figure (III-1) - Sign Changes of $\phi(\tilde{\nu})$ w.r.t. $(\tilde{\nu})$

is a critical time

$$t_{cr} = \frac{(\theta_o(y))^{\tilde{\nu}+1}}{\eta|(\tilde{\nu}+1)|} \qquad \text{(III.17)}$$

at which f becomes zero; f is negative for $t > t_{cr}$. Three types of behavior can be distinguished.

(i) Thermal hardening for $\tilde{\nu} > 0$

For $\tilde{\nu} > 0$, $\phi(\tilde{\nu})$ is negative and $f(y,t,\nu)$ is positive. Then, from (III.13-III.15) the quantities $\frac{\partial\theta}{\partial t}$, $\frac{\partial\gamma^p}{\partial t}$, and $\frac{\partial\theta}{\partial y}$ vanish as $t \to \infty$. Such solutions are strongly stable.

(ii) Thermal softening for $-1 < \tilde{\nu} < 0$

For $\tilde{\nu}$ in this range both $\phi(\tilde{\nu})$ and $f(y,t,\tilde{\nu})$ are positive. The quantities $\frac{\partial\theta}{\partial t}$, $\frac{\partial\gamma^p}{\partial t}$, $\frac{\partial\theta}{\partial y}$ become unbounded as $t \to \infty$. The solution grows in time as shown in Fig. (III.2) for the plastic strain rate. The shape of the plastic strain rate distribution varies slowly with time at small times and becomes independent of time as $t \to \infty$. There is no tendency for localization of shear straining. Based on the uniformity of the strain distribution; solutions such as those shown in Fig. (III.2) are said to "grow" rather than to become unstable. The term "instability" is reserved for bifuration phenomena in which the homogeneous and perturbed solutions grow at different rates so that differences between these solutions become large at late times as shown in Fig. (III.3). This notion of instability corresponds to experimental observations of shear bands with localized deformations which are large relative to deformations in neighboring regions.

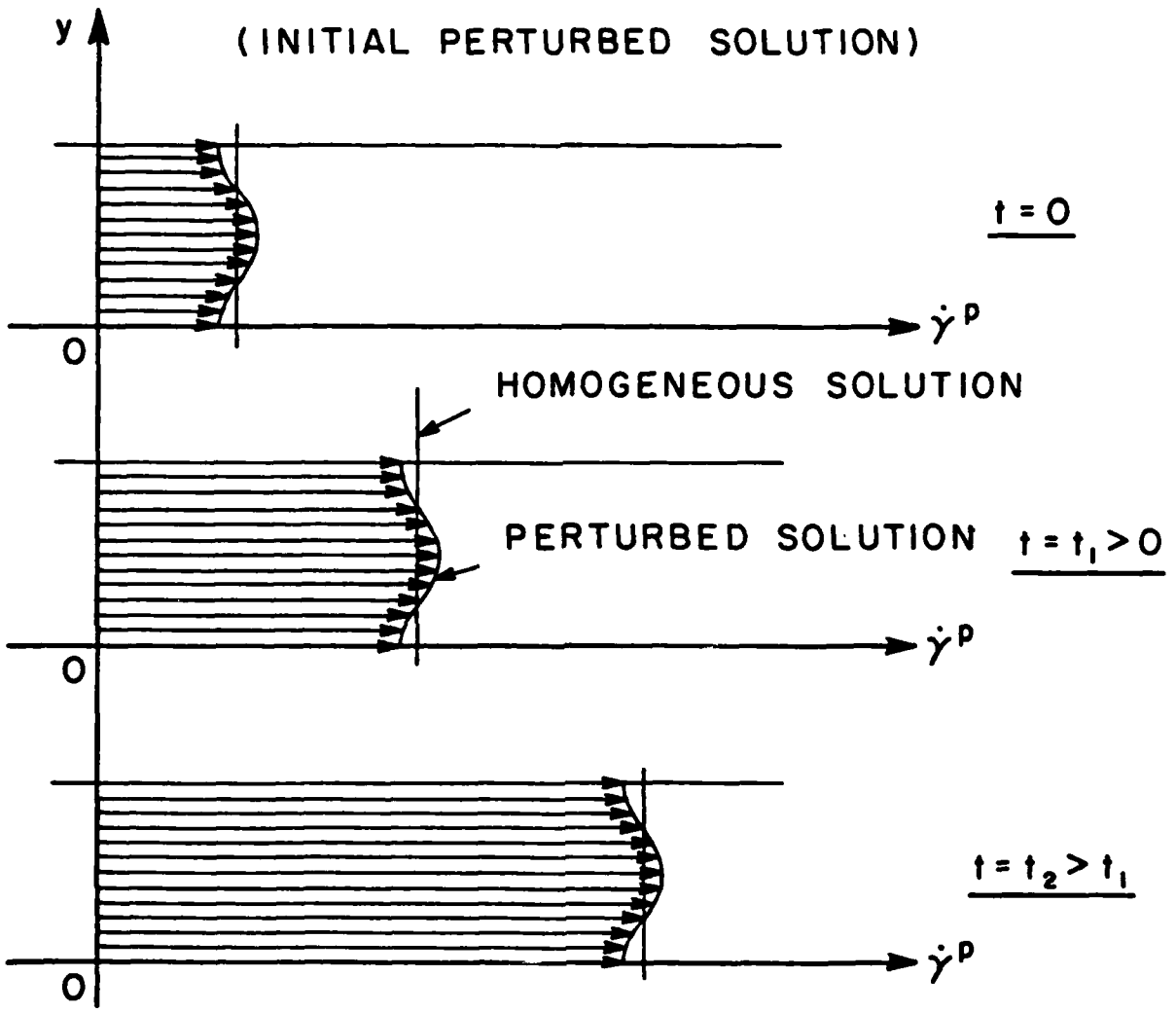

Figure (III-2) - Uniform Growth

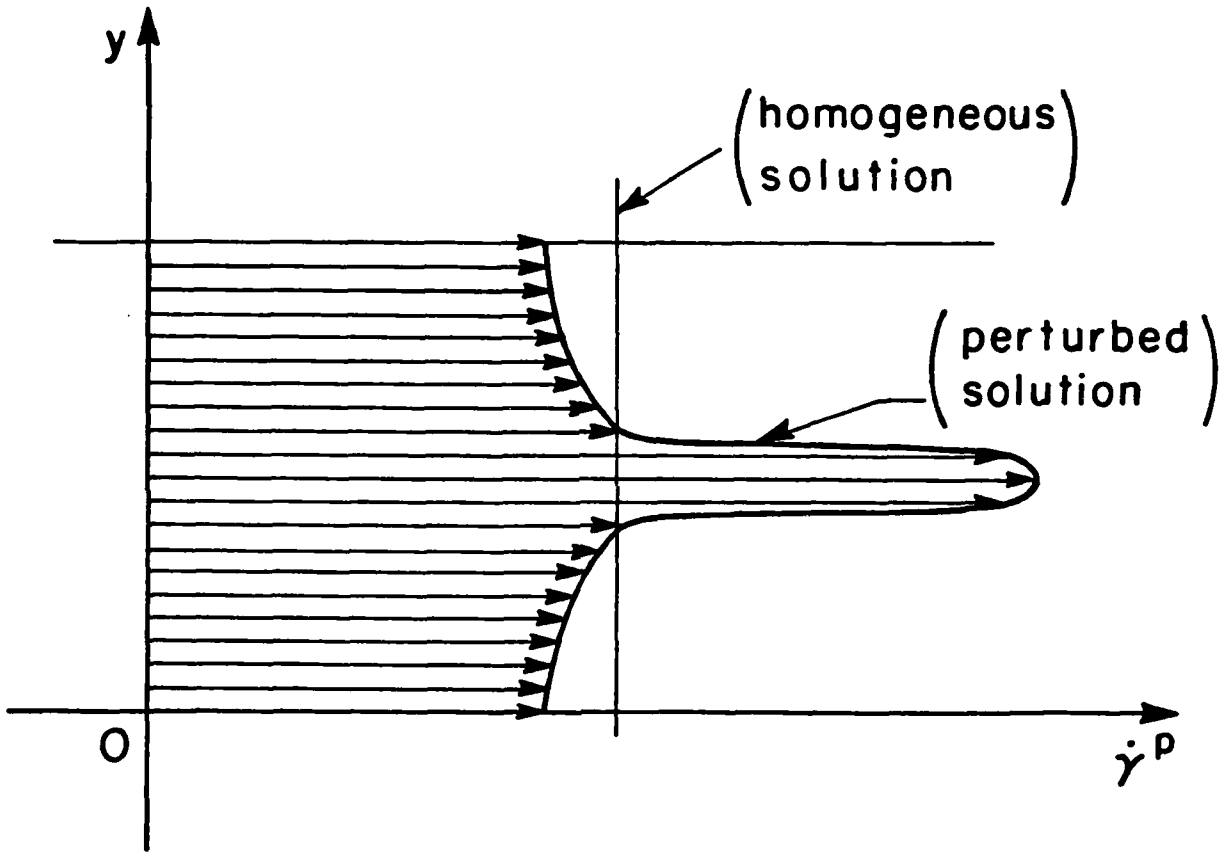

Figure (III-3) - Unstable Deformation

(iii) Thermal softening for $\tilde{\nu} < -1$

In this regime $\phi(\tilde{\nu})$ is negative; $f(y,t,\tilde{\nu})$ is positive for $t < t_{cr}$ and becomes negative for $t > t_{cr}$. All quantities in (III.11) and (III.13-III.15) become unbounded as $t \to t_{cr}$. Solutions exhibiting such behavior are termed unstable, although both the homogeneous and perturbed solutions become unbounded at the same time.

Concluding Remarks on Exact Solutions

1. The exact solution shows the possibility of a type of instability in which the solution becomes infinite in a finite time.

2. Less thermal softening is required to obtain unstable behavior for weakly strain-rate sensitive materials (i.e. $n << 1$) since Condition (iii) is $\nu < -n$.

IV. LINEAR STABILITY ANALYSES

In view of the extreme difficulty of solving the non-linear problem it is of interest to conduct stability analyses on a linearized version of the problem. Several authors have discussed this approach [9], [11]; however, for most of this discussion the homogeneous solution which is to be perturbed is held constant at the values corresponding to the instant at which the perturbation is introduced. This assumption, which is made to obtain linear equations with constant coefficients severely limits the applicability of the analyses. Extensions of the analysis to cases of time - varying coefficients have been presented by Clifton [14] and by T. J. Burns [10], who employed the direct Lyapunov's method for a thermo-viscous material. (i.e. elasticity and strain hardening are neglected)

In this study we seek a rigorous linear stability analysis to the general problem defined by Eqs. (II.9-II.12). Then, we present a modified stability criterion that extends the validity of the linear approach.

IV.1. Linearized system of equations

We consider the linearization of equations (II. 9-12) about the homogeneous (parallel flow) solution. We seek solutions of the form:

$$\begin{aligned} \tau(y,t) &= \tau^{o}(t) + \delta\tau(y,t) \\ v(y,t) &= v^{o}(y,t) + \delta v(y,t) \\ \gamma^{p}(y,t) &= \gamma p^{o}(t) + \delta\gamma^{p}(y,t) \\ \theta(y,t) &= \theta^{o}(t) + \delta\theta(y,t) \end{aligned} \qquad \text{(IV.1)}$$

where $\delta\tau$, δv, $\delta\gamma^{p}$, $\delta\theta$ are the differences between the solution τ, v, γ^{p}, θ, that includes the effects of a perturbation, and the

homogeneous solution τ^o, v^o, γ^{p^o}, θ^o. The homogeneous solution is assumed to be perturbed at (t = 0) by a small periodic fluctuation in the y-direction. We substitute solutions (IV.1) into the non-linear system (II. 9-12), and retain only first order terms in $\delta\tau$, δv, $\delta\gamma^p$, $\delta\theta$. In this way we obtain the following linear system of partial differential equations in $\delta\tau$, δv, $\delta\gamma^p$, and $\delta\theta$.

$$\frac{\partial}{\partial t}(\delta v) = \frac{1}{\rho_o}\frac{\partial}{\partial y}(\delta\tau) \qquad \text{(IV-2)}$$

$$\frac{\partial}{\partial t}(\delta\gamma^p) = \frac{\partial}{\partial y}(\delta v) - \frac{1}{G}\frac{\partial}{\partial t}(\delta\tau) \qquad \text{(IV-3)}$$

$$\frac{\partial}{\partial t}(\delta\theta) = r_o\frac{\partial^2}{\partial y^2}(\delta\theta) + r_1\tau^o\frac{\partial}{\partial t}(\delta\gamma^p) + r_1\phi^o\delta\tau \qquad \text{(IV-4)}$$

$$\frac{\partial}{\partial t}(\delta\gamma^p) = V^o\delta\tau + T^o\delta\theta + S^o\delta\gamma^p \qquad \text{(IV-5)}$$

where $r_o = \frac{k}{\rho_o c}$.

In these equations the coefficients V^o, T^o, S^o are defined by

$V^o = \left(\frac{\partial\phi}{\partial\tau}\right)^o$ is a measure of strain-rate sensitivity;

$T^o = \left(\frac{\partial\phi}{\partial\theta}\right)^o$ is a measure of thermal softening ($T^o > 0$), or hardening ($T^o < 0$) - thermal softening is the usual case for crystalline solids;

$S^o = \left(\frac{\partial\phi}{\partial\gamma^p}\right)^o$ is a measure of strain-hardening, (or softening if negative).

The functions V^o, T^o and S^o are evaluated at the homogeneous solution at time t, hence these are time dependent coefficients. For convenience of notation, we suppress the "δ" in the following analysis (e.g. $\delta\tau \to \tau$). We rewrite equations (IV.2,5) in matrix form for a solution vector

$$\underset{\sim}{\omega} = \begin{Bmatrix} v \\ \tau \\ \theta \\ \gamma^p \end{Bmatrix} \qquad \text{(IV.6)}$$

The resulting system of equations has the form

$$L(\underset{\sim}{\omega}) = A\,\underset{\sim}{\omega} + A^t\,\underset{\sim}{\omega}_{,t} + A^y\,\underset{\sim}{\omega}_{,y} + A^{yy}\,\underset{\sim}{\omega}_{,yy} = \underset{\sim}{0} \qquad \text{(IV.7)}$$

where a comma denotes differentiation with respect to the following subscripted variable and the coefficient matrices are given by:

$$A = \begin{bmatrix} 0 & 0 & 0 & 0 \\ 0 & V^o & T^o & S^o \\ 0 & -r_1(\tau^o V^o + \phi^o) & -r_1 \tau^o T^o & -r_1 \tau^o S^o \\ 0 & -V^o & -T^o & -S^o \end{bmatrix} \qquad A^t = \begin{bmatrix} \rho_o & 0 & 0 & 0 \\ 0 & \frac{1}{G} & 0 & 0 \\ 0 & 0 & 1 & 0 \\ 0 & C & 0 & 1 \end{bmatrix}$$

$$A^y = \begin{bmatrix} 0 & -1 & 0 & 0 \\ -1 & 0 & 0 & 0 \\ 0 & 0 & 0 & 0 \\ 0 & 0 & 0 & 0 \end{bmatrix} \qquad A^{yy} = \begin{bmatrix} 0 & 0 & 0 & 0 \\ 0 & 0 & 0 & 0 \\ 0 & 0 & -r_o & 0 \\ 0 & 0 & 0 & 0 \end{bmatrix} \qquad \text{(IV.8)}$$

The coefficient matrix A, is time-dependent, but it does not depend on the spatial coordinate y.

We introduce the Fourier transform defined by

$$\hat{F}(\xi,t) = \frac{1}{\sqrt{2\pi}} \int_{-\infty}^{+\infty} e^{-i\xi y}\, F(y,t)\, dy \,. \qquad \text{(IV.9.a)}$$

$$F(y,t) = \frac{1}{\sqrt{2\pi}} \int_{-\infty}^{+\infty} e^{i\xi y} \hat{F}(\xi,t)\, d\xi \,. \qquad \text{(IV.9.b)}$$

Then taking the Fourier transform of $L(\underset{\sim}{\omega}) = \underset{\sim}{0}$ we obtain

$$\frac{\partial \hat{\underset{\sim}{\omega}}}{\partial t}(\xi,t) = C(\xi,t)\ \hat{\underset{\sim}{\omega}}(\xi,t) \qquad \text{(IV.10)}$$

or, suppressing the dependence on ξ,

$$\frac{d\hat{\underset{\sim}{\omega}}}{dt}(t) = C(t)\ \hat{\underset{\sim}{\omega}}(t) \qquad \text{(IV.11)}$$

where C(t) is given by:

$$C(t) = \begin{bmatrix} 0 & -i\xi/\rho_o & 0 & 0 \\ -i\xi G & -GV^o & -GT^o & -GS^o \\ 0 & r_1(\tau^o V^o + \phi^o) & r_1\tau^o T^o - r_o\xi^2 & r_1\tau^o S^o \\ 0 & V^o & T^o & S^o \end{bmatrix} \qquad \text{(IV.12)}$$

Equation (IV.11) represent a system of linear, first order ordinary differential equations for the perturbation vector $\hat{\underset{\sim}{\omega}}(\xi,t)$.

IV.2) Solution of the Linear System:

Analytic solution of the system (IV.11) can be obtained in an iterative way as follows:

$$\hat{\underset{\sim}{\omega}}(t) = \hat{\underset{\sim}{\omega}}(0) + \int_o^t [C(\eta)\ \hat{\underset{\sim}{\omega}}]\, d\eta$$

$$= \hat{\underset{\sim}{\omega}}(0) + \int_o^t \left\{ C(\eta)\ [\ \hat{\underset{\sim}{\omega}}(0) + \int_o^\eta [C(x)\hat{\underset{\sim}{\omega}}]\, dx \right\} d\eta$$

Continuing the iteration process, we reach the solution:

$$\hat{\underset{\sim}{\omega}}(t) = S(t)\ \hat{\underset{\sim}{\omega}}(0) \qquad \text{(IV.13)}$$

where, the matrix S(t) is known as the matrizant of the differential equation, or the "solution operator", which is given explicitly by

$$S(t) = I + \int_o^t C(\eta)\, d\eta + \int_o^t C(\eta) \int_o^\eta C(x)dx\, d\eta + \ldots \quad \text{(IV.14)}$$

Or, in compact form,

$$S(t) = \sum_{n=o}^{\infty} C(t)^{(n)} \quad \text{(IV.15)}$$

where

$$C(t)^{(n)} = \int_o^t C(\eta)\ C(\eta)^{(n-1)}\ d\eta \quad \text{(IV.16)}$$

and

$$C(t)^{(o)} = I\,. \quad \text{(IV.17)}$$

The solution expressed by (IV.14,17) is the general solution of equation (IV.11); however in the special case where C(t) commutes with $C(t)^{(1)}$ the solution operator S(t) can be expressed concisely in the form

$$S(t) = \exp\left[\int_o^t C(\eta)\, d\eta\right] \quad \text{(IV.18)}$$

(see Appendix I).

IV.3. Stability of the Solution

Consider the solution in the general form (IV.14) which represents an infinite series. Taking the norm of each side, one obtains:

$$||S(t)|| = || \sum_{n=0}^{\infty} C(t)^{(n)} || \leq \sum_{n=0}^{\infty} ||C(t)^{(n)}||$$

However,

$$||C(t)^{(n)}|| = ||\int_0^t C(\eta)\ C(\eta)^{(n-1)} d\eta||$$

and for finite time intervals (0,t), we can write

$$||C(t)^{(n)}|| \leq \int_0^t ||C(\eta)\ C(\eta)^{(n-1)}||d\eta \leq \int_0^t ||C(\eta)||\ ||C(\eta)^{(n-1)}||d\eta$$

Then

$$||S(t)|| \leq 1 + \sum_{n=1}^{\infty} \left\{ \int_0^t ||C(\eta)||\ ||C(\eta)^{(n-1)}||d\eta \right\} . \qquad \text{(IV.19)}$$

Let us assume that $\sup||C(\eta)||$ exists and is equal to a finite value p, say. In this case we obtain:

$$||S(t)|| \leq 1 + pt + \frac{p^2t^2}{2!} + \ldots = e^{pt}$$

or

$$||S(t)|| \leq e^{[\sup||C(\eta)||]t};\ \forall\eta \in [0,t] \qquad \text{(IV.20)}$$

From (IV.20) we conclude that the series $S(t)$ is uniformly and absolutely convergent for all values of t as long as the maximum (supremum) norm of the coefficient matrix $C(t)$ is bounded for any finite time.

IV.4. Stability criterion for thermal-visco-plastic deformation

The solution (IV.13) gives a direct relation between the vector of initial perturbations and their corresponding values at a later time ($t > 0$). The argument usually used to determine the stability of such solutions is based on the signs of eigenvalues of the solution operator $S(t)$. Such a criterion serves to determine whether the initial disturbances grow (or decay) with increasing time. However, as mentioned in Chapter III, we seek a bifurcation process for which the perturbed solution grows much faster than the homogeneous solution. Also, we require the unstable growth to be confined to some region of the slab thickness. Motivated by this notion of instability, and in order to distinguish between a uniform growth Fig. (III.2) and an unstable deformation Fig. (III.3), we suggest the following criterion.

The system of equations (IV.7) is called "well-posed" and its solution given by (IV.13) is called stable if there exist constants κ and α, both positive, and independent of initial values $\hat{\underset{\sim}{\omega}}(0)$ such that:

$$\sup||S(t)|| \leq \kappa \exp(\alpha t). \qquad \text{(IV.21)}$$

The quantity $\sup||S(t)||$ in (IV.21) is the norm $||S(t)||_\infty$ defined in (IV.23).*

*If (IV.21) holds for $||S(t)||_\infty$, then it also holds for the L_2-norm defined by $||S(t)||_2 = \max_{\underset{\sim}{x}\neq\underset{\sim}{0}} \dfrac{||S(t)\underset{\sim}{x}||_2}{||\underset{\sim}{x}||_2}$ for each t.

The notion of well-posedness (IV.21) implies continuous dependence on the initial data. Moreover, this estimate (IV.21) implies that a stable solution can grow exponentially as long as it can be bounded by a suitable choice of (κ,α) for any finite time (t) and finite wave number (ξ). The inequality (IV.21) suggests much weaker conditions for stability than the requirement that all the eigenvalues λ_i of $S(t)$ satisfy $\lambda_i \leq 0$. An essential feature of the notion of instability adopted here is the requirement that there are solutions that become unbounded in a finite time.

In order to apply the criterion (IV.21) we note from (IV.20) that (IV.21) is satisfied if there exists an $\alpha > 0$ such that

$$\sup_{\eta\in[0,t]} ||C(\eta)|| \leq \alpha. \qquad \text{(IV.22)}$$

That is, the criterion (IV.21) is satisfied if the norm of $C(t)$ is bounded for any finite time. To express this constraint in terms of the elements of $C(t)$ we choose $\sup_{\eta\in[0,t]} ||C(\eta)||$ to be defined as follows:

$$\sup_{\eta\in[0,t]} ||C(\eta)|| = ||C(t)||_\infty = \max_{1\leq i\leq n} \sum_{j=1}^{n} |C_{ij}|. \qquad \text{(IV.23)}$$

Applying (IV.23) to the coefficient matrix $C(t)$ given by (IV.12), we find

$$\max(R_1,R_3,R_4) = \sup_{\eta\in[0,t]} ||C(\eta)||$$

where the row sums are

$$R_2 \equiv |G|[|V^o| + |S^o| + |T^o|] + |G\xi|$$

$$R_3 \equiv |r_1|\cdot[|\tau^o V^o + \phi^o| + |\tau^o S^o|] + |r_1\tau^o T^o - r_o\xi^2|$$

$$R_4 \equiv |V^o| + |S^o| + |T^o|$$

Since for constant strain rates ϕ^0 the time dependence in the expressions for the row sums is restricted to the functions T^0, S^0, V^0 and τ^0, we can write the stability criterion (IV.22) in the form

$$\{ |T^o(\eta)| + |S^o(\eta)| + |V^o(\eta)| \} \leq \alpha \qquad \text{(IV.24a)}$$

and

$$|\tau^o(\eta)| \cdot \{ |T^o(\eta)| + |S^o(\eta)| + |V^o(\eta)| \} \leq \beta \qquad \text{(IV.24b)}$$

provided that

$$\tau^o(\eta) > \tau_y \ , \forall \eta \epsilon [0, t] \ , \ (t < \infty) \ , \ \alpha > o \ , \ \beta > o \ ,$$

where the restriction on $\tau^o(\eta)$ is imposed because the shear stress must be greater than some yield value, say τ_y, for constitutive equations of the form (II.12) to apply.

The stability criteria (IV.24) have been derived for the case of finite wave numbers ξ. This restriction can be removed by considering directly the rate of growth of the L_2-norm of the solution $\underset{\sim}{\omega}$ of the system (IV.7). (See Appendix IV)

IV.5. APPLICATIONS OF THE STABILITY CRITERION

IV.5.1. The quasi-static model (III.5-III.8)

The analytical solution for this model is given in Chapter (III). For the constitutive law (III.8)

$$T^0 = \left.\frac{\partial\phi}{\partial\theta}\right|^0 = -\tilde{\nu}\left(\frac{\tau_1}{\mu_o}\right)^{1/n} \cdot (\theta^0(t))^{-(\tilde{\nu}+1)}$$

$$S^0 = 0$$

$$V^0 = \left.\frac{\partial\phi}{\partial\tau}\right|^0 = \left(\frac{1}{\mu_o n}\right)\left(\frac{\tau_1}{\mu_o}\right)^{\frac{1-n}{n}} (\theta^o)^{-\tilde{\nu}}$$

Substituting the values of τ^0, T^0, S^0 and V^0 in the inequality (IV.24) we obtain

$$(\frac{1}{n}) \cdot \left\{ |\nu| \tau_1 \theta^0(t)^{-(\tilde{\nu}+1)} + \theta^0(t)^{-\tilde{\nu}} \right\} \leq \bar{\alpha}. \qquad \text{(IV.25)}$$

where

$$\bar{\alpha} = \beta (\frac{\mu_o}{\tau_1})^{\frac{1}{n}} .$$

Substituting the homogeneous solution

$$\theta^0(t) = [1 + \eta(\tilde{\nu}+1)t]^{\frac{1}{\tilde{\nu}+1}}$$

into (IV.25) gives the stability requirement

$$(\frac{1}{n}) \cdot \left\{ f(t;\tilde{\nu})^{\phi(\tilde{\nu})} + |\nu| \tau_1 f(t;\tilde{\nu})^{-1} \right\} \leq \bar{\alpha} \qquad \text{(IV.26)}$$

where

$$f(t;\tilde{\nu}) = 1 + \eta(\tilde{\nu}+1)t.$$

Obviously, the inequality (IV.26) is only violated for $\tilde{\nu} < -1$. In this case the function f becomes zero at a critical time

$$\bar{t}_{cr} = \frac{1}{\eta|\tilde{\nu}+1|} . \qquad \text{(IV.27)}$$

Therefore, we conclude that the deformation described by this model is stable for $\tilde{\nu} > -1$. This is the same conclusion obtained from the exact solution (III.11-III.16). Furthermore, the linear stability analysis predicts the same type of singularity as that obtained for the exact solution, as well as the same critical time. Thus, the criterion (IV.21) appears to have promise for characterizing the stability of homogeneous deformations.

IV.5.2. General polynomial constitutive law with velocity boundary conditions

We consider the general system of equations (II.9-II.12) with the constitutive equation (III.1) written in the form

$$\phi = [\frac{\tau}{\mu_0} \theta^{-\nu} (\gamma^p)^{-m}]^{1/n} \qquad \text{(IV.28)}$$

A homogeneous solution for this model (neglecting elasticity) has been given by Clifton, et al [14]. The temperature and stress in this solution, obtained for a constant strain rate ϕ_0, are

$$\theta^0(t) = \{\gamma \hat{f}(\nu,m) \cdot t^{(1+m)} + \theta_0^{1-\nu}\}^{\frac{1}{1-\nu}} \qquad \text{(IV.29)}$$

$$\tau^0(t) = \bar{\mu} \cdot [\theta^0(t)]^{\nu} \cdot t^m \qquad \text{(IV.30)}$$

where,

$$\gamma \equiv r_1 \mu_0 \phi_0^{(1+m+n)} > 0$$

$$\hat{f}(\nu,m) \equiv \frac{1-\nu}{1+m}$$

$$\bar{\mu} \equiv \mu_0 \phi_0^{n+m} > 0.$$

For the constitutive equation (IV.28) the coefficients T^0, S^0, V^0 are

$$T^0 = -\frac{\phi_0}{n} (\frac{\nu}{\theta^0}) \qquad \text{(IV.31a)}$$

$$s^0 = -\frac{\phi_0}{n}\left(\frac{m}{\phi_0 t}\right) \qquad \text{(IV.31b)}$$

$$v^0 = \frac{\phi_0}{n}\left(\frac{1}{\tau^0}\right) \qquad \text{(IV.31c)}$$

From (IV.29-IV.31) the stability criterion (IV.24) becomes

$$\frac{\phi_0}{n} \cdot \{1 + |m|\frac{\bar{\mu}}{\phi_0} \quad (\theta^0)^{\nu} t^{m-1} + |\nu|\bar{\mu}(\theta^0)^{\nu-1} t^m\} \leq \beta \qquad \text{(IV.32)}$$

From (IV.32) the stability criterion is satisfied as long as neither of the functions $(\theta^0)^{\nu}$, $(\theta^0)^{\nu-1}$ becomes unbounded. Such singularities can occur only for $\hat{f}(\nu,m) < 0$ and at

$$\bar{t}_{cr} = \left\{ \frac{\theta_0^{1-\nu}}{\gamma|\hat{f}(\nu,m)|} \right\}^{1/1+m} \qquad \text{(IV.33)}$$

Stability boundaries based on the sign of $\hat{f}(\nu,m)$ are shown in Fig. (IV.1).

The function $\hat{f}(\nu,m)$ is negative in regions (I) and (III) defined by

I: $\nu > 1$ and $m > -1$

III: $\nu < 1$ and $m < -1$

Regions I and IV are of little interest in applications since materials are generally thermally soft. Region III is seldom, if ever, applicable because few materials exhibit the strong strain softening that is characteric of this region. Region II is characteristic of most metals. Thus, it appears that the stability criterion is satisfied for most metals that could be modeled by (IV.28). In view of the fact that Region II contains points corresponding to both strain

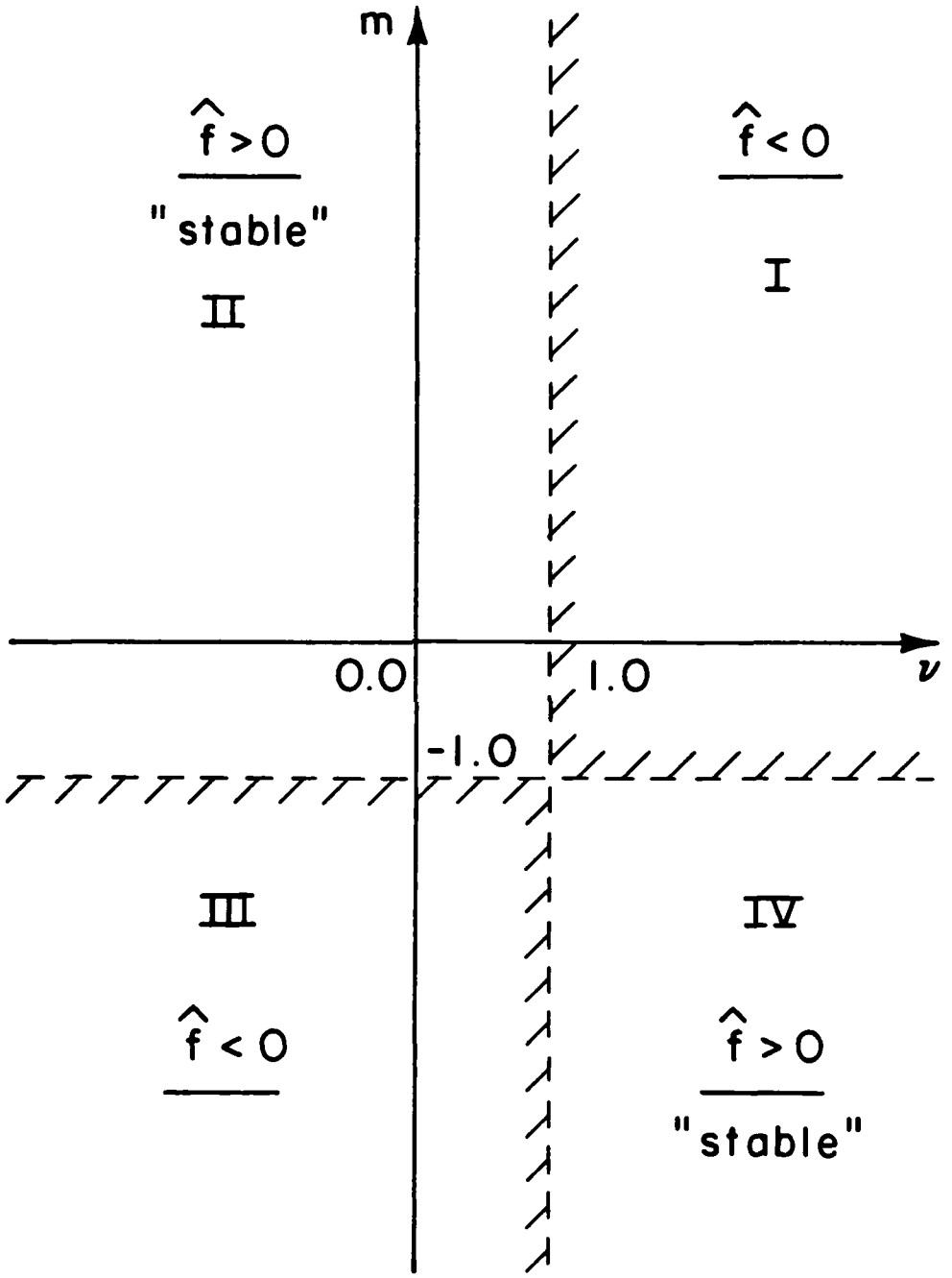

Figure (IV•1) - Sign of $\hat{f}$ (ν,m) in the $(\nu\text{-}m)$ Plane

softening ($m < 0$) and thermal softening ($\nu < 0$), it appears that stability in the sense of (IV.21) is satisfied for a wide class of materials.

Consider the term in { } in equation (IV.32); and denote it p(t), then equation (IV.32) becomes

$$\left(\frac{\phi_o}{n}\right) P(t) \leq \alpha$$

If P(t) is bounded, say by $P_{max.}$, then the solution to the perturbed problem grows no faster than $e^{\beta t}$ with $\beta = \frac{\phi_o P_{max.}}{n}$. Whether such a solution to the perturbed problem grows or decays depends on the thermal softening and strain hardening parameters, ν and m, respectively. In either case, the rate of growth or decay is affected by the strain-rate sensitivity parameter (n). Small values of n (i.e. weak strain-rate sensitivity) allow high rates of growth or decay.

If P(t) is unbounded, then the problem (IV.11) is not well-posed.

IV.5.3 Bodner-Merzer Constitutive Model

Consider the system of equations (II.9-II.12) with the constitutive model (introduced by Bodner and used by Merzer [13]):

$$\tau \equiv \tau(\dot{\gamma}^p, \theta, W^p) = \frac{\tau_1(W^p)}{\sqrt{3}} [f(\eta)]^{c(\theta)} \qquad \text{(IV.34)}$$

where

$$f(\eta) \equiv 2 \ell n \eta, \qquad \eta \equiv \frac{2D_o}{\dot{\gamma}^p};$$

$$c(\theta) \equiv \frac{-1/2}{n(\theta)}, \qquad n(\theta) = \frac{a}{\theta} + b, \; a > 0, \; b < 0;$$

$$\tau_1(W^p) = \tilde{\tau}_1 - (\tilde{\tau}_1 - \tilde{\tau}_o) e^{-mW^p}, \; m > 0, \; \tilde{\tau}_1 > \tilde{\tau}_o.$$

Neglect elastic strain rates in (II.10) and combine (II.9) and (II.10) to obtain

$$\rho_o \frac{\partial \phi}{\partial t} = \frac{\partial^2 \tau}{\partial y^2} \tag{IV.35}$$

where ϕ is the plastic strain rate, as in (II.12a). Substitution of (IV.34) in (IV.35) gives

$$\begin{aligned} \rho_o \frac{\partial \phi}{\partial t} = (S_1 \phi_{,yy} + S_2 \theta_{,yy} + S_3 w^p{}_{,yy}) \\ + \left(\frac{\partial S_1}{\partial y} \phi_{,y} + \frac{\partial S_2}{\partial y} \theta_{,y} + \frac{\partial S_3}{\partial y} w^p{}_{,y} \right) \end{aligned} \tag{IV.36}$$

where the coefficients S_i are for the model IV-34, given by

$$S_1 \equiv \frac{\partial \tau}{\partial \dot{\gamma}^p} = \tau / [n\phi \cdot f(n)] \tag{IV.37a}$$

$$S_2 \equiv \frac{\partial \tau}{\partial \theta} = - a\tau \cdot \ell n[f(n)]/(2\theta^2 n^2) \tag{IV.37b}$$

$$S_3 \equiv \frac{\partial \tau}{\partial w^p} = m\tau \left(\frac{\tilde{\tau}_1}{\tau_1} - 1 \right), \tag{IV.37c}$$

Equations (II.11) and (IV.36) constitute the governing equations for the evolution of the temperature θ and the plastic strain rate $\phi = \dot{\gamma}^p$, τ in these equations is obtained from (IV.34) and w^p is obtained from the integration of the second part of (II.5).

For a homogeneous deformation the coefficients S_i are y-independent, i.e.

$$\left.\begin{aligned} S_i &= S_i(t) \\ \text{and} \quad \frac{\partial S_i}{\partial y} &= 0 \end{aligned}\right\} \quad \text{for } i = 1, 2, 3 \tag{IV.38}$$

Moreover, if we confine attention to the late time response; then we can set

$$S_3(t \to \infty) = 0 \tag{IV.39}$$

Based on these assumptions the governing equations reduce to

$$\rho_o \frac{\partial \phi}{\partial t} = S_1 \phi_{,yy} + S_2 \theta_{,yy} \tag{IV.40.a}$$

$$\frac{\partial \theta}{\partial t} = r_o \theta_{,yy} + r_1 \hat{\tau}(\theta,\phi) \cdot \phi \tag{IV.40.b}$$

where

$$\hat{\tau}(\theta,\phi) \equiv \frac{\tilde{\tau}_1}{\sqrt{3}} [f(\eta)]^{c(\theta)} . \tag{IV.40.c}$$

Introduction of the solution vector

$$\underset{\sim}{z} \equiv \begin{Bmatrix} \phi \\ \theta \end{Bmatrix} \tag{IV.41}$$

allows equations (IV.40.a,b) to be written in the form

$$\underset{\sim}{Z}_{,t} = A^{(2)} \underset{\sim}{Z}_{,yy} + A^{(0)} \underset{\sim}{Z} \tag{IV.42}$$

where the coefficient matrices $A^{(2)}$ and $A^{(o)}$ are given by

$$A^{(2)} = \begin{pmatrix} S_1/\rho_0 & S_2/\rho_0 \\ 0 & r_0 \end{pmatrix} , \quad A^{(0)} = \begin{pmatrix} 0 & 0 \\ r_1\hat{\tau} & 0 \end{pmatrix} \tag{IV.43}$$

Taking the Fourier transform (cf. (IV.9)) of equation (IV.42) one obtains

$$\hat{\underset{\sim}{Z}}_{,t} = c(t) \hat{\underset{\sim}{Z}} \tag{IV.44}$$

where

$$c(t) = \begin{pmatrix} \frac{-\xi^2 S_1}{\rho_o} & \frac{-\xi^2 S_2}{\rho_o} \\ r_1\hat{\tau} & -\xi^2 r_o \end{pmatrix} . \tag{IV.44.a}$$

For the stability criterion (IV.22), stability requirements for the considered model can be given by

$$\frac{\xi^2}{\rho_o}\left(|S_1| + |S_2|\right) < \alpha \; ; \qquad \alpha > 0 \tag{IV.45.a}$$

$$\left(r_1 \hat{\tau} + \xi^2 r_o\right) < \beta \; ; \qquad \beta > 0 \tag{IV.45.b}$$

The inequality (IV.45.b) is always satisfied; however the inequality (IV.45.a) is violated as soon as either

$$\dot{\gamma}^p \to 2D_o \; , \qquad \text{i.e. } \eta \to 1 \tag{IV.46.a}$$

or

$$\theta \to \frac{a}{|b|} \; , \qquad \text{i.e. } n(\theta) \to 0 \tag{IV.46.b}$$

The second limit is reached for all homogeneous deformations without heat loss, if these deformations are carried to sufficiently large strains. Thus, the material model characterized by (IV.34) is especially sensitive to temperature increases. For the numerical values given in [13] for a and b the limit (IV.46.b) is reached at a temperature $\tilde{\theta} = 1.72$; for adiabatic deformation from room temperature this temperature is reached at a strain of approximately 200%. This limitation on homogeneous deformations for the model (IV.34) will be discussed further in chapter (V).

V. FINITE-DIFFERENCE SOLUTION OF THE NONLINEAR PROBLEM

In order to obtain a better understanding of the onset of localization in simple shear deformation, we seek a finite-difference numerical solution to the system (II.9,12) for the general form of the constitutive equation (II.12). Numerical solutions of this problem have been presented to interpret torsional Kolsky bar experiments [13], [15]. An important feature of these solutions is the introduction of a geometric imperfection in the specimen. The numerical calculations by Costin [12] show evidence of localized deformation in a low-carbon cold-rolled steel (CRS) at high strain rates, and stable deformation for a hot-rolled steel (HRS) of the same composition. These results are in agreement with experimental observations. Merzer [13] discusses the effect of thermal diffusion on band spreading in Kolsky bar experiments. He shows that for a thermal, visco-plastic model of an aluminum alloy the band does not spread significantly at strain rates of 500 s^{-1} and higher.

The objective of the present study is to examine, through numerical solutions, the response of different materials to different types of initial perturbations in the field quantities, for various combinations of boundary and loading conditions. A number of constitutive equations is considered in order to study the relative effects of strain-hardening and thermal softening. We consider the following system of equations:

$$\frac{\partial v}{\partial t} = \frac{1}{\rho_0} \frac{\partial \tau}{\partial y} \tag{V.1}$$

$$\frac{\partial \gamma^P}{\partial t} = \frac{\partial v}{\partial y} \tag{V.2}$$

$$\frac{\partial \theta}{\partial t} = r_0 \frac{\partial^2 \theta}{\partial y^2} + r_1 \tau \frac{\partial \gamma^P}{\partial t} \tag{V.3}$$

$$\tau = \psi(\theta, \gamma^P, \dot{\gamma}^P). \tag{V.4}$$

Elastic effects are not considered in this model, in order to facilitate the calculations; however, this approximation is not expected to affect the results significantly since elastic strain rate is much smaller than the plastic strain rate. Equation (V.3) has a quasi-linear term, while equation (V.4) is, in general, fully nonlinear.

Before presenting the finite difference formulation, we point out that we seek the qualitative behavior of the solution, which makes the stability of the difference method our primary concern and the method's accuracy of secondary importance. However, accuracy has to be kept within reasonable limits to satisfy the consistency requirement. An essential objective in this formulation is to be able to resolve the time scale on which major changes in the solution occur. This makes an explicit formulation preferable to an implicit one since small time steps are required for good time resolution and the implicit schemes have the associated difficulty of requiring the solution of a system of simultaneous equations at each time step. Thus, the unconditional stability feature of implicit schemes is less attractive for the type of problems considered. Use of an explicit scheme requires the choice of a "proper" time increment, where a "proper" time increment is the one that maintains scheme stability and is large enough to give good computational efficiency.

The difference formulation is presented for the system (V.1-4) with the following auxiliary conditions.

A. Initial Conditions

For a constant overall strain-rate, initial conditions for velocity, strain and strain-rate are:

$$v(y,0) = y, \quad \gamma^P(y,0) = \gamma_0, \quad \dot{\gamma}^P(y,0) = 1.$$

The initial condition for the temperature is assumed to be

$$\theta(y,0) = 1 + \theta_p(y)$$

where $\theta_p(y)$ is a small perturbation. The perturbation is taken to be either a smooth periodic fluctuation, or a step perturbation over a narrow region near the center of the slab thickness.

The initial conditions on $\gamma^P, \dot{\gamma}^P$ and θ are used to calculate the initial stress $\tau(y,0)$ from equation (V.4).

Alternatively, for quasi-static deformations with a geometric imperfection, we take the thickness in the direction z to be a function $T(y)$. From equilibrium the shear stress must satisfy

$$\tau(y,0)T(y) = \text{Const.} \qquad (V.6)$$

The initial temperature is taken to be $\theta(y,0) = 1$. The corresponding initial strain rate $\dot{\gamma}^P(y,0)$ and initial strain $\gamma^P(y,0)$ for which (V.4) is satisfied is obtained by assuming $\dot{\gamma}^P(y,0)$ and $\gamma^P(y,0)$ to be proportional, i.e.

$$\gamma^P(y,0) = \gamma_0 \dot{\gamma}^P(y,0).$$

Substituting this expression and (V.6) into (V.4), and requiring the mean strain rate to be unity, we obtain the constant in (V.6) and the initial strain rate distribution.

B. Boundary Conditions

We can prescribe either velocities or stresses at the boundaries $y = 0$ and $y = 1$. For most of this analysis we assume velocity boundary conditions of the form

$$\left.\begin{aligned} V(0,t) &= 0 \\ V(1,t) &= 1 \end{aligned}\right\} . \qquad (V.7)$$

We assume that the deformation occurs without heat transfer from the slab. This condition is ensured by the boundary conditions

$$\frac{\partial \theta}{\partial y}(0,t) = \frac{\partial \theta}{\partial y}(1,t) = 0 . \qquad (V.8)$$

V.1. Finite difference formulation

Our basic formulation is concerned with the dynamic problem in which inertial effects are retained. We confine our attention in this part to the case of velocity boundary conditions.

The key idea in this analysis is to rewrite the system of equations (V.1,4) in a modified form that reflects its "parabolic" nature. For this, differentiate (V.4) with respect to y to obtain

$$\frac{\partial \tau}{\partial y} = S_1 \frac{\partial \dot{\gamma}^P}{\partial y} + S_2 \frac{\partial \theta}{\partial y} + S_3 \frac{\partial \gamma^P}{\partial y} \qquad (V.9)$$

where

$$S_1 = \frac{\partial \psi}{\partial \dot{\gamma}^P} \qquad (V.10a)$$

$$S_2 = \frac{\partial \psi}{\partial \theta} \qquad (V.10b)$$

and

$$S_3 = \frac{\partial \psi}{\partial \gamma^P} . \tag{V.10c}$$

From the compatability relation (V.2), we get*

$$\frac{\partial \dot{\gamma}^P}{\partial y} = \frac{\partial}{\partial y} \left(\frac{\partial v}{\partial y}\right) = \frac{\partial^2 v}{\partial y^2} . \tag{V.11}$$

Substitution of (V.11) and (V.9) in (V.1) gives

$$\frac{\partial v}{\partial t} = \frac{1}{\rho_0}\{S_1 \frac{\partial^2 v}{\partial y^2} + S_2 \frac{\partial \theta}{\partial y} + S_3 \frac{\partial \gamma^P}{\partial y}\}. \tag{V.12}$$

This form of the momentum equation can be viewed as a <u>parabolic</u> equation for the velocity $v(y,t)$ which is similar to the well known diffusion equation

$$\frac{\partial u}{\partial t} = \nu \frac{\partial^2 u}{\partial x^2} \tag{V.13}$$

but with variable coefficient $S_1(y,t)$ and lower order terms. Substitution of the shear stress of (V.4) into (V.3) allows the governing equations to be written as the following system of three evolutionary equations.

$$\frac{\partial v}{\partial t} = \frac{1}{\rho_0}\{S_1 \frac{\partial^2 v}{\partial y^2} + S_2 \frac{\partial \theta}{\partial y} + S_3 \frac{\partial \gamma^P}{\partial y}\} \tag{V.14}$$

$$\frac{\partial \gamma^P}{\partial t} = \frac{\partial v}{\partial y} \tag{V.15}$$

$$\frac{\partial \theta}{\partial t} = r_0 \frac{\partial^2 \theta}{\partial y^2} + r_1 \cdot \psi(\theta, \gamma^P, \dot{\gamma}^P) \cdot \frac{\partial \gamma^P}{\partial t} . \tag{V.16}$$

---

*This step is the reason for not considering elastic effects.

Introducing the solution vector

$$\underset{\sim}{\omega} = \begin{Bmatrix} v \\ \gamma^P \\ \theta \end{Bmatrix} \tag{V.17}$$

we can write the system (V.14-V.16) as

$$\underset{\sim}{\omega}_{,t} = A^y \underset{\sim}{\omega}_{,y} + A^{yy} \underset{\sim}{\omega}_{,yy} \tag{V.18}$$

where

$$A^y = \begin{Bmatrix} 0 & S_3/\rho_0 & S_2/\rho_0 \\ 1 & 0 & 0 \\ r_1\psi & 0 & 0 \end{Bmatrix} \tag{V.19}$$

$$A^{yy} = \begin{Bmatrix} S_1/\rho_0 & 0 & 0 \\ 0 & 0 & 0 \\ 0 & 0 & r_0 \end{Bmatrix} . \tag{V.20}$$

We introduce the following terminology for finite difference quantities

$h \equiv \Delta y$ ... spatial increment

$k \equiv \Delta t$ ... time increment

$x_j^n \equiv x(jh,nk)$ ··· Value of the variable x at the j^{th} node and the n^{th} time level (assuming that $x(y,t)$ coincides - at least locally - with the described values x_j^n at the respective nodes).

We make use of the difference operators

$D_+(h)$ .... forward difference operator

$D_-(h)$ .... backward difference operator

$D_0(h)$ .... central difference operator

where

$$D_+(h)x_j^n = (x_{j+1}^n - x_j^n)/h \tag{V.21}$$

$$D_-(h)x_j^n = (x_j^n - x_{j-1}^n)/h \tag{V.22}$$

$$D_0(h)x_j^n = (x_{j+1}^n - x_{j-1}^n)/2h \tag{V.23}$$

The difference operator $D_+(h)D_-(h) = D_-(h)D_+(h)$ represents the symmetric second order difference operator, i.e.

$$D_+(h)D_-(h)x_j^n = (x_{j+1}^n - 2x_j^n + x_{j-1}^n)/h^2. \tag{V.24}$$

We will use the operators $D_0(h)$ and $D_+(h)D_-(h)$ to approximate first and second order spatial derivatives, respectively. Also, $D_+(k)$ will be used to approximate the time derivatives.

We will solve the evolution equations (V.14,16) in the given order,

using the updated values to modify the calculation. Therefore, difference equations can be given, for interior nodal points, as follows:

$$D_+(k)v_j^n = \frac{1}{\rho_0}\{S_{1j}^n D_+(h)D_-(h)V_j^n + S_{2j}^n D_0(h)\theta_j^n + S_{3j}^n D_0(h)(\gamma^P)_j^n\} \quad (V.25)$$

$$D_+(k)(\gamma^P)_j^n = D_0(h)v_j^{n+1} \quad (V.26)$$

and

$$D_+(k)\theta_j^n = r_0 D_+(h)D_-(h)\theta_j^n + r_1[\psi(\theta_j^n, \gamma_j^{n+1}, \dot{\gamma}_j^{n+1})]D_0(h)v_j^{n+1}. \quad (V.27)$$

The shear stress τ_j^{n+1} is evaluated from

$$\tau_j^{n+1} = \psi\{\theta_j^{n+1},\ (\gamma^P)_j^{n+1},\ [D_0(h)v_j^{n+1}]\}. \quad (V.28)$$

Spatial derivatives at the boundaries are approximated by a second order discretization derived by the method of undetermined coefficients. The results are

$$\left.\frac{\partial f}{\partial y}\right|_{y=0} \simeq (-\frac{3}{2}f_0 + 2f_1 - \frac{1}{2}f_2)/h + O(h^2) \quad (V.29)$$

$$\left.\frac{\partial f}{\partial y}\right|_{y=1} \simeq (\frac{3}{2}f_N - 2f_{N-1} + \frac{1}{2}f_{N-2})/h + O(h^2) \quad (V.30)$$

$$\left.\frac{\partial^2 f}{\partial y^2}\right)_{y=0} \simeq (f_0 - 2f_1 + f_2)/h^2 + O(h) \quad (V.31)$$

$$\left.\frac{\partial^2 f}{\partial y^2}\right)_{y=1} \simeq (f_N - 2f_{N-1} + f_{N-2})/h^2 + O(h) \quad (V.32)$$

Since the boundary conditions are prescribed for the velocity $v(y,t)$ and the temperature $\theta(y,t)$, we do not need to use (V.31,32). Therefore the order of accuracy of the scheme (V.25,30) becomes

$$\epsilon = O(h^2,k) \quad \text{i.e.} \quad O(2,1). \tag{V.33}$$

Consistency of the scheme with the original system (V.18) requires that ϵ is at least $O(1,1)$, therefore (V.33) implies consistency as well.

V.2. Stability of the difference scheme

The notion of scheme stability we use is a modification of the Von-Neumann stability criterion [18] discussed by Strang [20] which, for the system (V.18), gives the stability requirement:

$$\frac{k}{h^2} \cdot \left|\text{Max eigenvalue of } A^{yy}\right| \leq \frac{1}{2} .$$

From (V.20) this requirement is

$$\left(\frac{k}{h^2}\right) \max\left\{\frac{S_1(y,t)}{\rho_0}, \frac{k}{\rho_0 c}\right\} \leq \frac{1}{2} .$$

In general, $S_1(y,t) > k/c$ so that the limit on the time step is

$$k \leq \frac{\rho_0 h^2}{2S_1(y,t)} . \tag{V.34}$$

The criterion (V.34) used to bound the time increment k is an approximate one based on freezing the coefficient $S_1(y,t)$ between time levels. We evaluate the right hand side of the inequality at each time level and set

$$k_j^{n+1} = (0.97) \cdot \min_j \left\{ \frac{\rho_0 h^2/2}{(S_1)_j^n} \right\} \tag{V.35}$$

where k_j^{n+1} is the time increment between levels (n) and (n+1).

V.3. Formulation for stress boundary conditions

The analysis of the case where stresses are prescribed at the boundaries is simplified by rewriting the governing equations in a form that allows the solution to be obtained following the same procedures used in the case of velocity boundary conditions. Differentiating the constitutive equation (V.4) with respect to time, one obtains

$$\frac{\partial \tau}{\partial t} = S_1 \frac{\partial^2 \gamma^P}{\partial t^2} + S_2 \frac{\partial \theta}{\partial t} + S_3 \frac{\partial \gamma^P}{\partial t} \tag{V.36}$$

where, S_1, S_2 and S_3 are defined by (V.10,a,b,c). From (V.1) and (V.2) we have

$$\frac{\partial^2 \gamma^P}{\partial t^2} = \frac{1}{\rho_0} \frac{\partial^2 \tau}{\partial y^2} . \tag{V.37}$$

Then, substitution of (V.3), (V.2), and (V.37) into (V.36) gives the following evolutionary equation for the flow stress

$$\frac{\partial \tau}{\partial t} = \frac{S_1}{\rho_0} \frac{\partial^2 \tau}{\partial y^2} + S_2 \left(r_0 \frac{\partial^2 \theta}{\partial y^2} + r_1 \tau \frac{\partial v}{\partial y} \right) + S_3 \frac{\partial v}{\partial y} . \tag{V.38}$$

Introducing the solution vector

$$\underset{\sim}{z} = \begin{Bmatrix} \tau \\ v \\ \gamma^P \\ \theta \end{Bmatrix} \tag{V.39}$$

we can write the governing equations in the form

$$\underset{\sim}{z}_{,t} = B^{y}\underset{\sim}{z}_{,y} + B^{yy}\underset{\sim}{z}_{,yy} \tag{V.40}$$

where

$$B^{y} = \begin{bmatrix} 0 & r_1\tau S_2 + S_3 & 0 & 0 \\ 1/\rho_0 & 0 & 0 & 0 \\ 0 & 1 & 0 & 0 \\ 0 & r_1\tau & 0 & 0 \end{bmatrix} \tag{V.41}$$

and

$$B^{yy} = \begin{bmatrix} S_1/\rho_0 & 0 & 0 & r_0 S_2 \\ 0 & 0 & 0 & 0 \\ 0 & 0 & 0 & 0 \\ 0 & 0 & 0 & r_0 \end{bmatrix}. \tag{V.42}$$

The numerical solution of equation (V.40) is obtained by an explicit finite difference scheme analogous to that described in the previous section. The spatial derivatives are replaced by central differences while time derivatives are replaced by forward differences. The system of evolutionary equations is solved in the order of the components of the vector.

The scheme stability is analogously determined by the requirement

$$\left|\text{Max eigenvalue of } \underset{\sim}{B}^{yy}\right| \frac{k}{h^2} \leq \frac{1}{2}. \tag{V.43}$$

Computational evidence show that scheme stability is ensured by using

$$k = 0.97 \left(\frac{\rho_0 h^2}{2S_1}\right) \qquad (V.44)$$

which is the same step size used for the case of velocity boundary conditions.

V.4. Formulation for the case of geometric inhomogeneity

We seek a finite-difference solution to the general nonlinear system (II.9,12) for the case of a thin-walled tube with a groove in it as shown in Fig. (V.1). The tube is subjected to torsion which, for sufficiently small values of the ratio of wall thickness to tube radius, is a good approximation of simple shear.

Numerical simulation of this problem has been presented by Litonski [15], Costin, et al, [12] and Merzer [13] for the case of quasi-static deformation. They assumed homogeneous deformation conditions in each uniform thickness section of the tube. Merzer [13] included heat conduction.

A complete numerical solution for this problem is presented -- accounting for inertial effects, and without imposing the assumption of deformation homogeneity in uniform thickness regions. The system of governing equations is taken to be (V.1,4). Due to the geometric discontinuity, modifications are required in the initial conditions. In addition, boundary conditions are required at the surface of discontinuity. To obtain these conditions, consider a strip of width 2ϵ at the edge of the groove as shown in Fig. (V.2).

Let '-' and '+' denote evaluations of the various quantities at the left and right hand sides of the edge shown in Fig. (V.2).

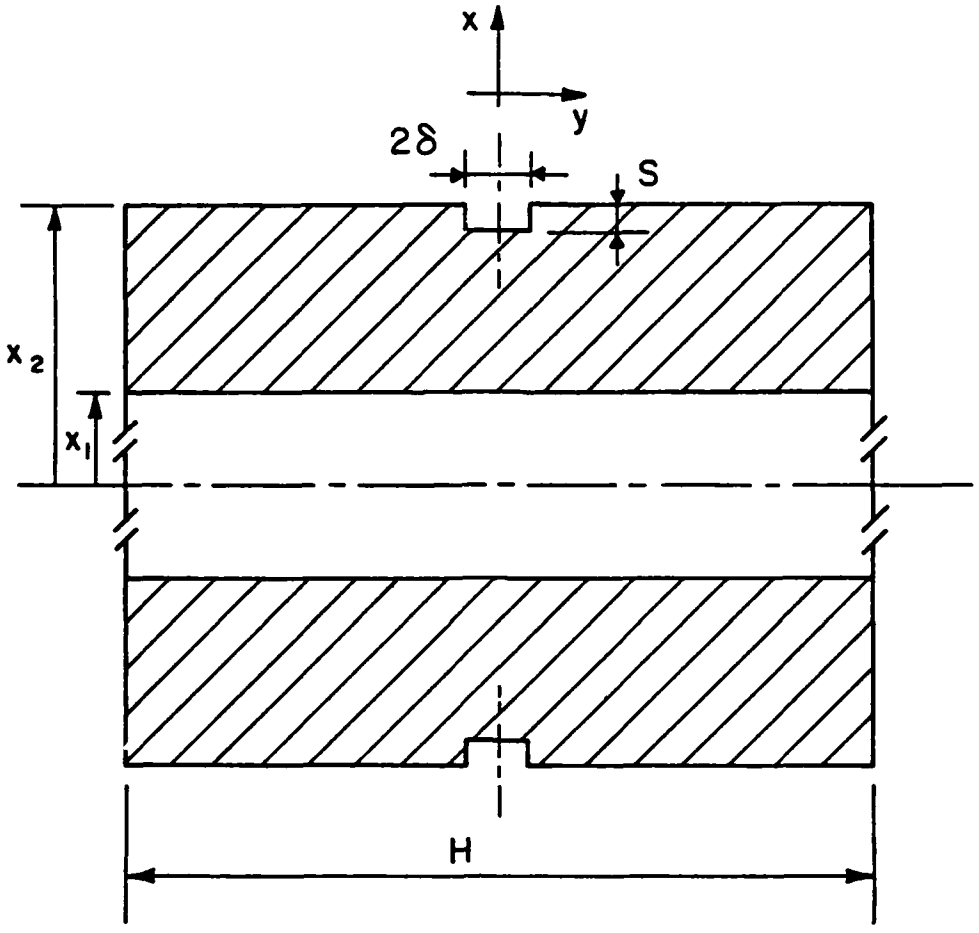

Figure (V.1) - Longitudinal Cross-section in the thin-walled tube with the groove (δ, S)

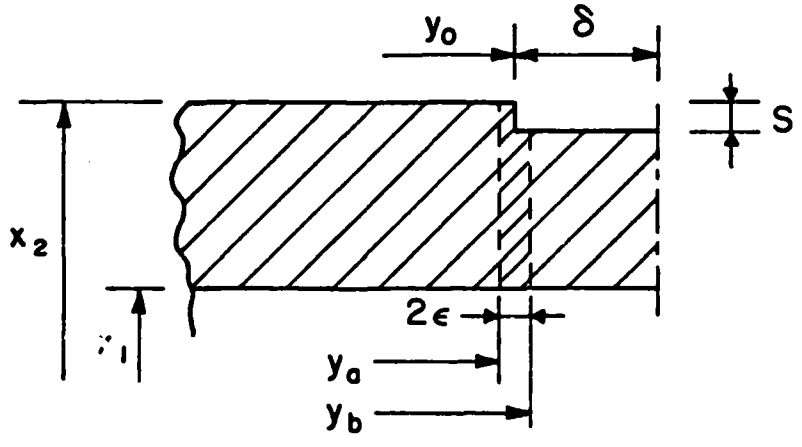

Figure (V.2) - Imaginary strip at the border of the groove.

Continuity of particle velocity, temperature, and shear force (or torque) gives

$$v^- = v^+ \tag{V.45a}$$

$$\theta^- = \theta^+ \tag{V.45b}$$

$$\tau^- = \lambda\tau^+ \; ; \quad \lambda < 1 \tag{V.45c}$$

where $\lambda = A^+/A^-$ is the ratio of the cross-sectional areas.

Consideration of energy flux into the strip of width 2ϵ, and taking the limit as $\epsilon \to 0$ gives the additional relations

$$(\frac{\partial\theta}{\partial y})^- = \lambda(\frac{\partial\theta}{\partial y})^+ . \tag{V.45d}$$

Equations (V.45a-d) are the conditions that are to hold at the interface $y = y_0$.

V.4.a. Finite-difference solution

The symmetry of the problem allows us to consider only the solution in the half $y \in [0,1/2]$. The initial conditions are chosen such that the system of governing equations (V.1-4) and the continuity requirements (V.45) are met. Plastic strain and temperature are taken to be homogeneous. Plastic strain rate $\dot{\gamma}^P$ is assumed to jump at the interface in order to give the required jump in the flow stress. The overall strain rate is maintained constant.

The difference method is the same as described in section V.1, except for the treatment of the geometric discontinuity at $y = y_0$. Discretization at nodes j^+ and j^- (see Fig. (V.3)) is performed by replacing the spatial derivative $\partial/\partial y$ by forward and backward

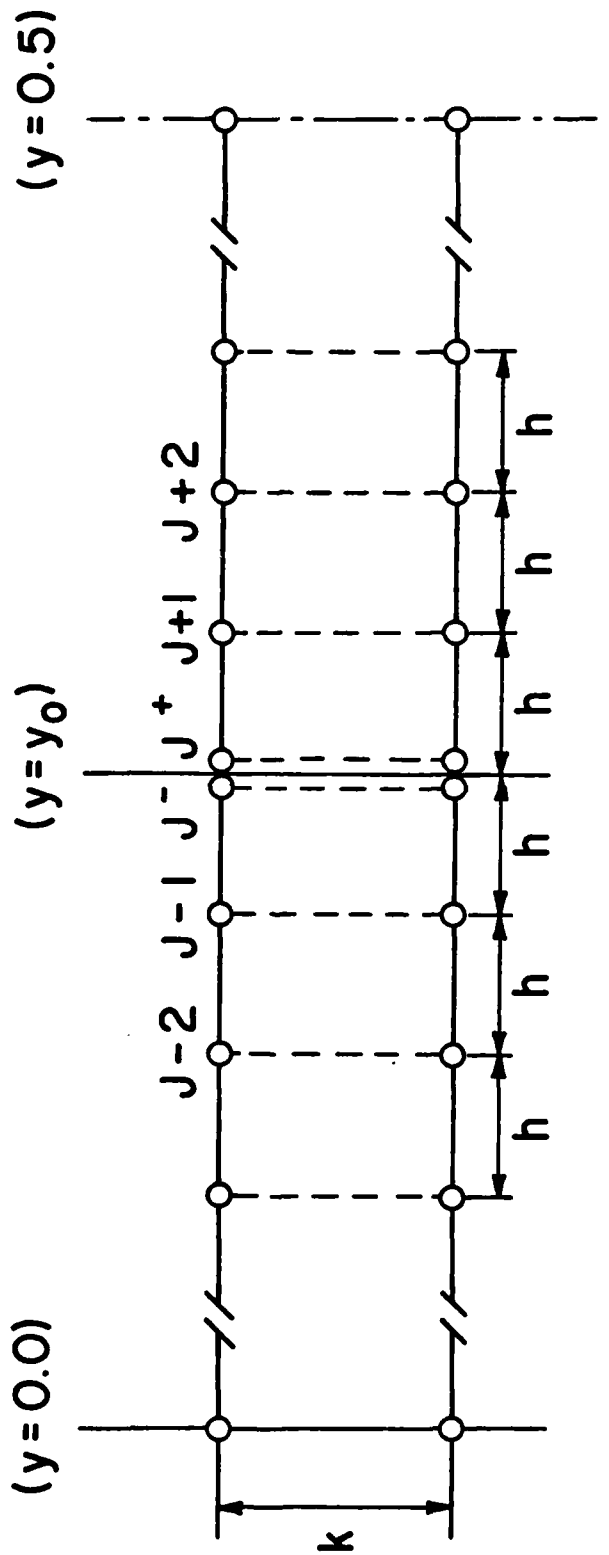

Figure (V.3) - Two levels of the Computational grid

differences analogous to (V.29) and (V.30). The velocity at level $n + 1$ is obtained by proceeding from the boundary $y = 0$ at which $v(0,t) = 0$ to the nodal point $j - 1$ using equation (V.25) and similarly proceeding from the boundary $y = \frac{1}{2}$ at which $v(\frac{1}{2},t) = \frac{1}{2}$ to the nodal point $j + 1$. In order to evaluate (v_j^{n+1}) we use the jump relations (V.45b) and (V.45c) and the constitutive equation (V.4)

$$\lambda \cdot \psi(\theta_j, \gamma^P_{j^+}, \frac{\partial v^+}{\partial y}) = \psi(\theta_j, \gamma^P_{j^-}, \frac{\partial v^-}{\partial y}) \qquad (V.46)$$

where all quantities are to be evaluated at the level $n + 1$. The velocity gradients in (V.46) are approximated by the one-sided expressions (V.29), (V.30). With the continuity of the velocity field at $y = y_0$, equation (V.46) becomes an equation for the velocity at the interface v_j^{n+1}. This equation is solved by either taking θ_j and $\gamma^P_{j^+}, \gamma^P_{j^-}$ to be the values at the level n or by an iterative procedure in which the values of $\theta_j, \gamma^P_{j^+}, \gamma^P_{j^-}$ are updated as they are obtained from (V.26) and (V.27), with centered differences replaced by one-sided differences.

The temperature is evaluated by means of equation (V.27) for all nodal points except the nodes j^+, j^- at the interface. The temperature at these nodes is obtained from (V.45b) and (V.45d), using one-sided difference operators. Finally, the flow stress is obtained from equation (V.28).

V.5. Numerical results

The numerical solution to the fully nonlinear system (V.1-V.4) is presented for a number of constitutive equations modelling the response

of visco-plastic materials. Initial imperfections of the homogeneous solution are taken as a periodic temperature perturbation or as a permanent geometric defect (cf. V.4). Numerical results are presented for both velocity as well as traction boundary conditions. The dynamic problem is considered for all models discussed. An essential objective is to compare numerical results with linear analysis predictions (Chapter IV) in order to determine the usefulness of these predictions.

A. Velocity boundary conditions

We present herein numerical results for the case where velocities are prescribed at the boundaries as given by conditions (V.7).

A.1 Initial temperature perturbation

The initial imperfection is taken here as a periodic fluctuation in the specimen temperature. This imperfection is considered to be weaker than the geometric defect described in (V.4). This is due to the transient nature of such defects in contrast to the permanent effect of the existence of a groove.

A.1.a Power law

Consider the constitutive equation

$$\tau = (\theta)^{\nu}(\gamma^{p})^{m}(\dot{\gamma}^{p})^{n} \qquad (V.47)$$

where

ν = thermal softening (hardening) exponent

m = strain hardening exponent

n = strain-rate exponent

A series of numerical solutions has been obtained for n=1 and for different values of ν and m in order to study the relative effects of thermal softening and strain-hardening. Most visco-plastic materials exhibit

strain-hardening and thermal softening. Under such circumstances, it is believed that at high strain rates deformation instability occurs as soon as the net hardening rate $\left.\frac{d\tau}{dt}\right\}_A$ vanishes, where 'A' refers to an adiabatic deformation.

From the numerical solutions it appears that the vanishing of the adiabatic hardening rate is not sufficient to ensure the onset of localization. Indeed, the numerical solution for n=1 shows remarkably stable deformation even when the slope of the isothermal stress-strain curve becomes negative.

Numerical results have been obtained for the following values of the model parameters corresponding to an aluminum alloy.

Thermal properties

k ($Wm^{-1}{}^{\circ}C^{-1}$)	ρ_0 (kg/m^3)	C ($Jkg^{-1}{}^{\circ}C^{-1}$)
222	2700	903

The overall strain rates considered are in the range $[10^3 s^{-1} - 10^6 s^{-1}]$.

The initial homogeneous strain is taken as $\gamma_0 = 0.01$, while the perturbation in the initial temperature distribution is chosen as

$$\theta_p(y) = \epsilon \sin[2\pi(\frac{1}{4} - y)] \qquad (V.48)$$

where $\epsilon = 0.005$ or $\epsilon = 0.05$. The dimensional value of the homogeneous (unperturbed) initial temperature distribution is $\hat{\theta}_0 = 300°K$. The slab thickness is $\hat{H} = 0.01\,m$. The homogeneous initial value of the flow stress is taken as $\hat{\tau}_0 = 10^8\,Pa$.

The dimensionless spatial step size is chosen as $\Delta y = 1/40$, while the temporal step size is monitored throughout the calculation to meet the stability requirement (V.35).

Numerical solutions for the power law (V.47) with $m > 0$, $\nu < 0$, and $n = 1$ show a slight departure from the homogeneous solution at small strains $\gamma^P \leq 0.05$. Then, the deviation from the homogeneous solution reaches an upper bound at which the inhomogeneous solution retracts back towards the homogeneous solution, but at much slower rate, Figure (V.4). For the material considered, the rate of temperature rise is slow, with only a 1 percent temperature rise for a 5 percent plastic strain increment. The stabilizing effect of thermal diffusion seems to be almost negligible in the deformation considered, Figure (V.6). An increase in the amplitude of the initial inhomogeneity to $\epsilon = 0.05$ causes a proportionate increase in the excursion from the homogeneous solution, but it does not change the qualitative features of the solution, i.e. an envelope is attained and the deformation remains stable.

Finite-difference solutions have also been obtained for cases with $-1 < m < 0$ and $\nu < 0$ for which elementary linear stability analysis (e.g.[11]) allows the possibility of exponential growth. For cases of thermal softening and strain softening with $n = 1$, the flow stress decreases monotonically as the solution evolves while the numerical solution continues to become more inhomogeneous as time increases; however, the time scale on which significant departure from the homogeneous solution occurs is extremely long -- apparently too long for the localization to correspond to the shear band development observed in experiments. A typical situation is illustrated in Figure (V.5) which corresponds to $\nu = -0.75$,

$m = -0.95$ and $n = 1$ at a dynamic global strain rate of $(10^4)s^{-1}$. Clearly, the profiles at later times are getting closer to each other. This appears to be due to a decrease in the plastic working as a result of the rate of decreasing stress values. It appears that the solutions for $(m < 0)$ tend asymptotically to the limiting situation of a localized deformation. However, if we confine ourselves to strain amplitudes that are commonly obtained in the plastic deformation of real materials, we reach the conclusion that the deformation described by the model (V-47) is remarkably stable for $n = 1$.

The accuracy of the finite difference code has been examined by calculating a solution for a special case ($\nu = m = 0$, $n = 1$) for which an exact solution is available. Close agreement with the exact solution was obtained.

A.1.b Arrhenius law

Consider the constitutive equation

$$\tau = \tau_B(\gamma^P) - \left(\frac{K_b\theta}{W}\right) \ell n\left(\frac{\omega}{\dot{\gamma}^P}\right) \qquad (V.49)$$

discussed in Chapter III.

Numerical results have been obtained for the same Aluminum alloy as in A. Other constants required in (V.49) are

$$\left.\begin{aligned} \omega &= 10^{12} s^{-1} \\ K_b &= 1.38 \times 10^{-23} J/°K \\ W &= 0.5 \times 10^{-26} m^3 \end{aligned}\right\} \qquad (V.50)$$

while the strain hardening function has the form

$$\tau_B(\gamma^P) = \tau_B(0) \cdot [1 + b(1 - e^{-c\gamma^P})] \qquad (V.51)$$

where

$$\tau_B^{(0)} = 10^8 \text{ Pa}$$

$$b = 0.5$$

$$c = 4.0.$$

We also introduce the following additional dimensionless quantities (cf. [14])

$$\left.\begin{aligned} \omega = \frac{\hat{\omega}}{\dot{\hat{\gamma}}_0^P}, \quad \tau_B(\gamma^P) &= \frac{\hat{\tau}_B(\hat{\gamma}^P)}{\hat{\tau}_0} \\ \frac{W}{K_b} &= \frac{\hat{\tau}_0 \hat{W}}{\hat{K}_b \hat{\theta}_0} \end{aligned}\right\}. \qquad (V.52)$$

Numerical results obtained for this deformation are shown in Fig. (V.8). The qualitative nature of the deformation behavior is similar to model (A.1.a) for $m < 0$ and $\nu < 0$, in the sense that the solution has a tendency to become more inhomogeneous as time increases, however, the deviation from the homogeneous solution again occurs very slowly. The deformation governed by the Arrhenius law remains contained even when the point of maximum stress is reached, which appears to be strong evidence for stability. In this sense the numerical results appear to be consistent with the predictions of the linear stability analysis by Clifton et al. [14].

The numerical result shown in Fig. (V.8) is obtained using the hardening function given by

$$\tau_B(\gamma^P) = \left(\frac{f_1 - f_0}{\gamma^*}\right) \cdot \gamma^P + f_0 \,, \qquad \text{for } \gamma^P \leq \gamma^*$$
$$= f_1 \,, \qquad \text{for } \gamma^P > \gamma^* \tag{V.53}$$

where the dimensional values of the parameters are

$$\left.\begin{aligned} f_0 = 10^8 \text{ pa} \,, \quad f_1 = 1.5 \times 10^8 \text{ pa} \\ \text{and} \\ \gamma^* = 0.15 \end{aligned}\right\} \tag{V.54}$$

A.1.c Bodner-Merzer law

Consider the constitutive equation

$$\tau = \frac{\tau_1(W^P)}{\sqrt{3}} [f(\eta)]^{c(\theta)} \tag{V.55}$$

defined in (IV.5.3). Numerical values for the material constants are taken to be the same values given by Merzer [13]. Non-uniformity of the strain-rate along the length of the specimen continues to increase as the deformation proceeds. For $\varepsilon = 0.05$ the deformation becomes strongly localized. Computed profiles for $\varepsilon = 0.005$ are shown in Figs. (V.9.a-d).

The instability obtained for the model (V.55) can be attributed to two main reasons:

1) The strong thermal softening that overcomes strain hardening throughout the deformation process, see Fig. (V.9.c);
2) The extreme sensitivity to temperature which has been discussed in (IV.5.3).

The instability reported by Merzer [13] for this model - in the case of a geometric imperfection - has been ascribed to the "persistency" of the geometric defect; however in view of the unstable response

of this model to a "transient" temperature perturbation it is evident that the details of the constitutive model as well as the nature and magnitude of the initial imperfection play important roles in the localization process.

A.2 Geometric imperfection

We consider numerical results for the problem described in (IV.4) in which a permanent groove is introduced in a thin-walled tube, Fig. (V.1). The groove is characterized by

$$\lambda = 1.04 \quad \text{and} \quad \delta = 0.1.$$

A.2.a Power law

The computed profiles for the model (V.47) are shown in Figs. (V.10.a-d) and (V.11.a-d). Clearly, for n = 1 the power law - again - gives strongly stable response in spite of the initial jump in the strain rate, Fig. (V.10.d). The difference between temperature levels inside and outside the groove remains less than one percent up to total strains of 40 percent, Figure (V.10.b).

For the case of $m > 0$; the stress rises monotonically while it decreases monotonically for $m < 0$, Figures (V.10.c), (V.11.c) respectively. The maximum rise of the strain rate from its initial value (inside the groove) is less than one percent which is strong evidence of the stability obtained for the power law given by (V.47), with n = 1.

The effect of strain-rate hardening on the response for the power law given by (V.47) is examined by choosing the parameters ν, m and n to correspond to two steels, namely a cold-rolled steel (CRS-1018) and a hot-rolled steel (HRS-1020). Experimental investigations [19] showed that deformation localizes into shear bands in the CRS whereas the HRS showed a stable response.

Numerical values for the parameters used in this computation are

CRS-1018	HRS-1020
ν = -0.38	ν = -0.51
m = +0.015	m = +0.12
n = +0.019	n = +0.0133
$\hat{\tau}_o$ = 436 MPa	$\hat{\tau}_o$ = 261 MPa

Thermal Properties:

k $Wm^{-1}\,{}^{o}C^{-1}$	ρ_o kg/m^3	C $Jkg^{-1}\,{}^{o}C^{-1}$
54	7800	500

The length of the specimen is taken as 2.5 mm and a dynamic global strain rate of $10^3\ s^{-1}$ is considered. The groove characteristics are

$$\lambda = 1.02 \text{ and } \delta = 0.05$$

The results of this calculation are shown in Figures (V.12.a-f) and (V.13.a-f) for the HRS and the CRS respectively. The solutions indicate remarkably distinct behavior for the two steels considered. The strong hardening rate exhibited by the HRS seems to stabilize the deformation, whereas the deformation of the CRS localizes inside the groove as soon as thermal softening overcomes strain and strain-rate

hardening. Furthermore, for the CRS the shape of the profiles inside the groove indicates a strong localization process. These results are - qualitatively - in agreement with experimental observations in [19]. The instability observed for the CRS with $n << 1$ and the stability shown in Figures (V.11) for $n = 1$ are consistent with the predictions of the linear stability analysis (cf. (IV.32)) which allows large growth rates for small values of n.

A.2.b Arrhenius law

The response for the case of the Arrhenius law (V.49) with a geometric defect is presented in Figs. (V.14.a-d), (V.15.a-d) and (V.16.a-d).

The computed profiles show a wave-like solution at early times ($\gamma^P \lesssim 0.25$). This feature is attributed to the strength of the strain hardening coefficient S_3 relative to the viscosity coefficient S_1 at early times. For $S_1 << S_3$, the momentum equation (V.14) can be written as

$$\rho_o \frac{\partial v}{\partial t} = S_2 \frac{\partial \theta}{\partial y} + S_3 \frac{\partial \gamma^P}{\partial y} . \qquad (V.56)$$

Moreover, if heat diffusion is neglected due to its small influence, we can set

$$\frac{\partial \theta}{\partial t} = r_1 \tau \phi . \qquad (V.57)$$

Using the compatability equation (V.15) to eliminate (v), we find

$$\frac{\partial^2 \gamma^P}{\partial t^2} = \left(\frac{S_3}{\rho_o}\right) \frac{\partial^2 \gamma^P}{\partial y^2} + \left(\frac{S_2}{\rho_o}\right) \frac{\partial^2 \theta}{\partial y^2} + \text{"L.O.D."} \qquad (V.58)$$

where "L.O.D." stands for "lower order derivatives". Differentiating (V.58) w.r.t. time, we get the following wave equation for the plastic strain rate

$$\frac{\partial^2 \phi}{\partial t^2} = \left[\frac{1}{\rho_o} (S_3 + r_1 \tau S_2)\right] \frac{\partial^2 \phi}{\partial y 2} + \text{L.O.D.} \qquad \text{(V.59)}$$

Observing that $S_2 < 0$ for the thermal softening features of the Arrhenius law, we can see that at early times when S_1 can be neglected with respect to S_3, a wave-like response is obtained when the strain hardening ($S_3 > 0$) dominates the thermal softening ($S_2 < 0$). This analysis is supported by the numerical results shown in Fig. (V.16.a-d) where no hardening is considered and the wave-like early response is totally eliminated.

Consideration of the late time response for the case of the Arrhenius law, suggests that the existence of a permanent groove in the specimen contributes to an instability. This can be seen by noting the large temperature increase inside the groove relative to that outside it, as well as the increase of strain rates inside the groove and their decrease outside the groove. In spite of these instability features we regard this response as essentially stable for practical purposes. That is, although the deformation begins with strain rates inside the groove which are 4.5 times larger than those outside, the final strain rates at $\gamma^P = 1.0$ are only 6 times larger than those outside the groove. Therefore the observed instability is very weak even with a substantial initial jump and with continuation of the deformation to large strains. We prefer to reserve the term instability for cases analogous to reported experimental

results on shear bands in which the strains within the bands are much larger than in neighboring regions.

The results shown in Figure (V.15.a-d) are obtained for a shallower groove, $\lambda = 1.004$, the difference between temperature levels in and out of the groove is less pronounced. Moreover the difference between strain rates is less than that obtained for $\lambda = 1.04$, and the strain rate inside the groove at $\gamma^P = 1.0$ remains well below the value at $\gamma^P = 0.0$.

The results obtained for the non-hardening idealization are presented in Figure (V.16.a-d). Wave-like early response is completely eliminated upon removal of the strain hardening. At late times the differences in strain rate are comparable to those obtained when strain hardening was included. This result is consistent with regarding the response as stable for the case of the Arrhenius law, since even for such strongly destabilizing conditions as a groove and no strain-hardening the deformation does not become much more non-uniform at late times than it is initially. Computational experiments performed for the Arrhenius law revealed negligible sensitivity of the results to heat conduction.

A.2.c Bodner-Merzer model

Numerical results for the model (V.55) have been reported by Merzer [13] for a specimen with a groove. Our results for the same problem are shown in Figs. (V.17.a-d). In order to improve the accuracy of the solution near the groove a finer mesh is used than in [13] and jumps across the groove boundaries are accounted for ex-

plicitly. A two-level, explicit, Du-Fort and Frankel algorithm is used. Details of the numerical method are given in Appendix II.

The qualitative features of the solution are the same as those obtained by Merzer [13]; however, the temperature and strain rate amplitudes inside the groove are higher than reported values [13]. This difference is believed to be a consequence of numerical errors caused by the use of a coarse computational mesh in [13].

The response obtained for this model is quite strongly unstable relative to other examples considered herein. One factor contributing to this instability is the relatively weak strain hardening, for which the material begins softening immediately, see Fig. (IV.17.c). Another is the fact that the strain rate can increase indefinitely without increase in stress as the temperature $\tilde{\theta} = 1.72$ is approached (cf. IV.46.b).

B. Stress boundary conditions

Numerical results are presented in this section for the case of simple shear of a uniform slab subjected to the stress boundary conditions

$$\tau(0,t) = \tau(1,t) = \tau(0, 0) = \tau(1, 0) \qquad (V.60)$$

The constitutive equation is taken to be the power law (V.47) with $n = 1$. An initial temperature perturbation (V.48) is considered, with $\varepsilon = 0.005$. Two cases are considered as being representative of the response of materials that can be modelled by (V.47); the first is for $\nu = -0.75$ and $m = +0.1$ while the second is for the same ν but with $m = -0.95$.

The behavior for $m > 0$ is remarkably stable. The deformation tends to become more homogeneous with increasing time, see Fig. (IV.18.a). This stable response results even when the point of maximum load is passed, i.e. for $\gamma^P > 0.025$. On the other hand, the response for $m < 0$ is remarkably unstable. Shear bands form at the two boundaries where strain rates are 24 times higher than their initial values (see Fig. (V.19.d)). Moreover this intense shearing occurs at relatively small strains ($\gamma^P = 0.05$), indicating a strong bifurcation process. As a result of thermal softening and strain softening, the flow stress decreases monotonically except at $y = 0$ and $y = 1$. Sustaining high stress levels at the boundaries leads to the softening of the material there and to the resulting shear strain localization.

A similar qualitative response is observed for the Arrhenius law given by (V.49) with no hardening. The deformation tends to become more inhomogeneous as time grows; however, the speed of deformation is slower than that obtained for the power law, see Figures (V.20.a-d). Strain rates are only (1.5) times their initial values at 50% of plastic straining. This slow localization can be explained by the weak thermal softening exhibited by the Arrhenius law as well as the absence of the isothermal strain-softening, see Figure (V.20.c).

The response for the Bodner-Merzer constitutive model is - again - qualitatively similar to earlier results; however, the rate of heat generation is much higher as compared to the power law or the Arrhenius law, see Figure (V.21.b). The limit (IV.46.b) imposed on temperature by the constitutive law (V.35) is reached at the specimen boundaries for total plastic strain of approximately (35) percent.

The remarkable feature of the solution of the simple shear problem with traction-controlled boundaries is that the same response is obtained whether or not the initial solution is perturbed. In other words, the solution of an unperturbed dynamic problem with stress boundary conditions becomes immediately inhomogeneous as deformation proceeds. The evolution of inhomogeneous deformation seems to be a consequence of the imposed stresses at the boundaries, since holding stresses to be constant there while allowing stress to decrease in the interior creates sharp stress gradients in the vicinity of specimen boundaries; as a result, strain rates become large - forming regions of localized deformation. This feature of the problem with stress boundary conditions is discussed further in Appendix (III).

V.6 Concluding remarks

For velocity boundary conditions, simple shearing deformations are remarkably stable for the three constitutive equations considered except for the Bodner-Merzer model and the power law with $n \ll 1$. The localization observed for the Bodner-Merzer model appears to be due to a non-physical degeneracy of the model at finite temperatures that may be reached during adiabatic experiments. The localization observed for the CRS with $n \ll 1$ is viewed as indicative of the effects of thermal softening, weak strain hardening and weak strain rate sensitivity in obtaining significant strain localization at moderate strains. Although a persistent geometric defect, such as a groove, appears to be slightly more destabilizing than an initial perturbation in, for example, temperature, the essential conclusions regarding the stability of simple shearing deformations do

not appear to be changed substantially by the type of inhomogeneity. However, the strength of the inhomogeneity plays a significant role.

For stress boundary conditions it appears that simple shearing deformations are much less stable. For a power law model with isothermal strain softening, localized deformations occur at relatively small strains.

Acknowledgements

This research has been supported by the U.S. Army Research Office under Grant DAAG 29-81-K-0121/3 with Brown University. The computations reported here were carried out on the Brown University, Division of Engineering VAX-11/780 computer. The acquisition of this computer was made possible by grants from the U.S. National Science Foundation, the General Electric Foundation and the Digital Equipment Corporation.

Helpful collaboration with Alain Molinari in the early stages of this investigation is gratefully acknowledged. Discussions with Jacques Duffy and Kathy Hartley on modelling the experiments for HRS-1020 and CRS-1018 are appreciated.

References:

1. Culver, R.S., "Thermal Instability Strain in Dynamic Plastic Deformation," in (Metallurgical Effects at High Strain Rates), R.W. Rohde, B.M. Butcher, J.R. Holland and C.H. Karnes, Eds. Plenum Press, N.Y., 1973, p. 519.

2. Zener, C., Holloman, J.H., "Effect of Strain Rate Upon Plastic Flow of Steel," 1944, J. Appl. Phys. 15, pp. 22-32.

3. Rogers, H.C., "Adiabatic Shearing - A Review," 1974, Drexel University Report.

4. Argon, A.S., 1973, "Stability of Plastic Deformation," Chapt. 7, in "The Inhomogeneity of Plastic Deformation," ASM, Metals Park, OH.

5. Asaro, R.J., "Micromechanics of Crystals and Polycrystals," 1983, in "Advances in Applied Mechanics," Volume 23, pp. 1-115.

6. Wright, P.K., "Metallurgical Effects at High Strain Rates in the Secondary Shear Zone of the Machining Operation," see Ref. 1, p. 531.

7. Moss, G.L., "Shear Strains, Strain Rates and Temperature Changes in Adiabatic Shear Bands," In "Shock Waves and High-Strain-Rate Phenomena in Metals," Plenum Press, Chapt. 19, 1981.

8. Bai, Y.L., "Thermo-Plastic Instability in Simple Shear," J. Mech. Physics of Solids, 1982, pp. 195-207.

9. Bai, Y.L., "A Criterion for Thermo-Plastic Shear Instability," 1981, Chapt. 14, in "Shock Waves and High Strain-Rate Phenomena in Metals," Plenum Press.

10. Burns, T.J., Trucano, T.G., "Instability in Simple Shear Deformation of Stress-Softening Materials," 1982, Sandia National Laboratories, SAND 82-0004; and

    Burns, T.J., "Approximate Linear Stability Analysis of a Model of Adiabatic Shear Band Formation," 1983, Sandia National Laboratories, SAND 83-1907.

11. Clifton, R.J., "Adiabatic Shear," 1978, A Report for the NCR Committee on Material Response to Ultra-High Loading Rates, National Materials Advisory Board Committee, Rep. No. NMAB-356.

12. Costin, L.S., Crisman, E.E., Hawley, R.H., Duffy, J., "On the Localization of Plastic Flow in Mild Steel Tubes Under Dynamic Torsional Loading," Brown University Report No. NSF 18532/7, 1979.

13. Merzer, A.M., "Modelling of Adiabatic Shear Band Development from Small Imperfections," 1982, J. Mech. Phys. Solids, 30, No. 5, pp. 323-338.

14. Clifton, R.J., Molinari, A., Shawki, T.G., "On the Stability of Simple Shearing of Thermal Visco-Plastic Materials," unpublished manuscript.

15. Litonski, J., "Plastic flow of a tube under adiabatic torsion", Bulletin De L'academie, Polonaise des sciences, Vol. XXV, No. 1, 1977.

16. Coddington, E. A., Levinson, N., "Theory of ordinary differential equations", 1955, McGraw-Hill, Inc.

17. Conte, de Boor, "Elementary Numerical Analysis", McGraw-Hill, Inc., second edition, 1972.

18. Kreiss, H. O., Oliger, J., "Methods for the approximate solution of time dependent problems", WMO-ICSV Joint Organizing Committee, No. 10, 1976.

19. Hartley, K. A., "Incremental strain rate and incremental temperature experiments and the development of Constitutive Laws for BCC metals", Sc.M. Thesis, Brown University, 1983.

20. Richtmyer, R.D. and Morton, K.W., "Difference methods for initial-value problems," John Wiley and Sons, 1967.

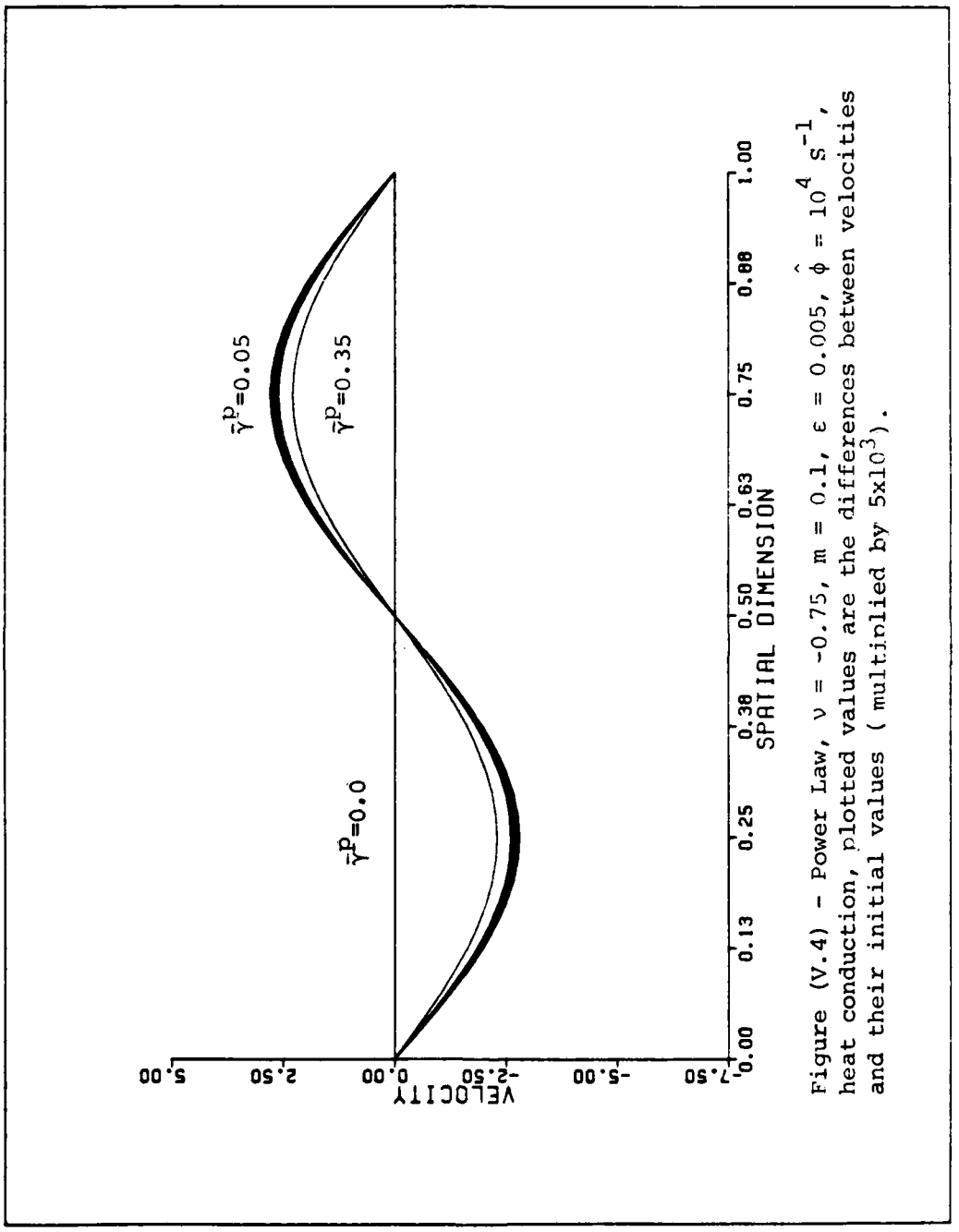

Figure (V.4) - Power Law, $\nu = -0.75$, $m = 0.1$, $\varepsilon = 0.005$, $\hat{\phi} = 10^4\ s^{-1}$, heat conduction, plotted values are the differences between velocities and their initial values (multiplied by $5x10^3$).

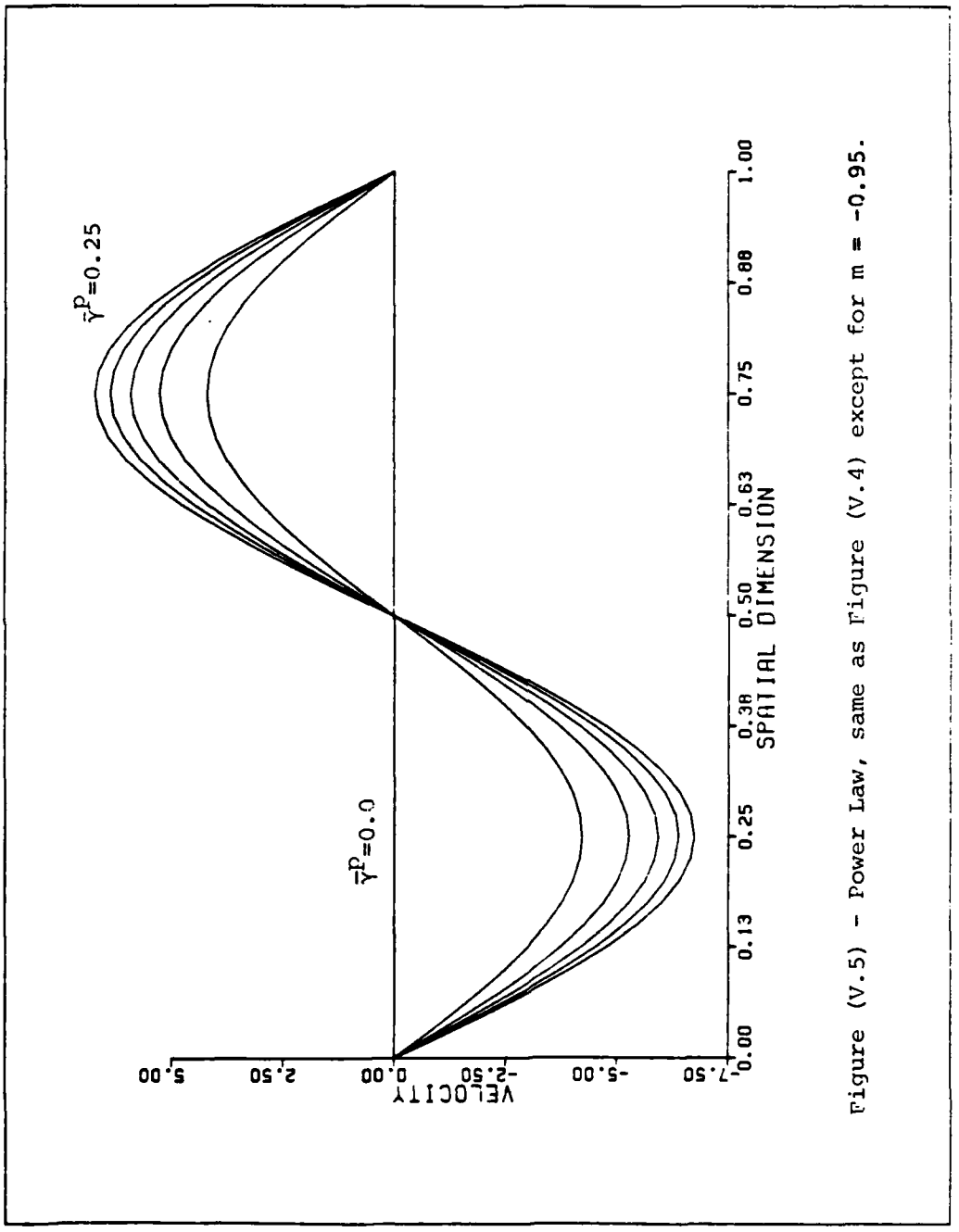

Figure (V.5) - Power Law, same as Figure (V.4) except for m = -0.95.

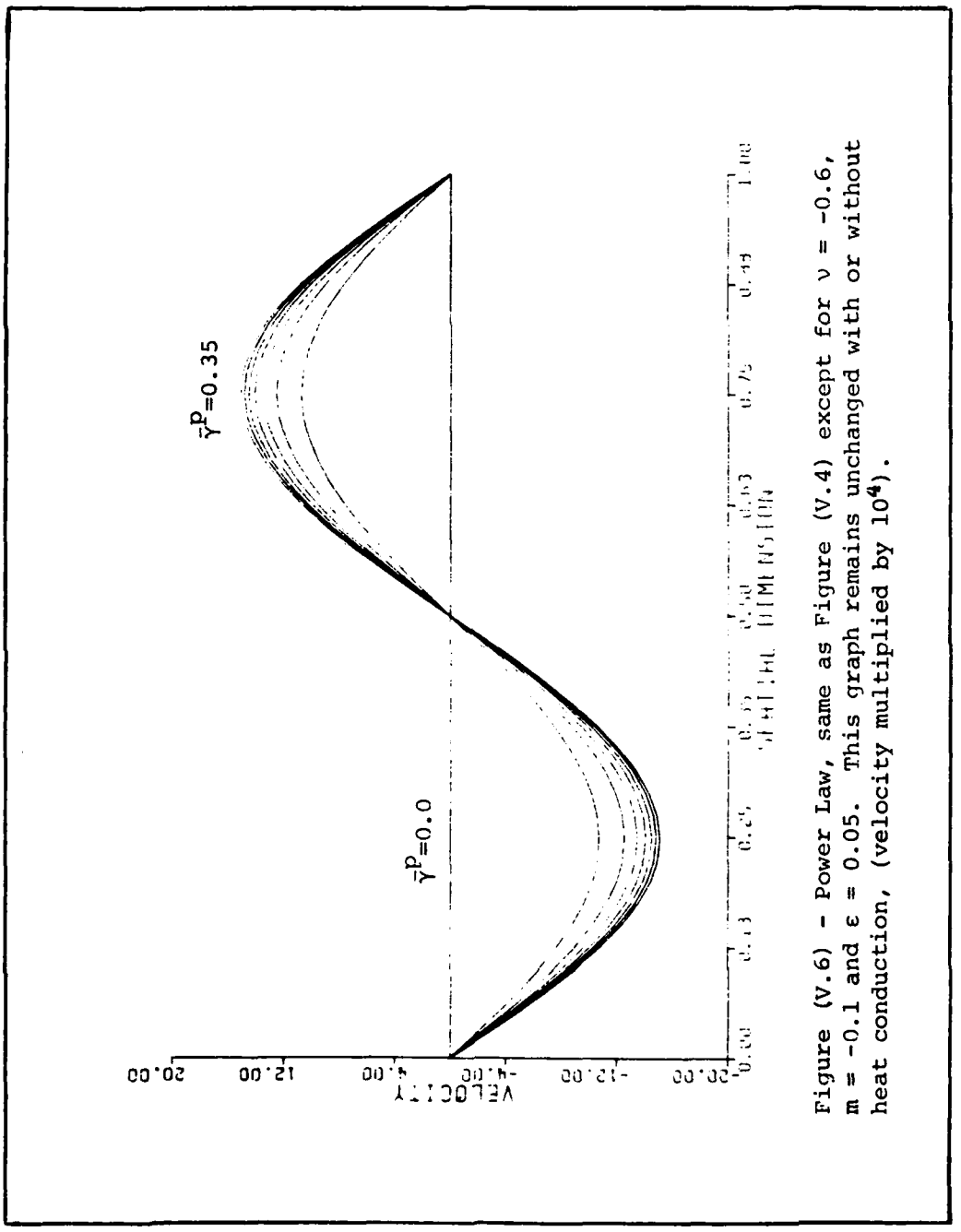

Figure (V.6) - Power Law, same as Figure (V.4) except for $\nu = -0.6$, $m = -0.1$ and $\varepsilon = 0.05$. This graph remains unchanged with or without heat conduction, (velocity multiplied by 10^4).

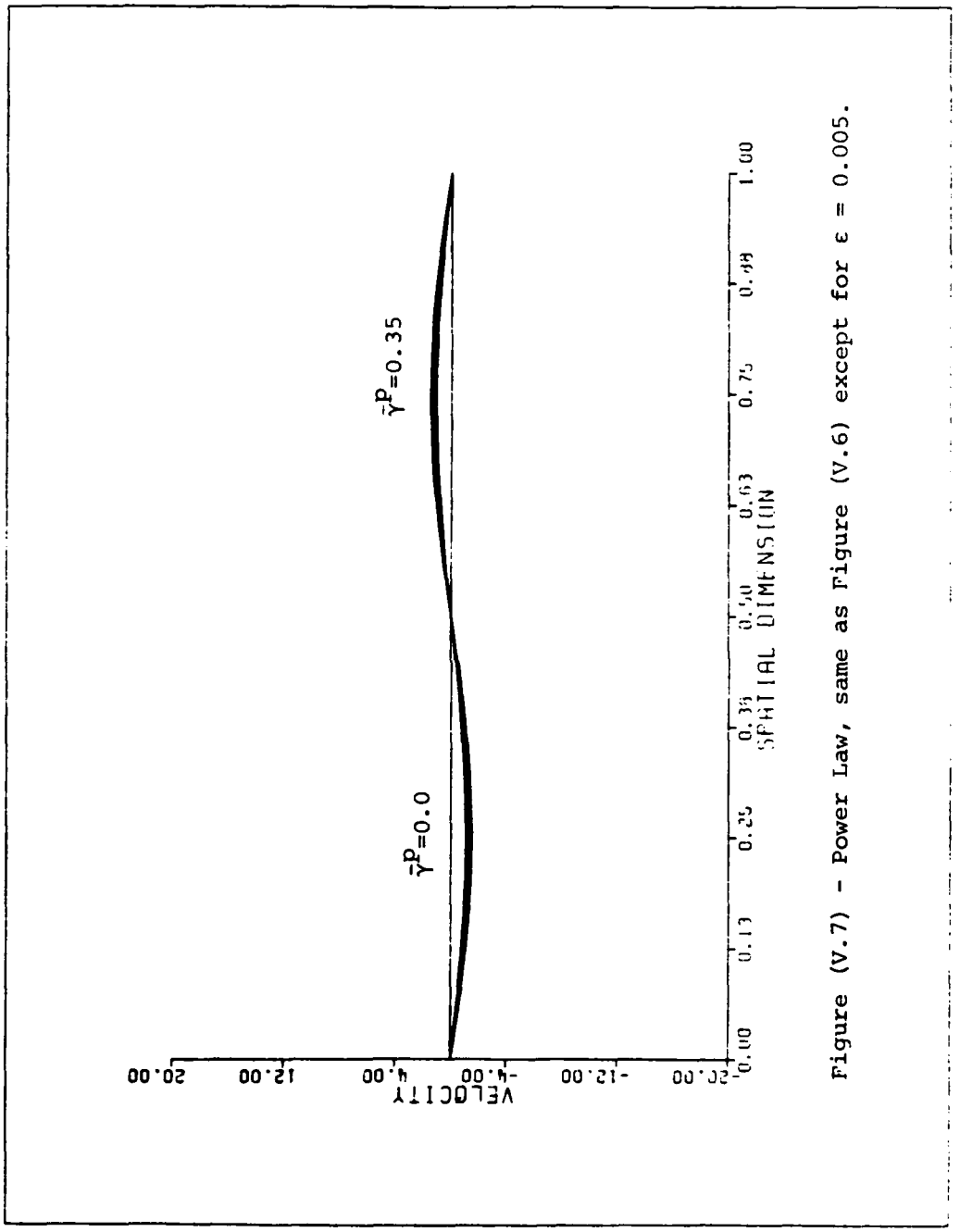

Figure (V.7) - Power Law, same as Figure (V.6) except for ϵ = 0.005.

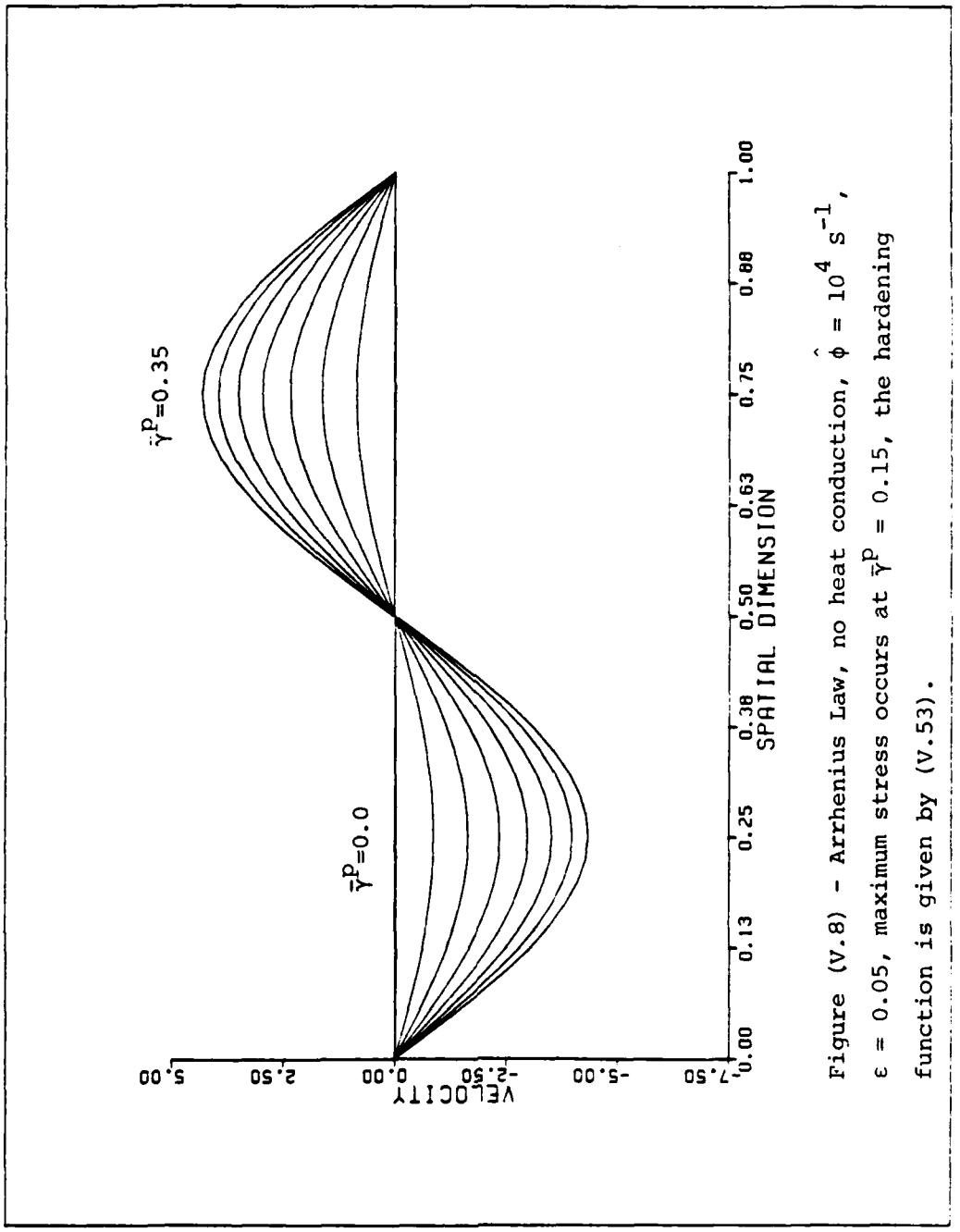

Figure (V.8) - Arrhenius Law, no heat conduction, $\hat{\phi} = 10^4\ s^{-1}$, $\varepsilon = 0.05$, maximum stress occurs at $\bar{\gamma}^p = 0.15$, the hardening function is given by (V.53).

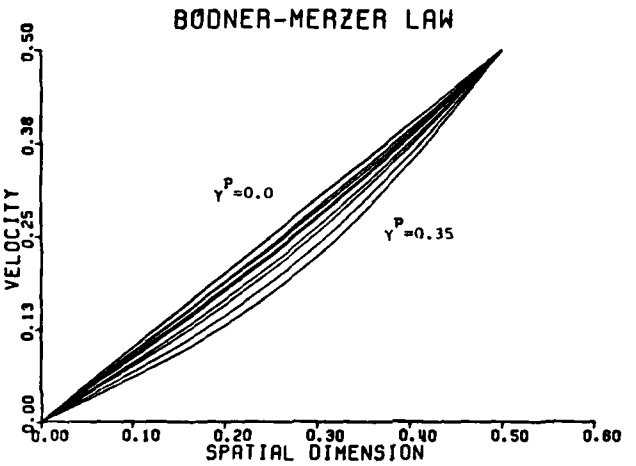

Figure (V.9.a) - Initial temperature perturbation, same parameters as in Merzer's Calculation, ϵ=0.005, profiles are obtained for intervals of (γ^P=0.05).

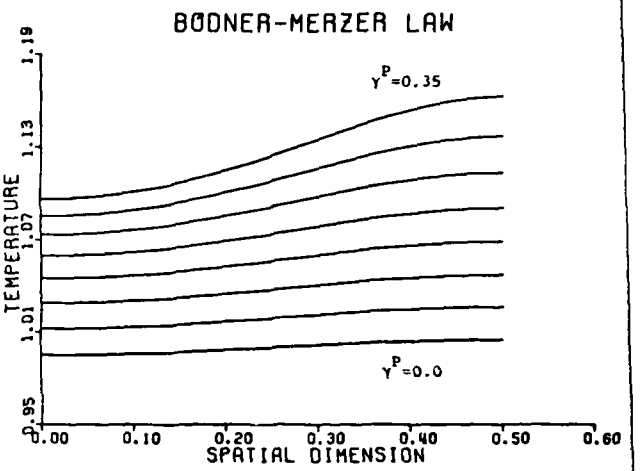

Figure (V.9.b) - Temperature profiles for the problem defined in Fig. (V.9.a).

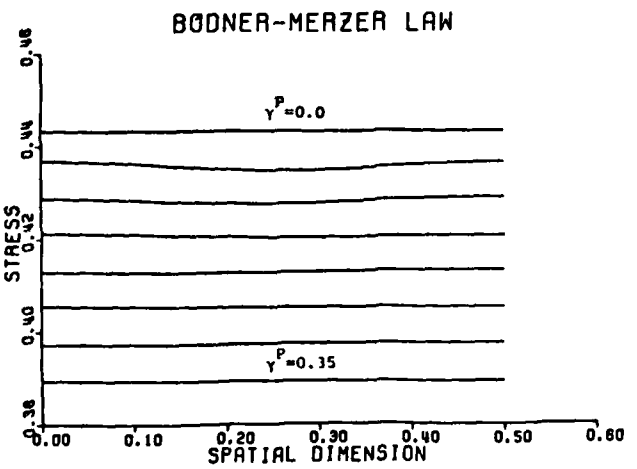

Figure (V.9.C) - stress profiles for the problem defined in Fig. (V.9.a).

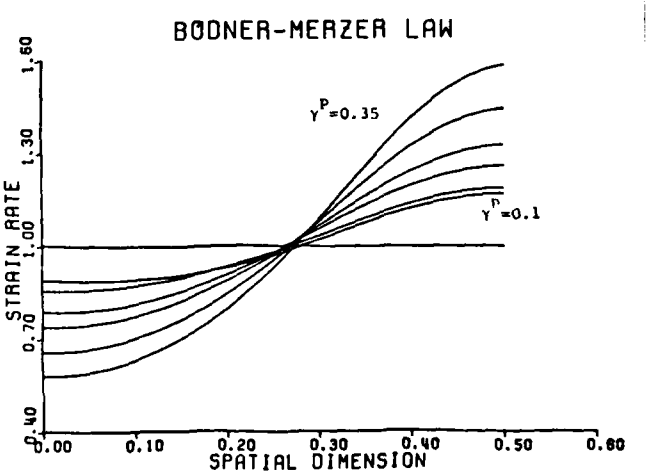

Figure (V.9.d) - strain rate profiles for the problem defined in Fig. (V.9.a).

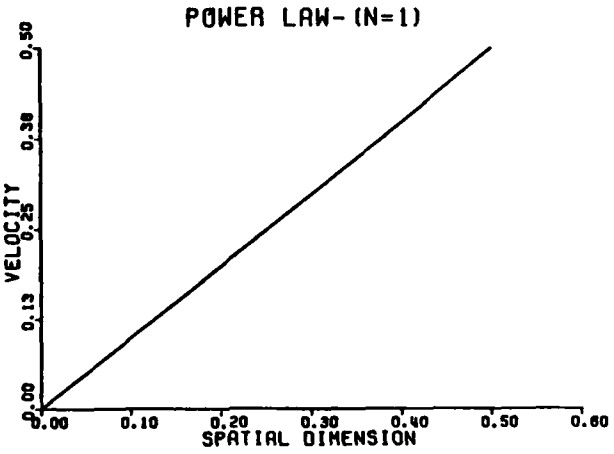

Figure (V.10.a) - Geometric imperfection, δ=0.1, λ=1.04, ν=-0.75, m=+0.25, ε=0.0, plotted values are identical in the range $\bar{\gamma}^P$=0.0-0.4 for the shown scale.

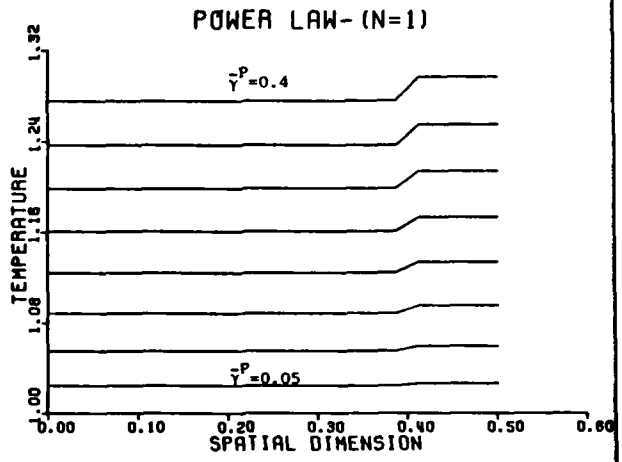

Figure (V.10.b) - Temperature profiles for the problem defined in Fig. (V.10.a).

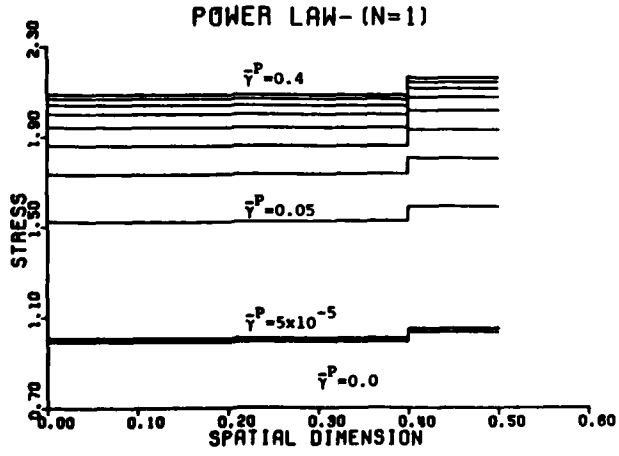

Figure (V.10.c) - stress profiles for the problem defined in Fig. (V.10.a).

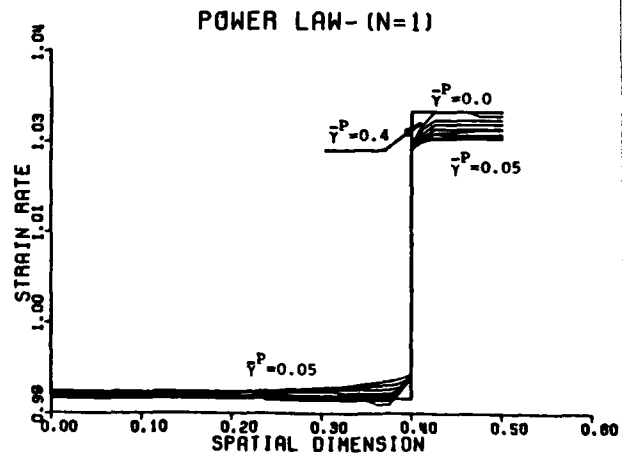

Figure (V.10.d) - strain rate profiles for the problem defined in Fig. (V.10.a).

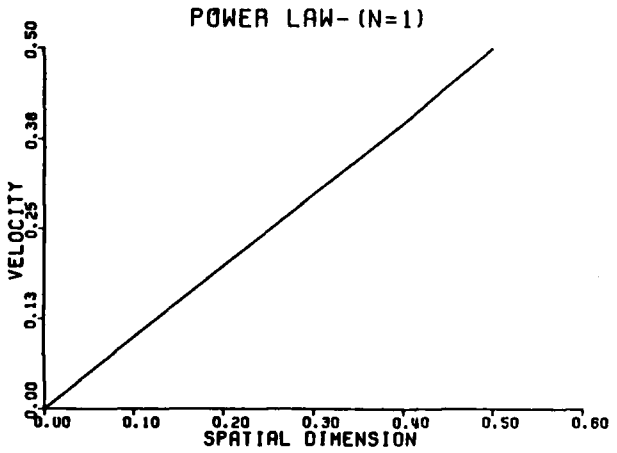

Figure (V.11.a) - Geometric imperfection, λ=1.04, δ=0.1, ν=0.75, m= -0.25, plotted values are identical in the range $\bar{\gamma}^P$= 0.0-0.4 for the scale shown.

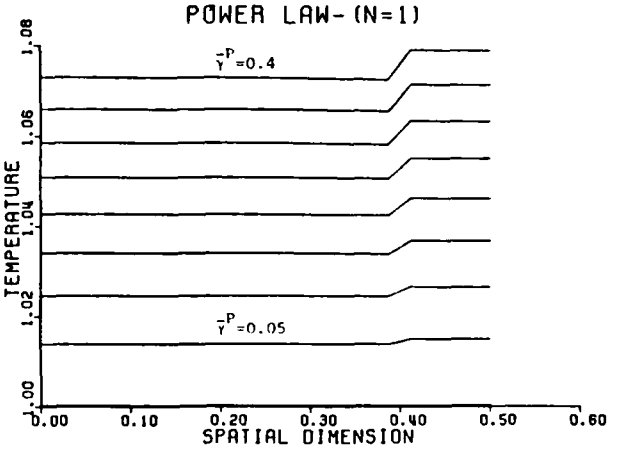

Figure (V.11.b) - Temperature profiles for the problem defined in Fig. (V.11.a).

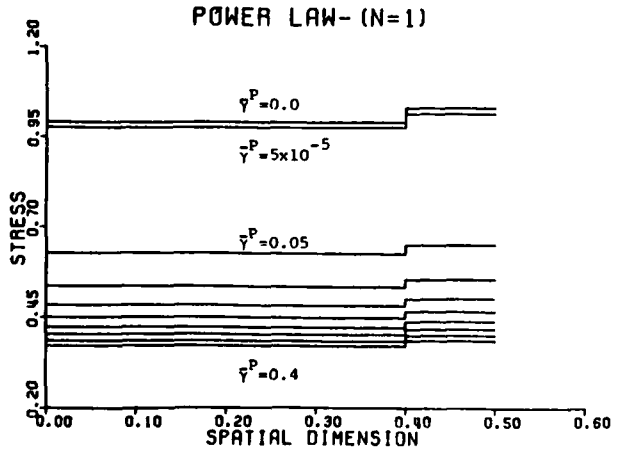

Figure (V.11.c) - stress profiles for the problem defined in Fig. (V.11.a).

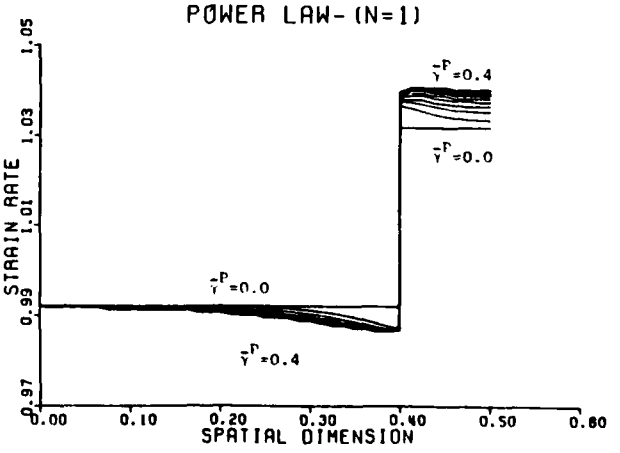

Figure (V.11.d) - strain rate profiles for the problem defined in Fig. (V.11.a).

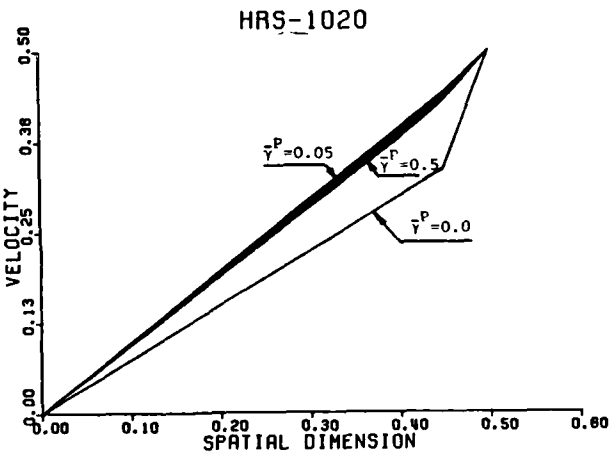

Figure (V.12.a) - Geometric imperfection, δ=0.05, λ=1.02, ν=-0.51, m=0.12, n=0.013, plots are obtained for intervals of $\bar{\gamma}^P$=0.05.

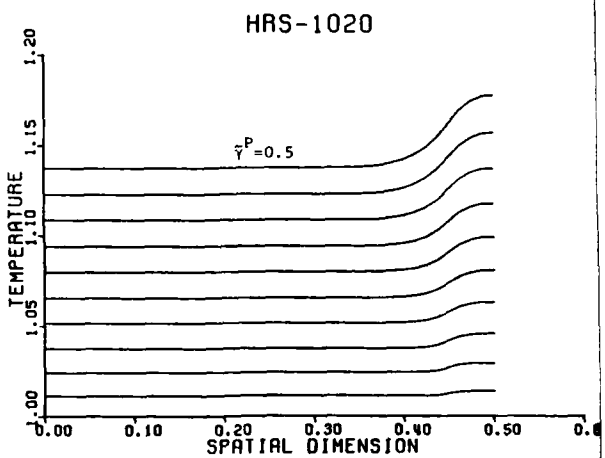

Figure (V.12.b) - Temperature profiles for the problem defined in Fig. (V.12.a).

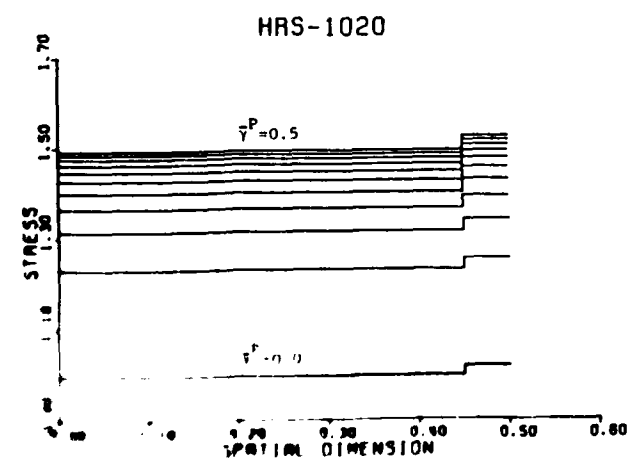

Figure (V.12.c) - [illegible] problem defined [illegible] behavior.

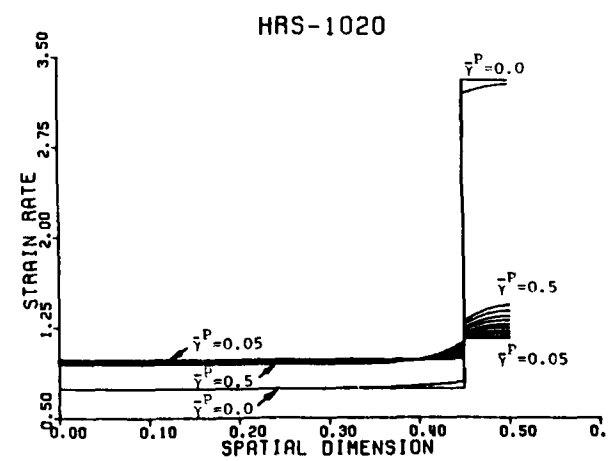

Figure (V.12.d) - Strain-rate profiles for the problem defined in Fig. (V.12.a).

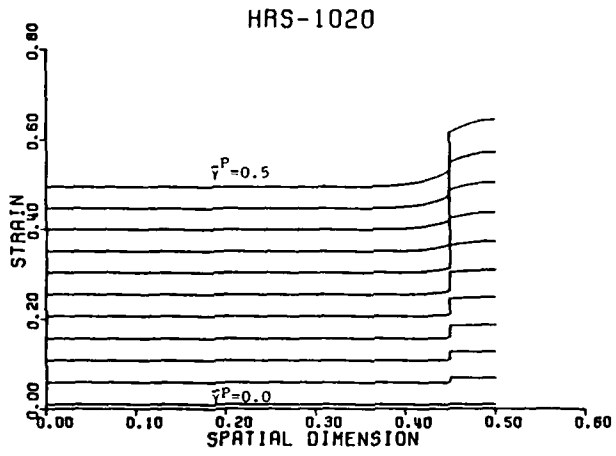

Figure (V.12.e) - Plastic strain profiles for the problem defined in Fig. (V.12.a).

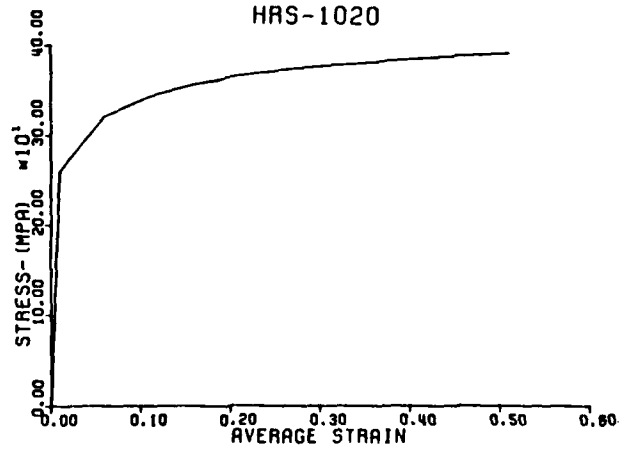

Figure (V.12.f) Computed nominal stress-strain relation.

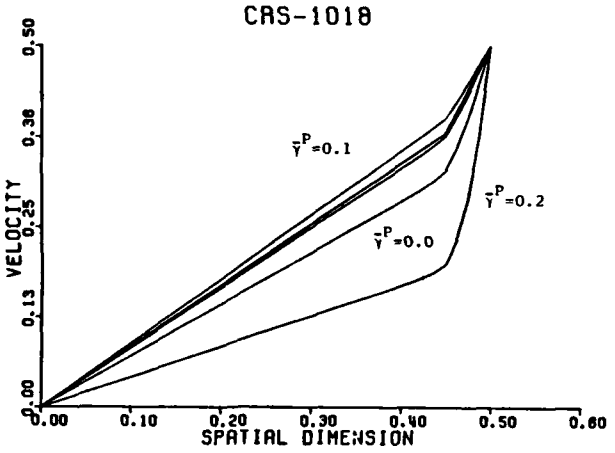

Figure (V.13.a) - Geometric imperfection, δ=0.05, λ=1.02, ν=-0.38, m=0.015, n=0.019, plots are obtained for intervals of $\bar{\gamma}^P$=0.05

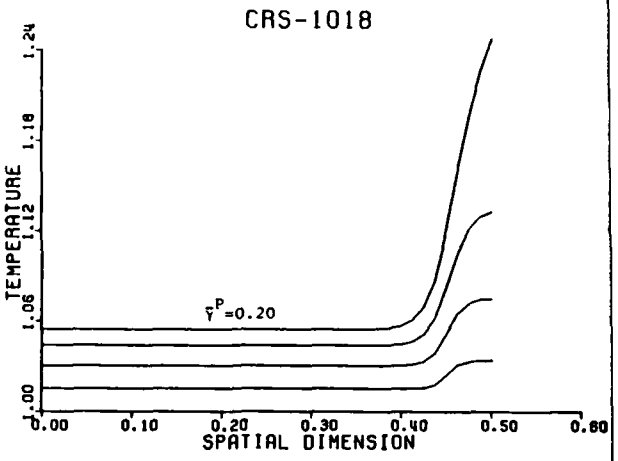

Figure (V.13.b) - Temperature profiles for the problem defined in Fig. (V.13.a).

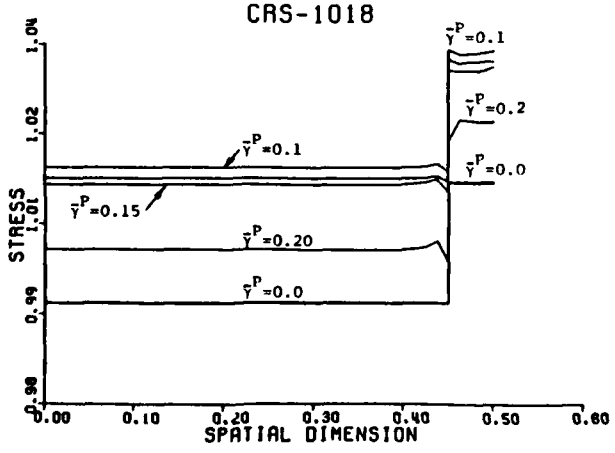

Figure (V.13.c) - Stress profiles for the problem defined in Fig. (V.13.a), stress decreases after $\bar{\gamma}^P$=0.1.

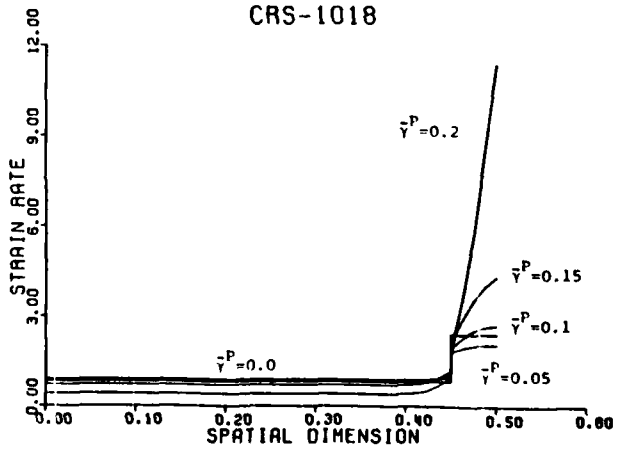

Figure (V.13.d) - Strain-rate profiles for the problem defined in Fig. (V.13.a), beyond $\bar{\gamma}^P$=0.05; strain-rate increases rapidly inside the groove whereas decreasing outside of it.

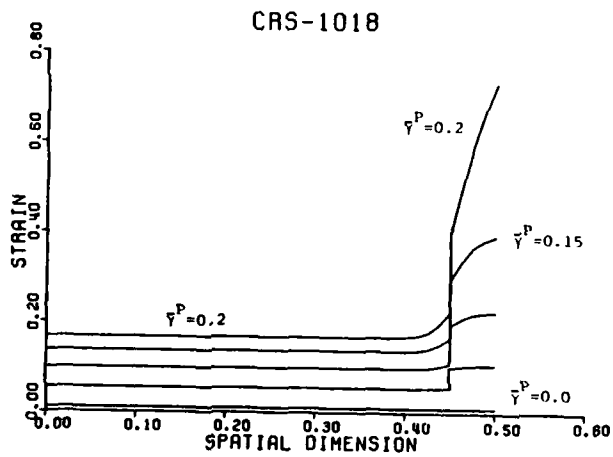

Figure (V.13.e) - Plastic strain profiles for the problem defined in Fig. (V.13.a).

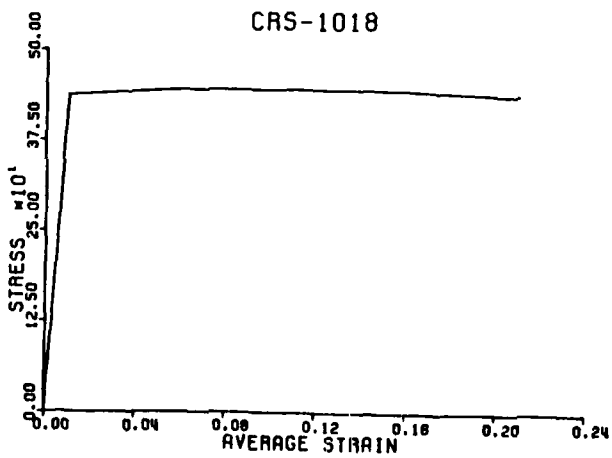

Figure (V.13.f) - Computed Nominal stress-strain relation; stress attains its maximum value at approximately $\bar{\gamma}^P$=0.1

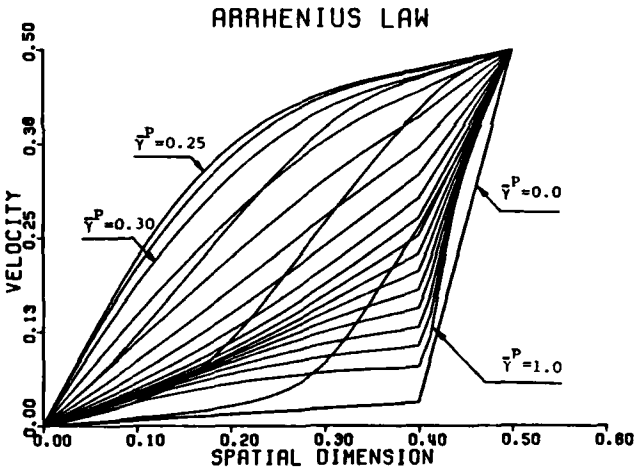

Figure (V.14.a) - Geometric imperfection, δ=0.1, λ=1.04, hardening function is given by (V.51), ε=0.0, Notice early time wave-like response.

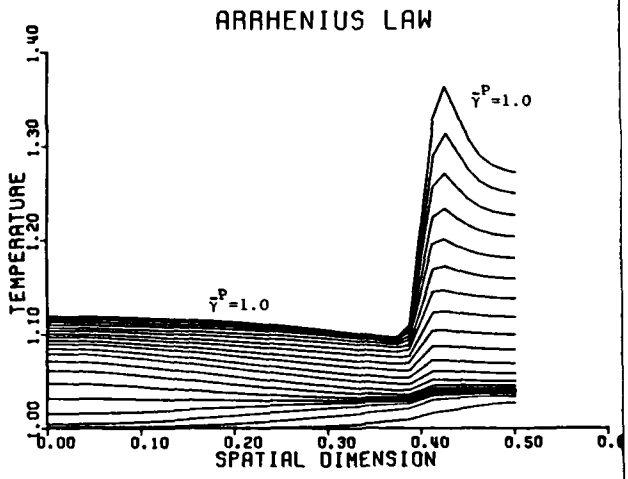

Figure (V.14.b) - Temperature profiles for the problem defined in Fig. (V.14.a).

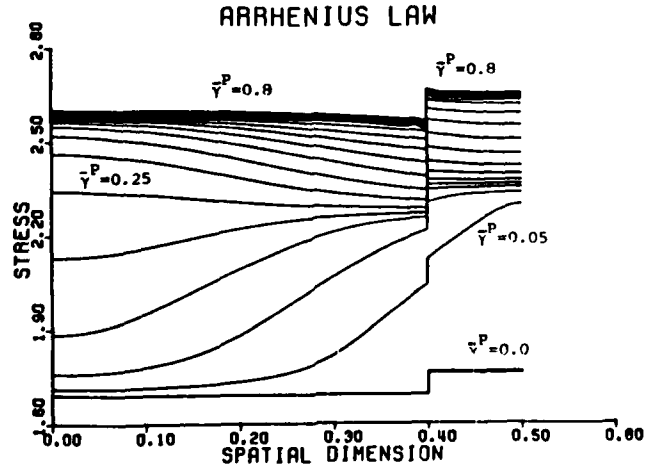

Figure (V.14.c) - stress profiles for the problem defined in Fig. (V.14.a), flow stress attains its maximum amplitude at $\bar{\gamma}^P$=0.80 then decreases, profiles are obtained up to ($\bar{\gamma}^P$=1.0).

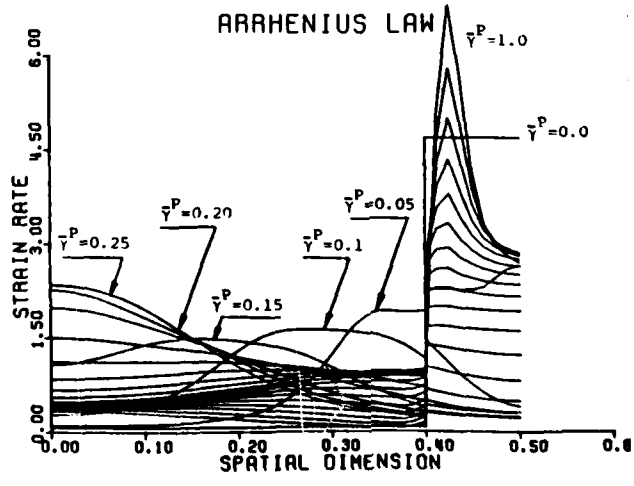

Figure (V.14.d) - strain rate profiles for the problem defined in Fig. (V.14.a), the early time profiles are labeled; afterwards, the strain rate decreases outside the groove and increases inside it up to ($\bar{\gamma}^P$=1.0).

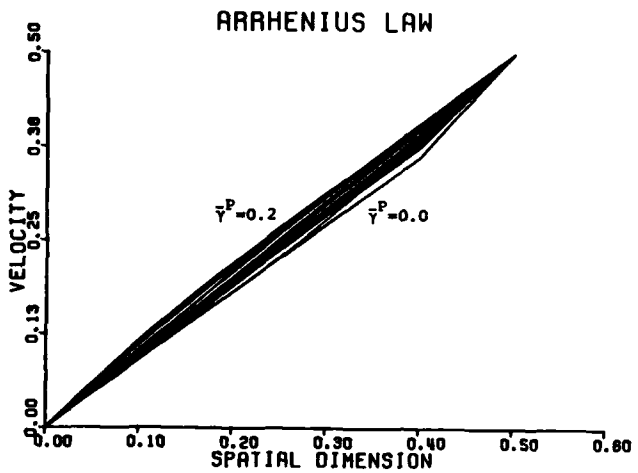

Figure (V.15.a) - same as Fig. (V.14.a) except for λ=1.004, profiles obtained for $\bar{\gamma}^P$>0.2 tend to move towards the initial profile ($\bar{\gamma}^P$=0.0).

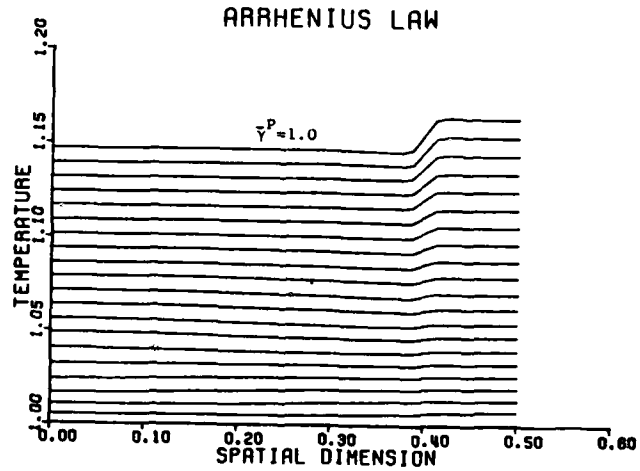

Figure (V.15.b) - Temperature profiles for the problem defined in Fig. (V.15.a), profiles are obtained for intervals of ($\bar{\gamma}^P$=0.05).

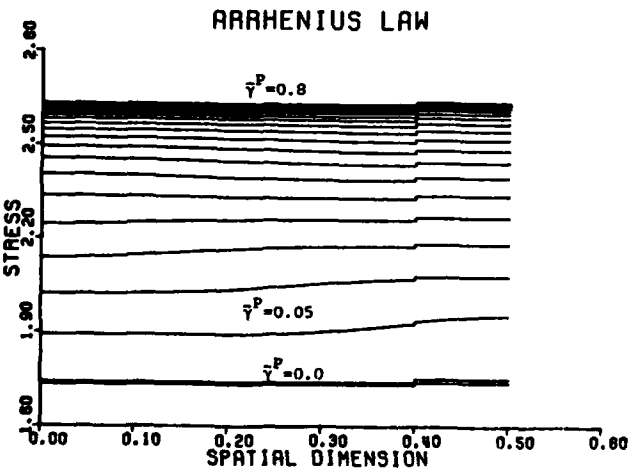

Figure (V.15.c) - stress profiles for the problem defined in Fig. (V.15.a).

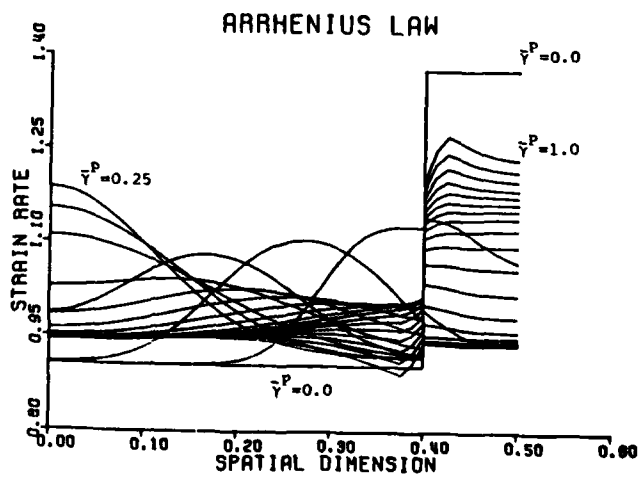

Figure (V.15.d) - strain-rate profiles for the problem defined in Fig. (V.15.a); a similar response to that in Fig. (V.14.d) is observed.

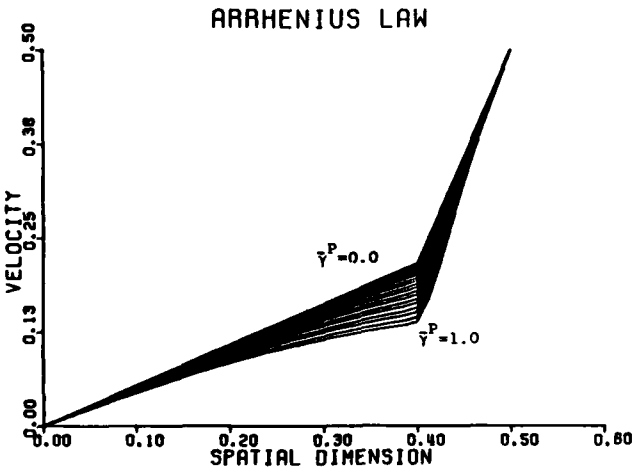

Figure (V.16.a) - same as Fig. (V.14.a) except that hardening is not considered, i.e. $\tau_B(\bar{\gamma}^P)$=Constant; no wave-like response is observed.

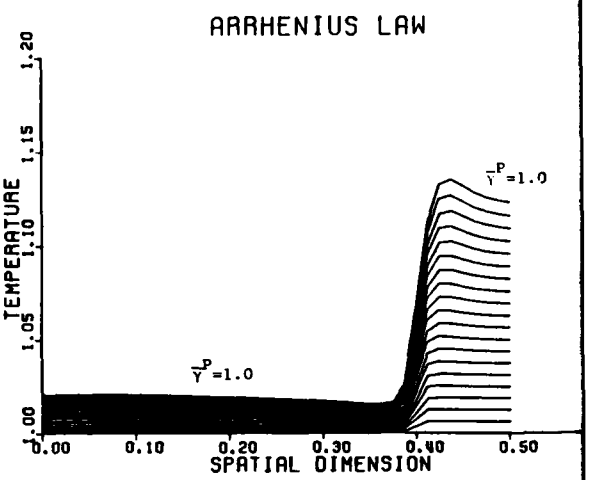

Figure (V.16.b) - Temperature profiles for the problem defined in Fig. (V.16.a).

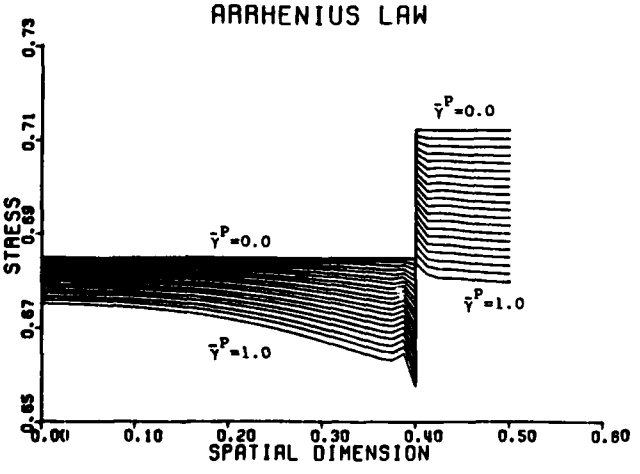

Figure (V.16.c) - stress profiles for the problem defined in Fig. (V.16.a), stress is decreasing monotonically due to non-hardening idealization.

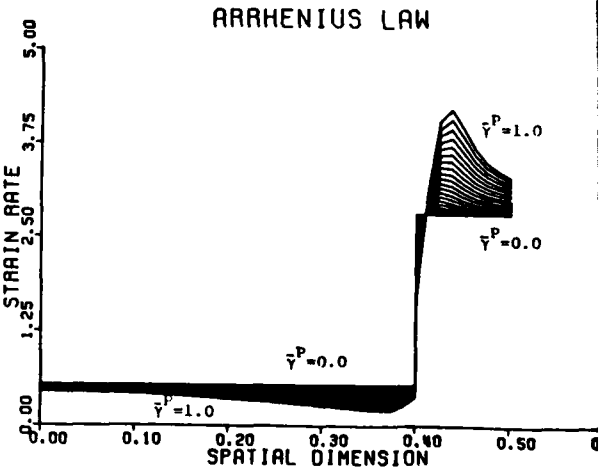

Figure (V.16.d) - strain rate profiles for the problem defined in Fig. (V.16.a).

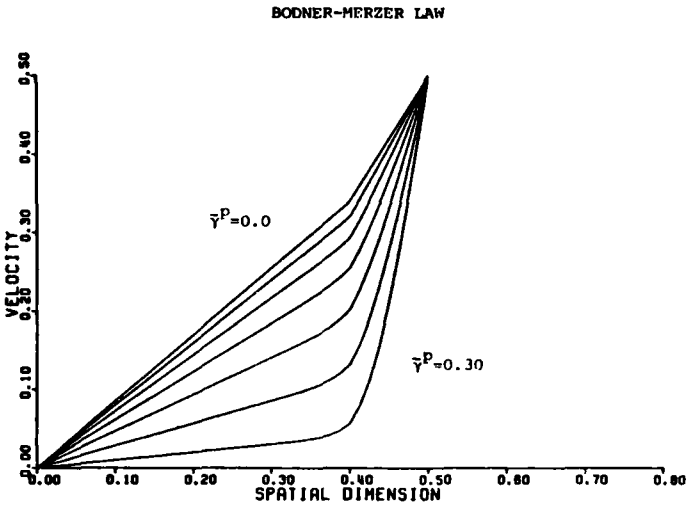

Figure (V.17.a) - Merzer's Model, $\delta = 0.1$, $\lambda = 1.04$, same parameters as in Merzer's Calculation; profiles are obtained for intervals of ($\bar{\gamma}^p = 0.05$).

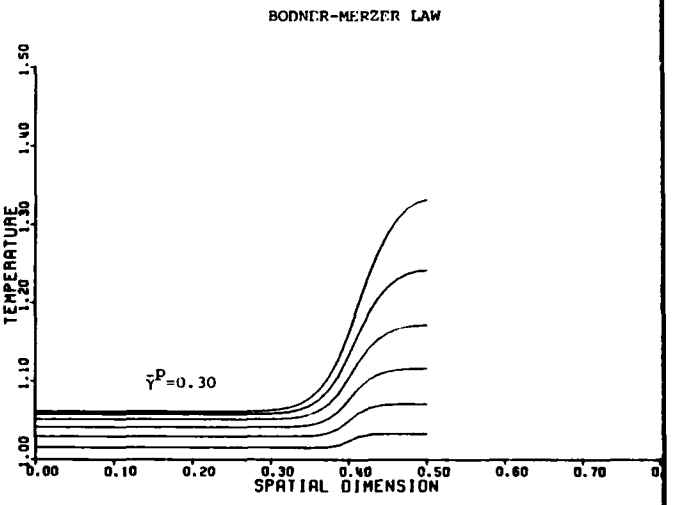

Figure (V.17.b) - Temperature profiles for Merzer's Model.

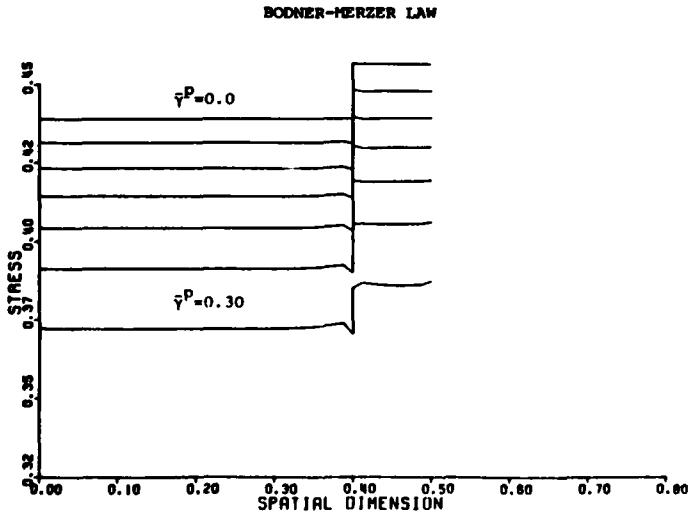

Figure (V.17.c) - stress profiles for Merzer's Model.

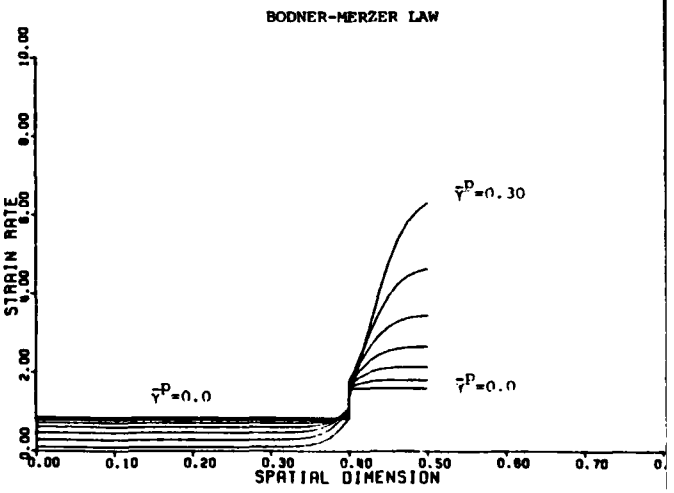

Figure (V.17.d) - strain rate profiles for Merzer's Model.

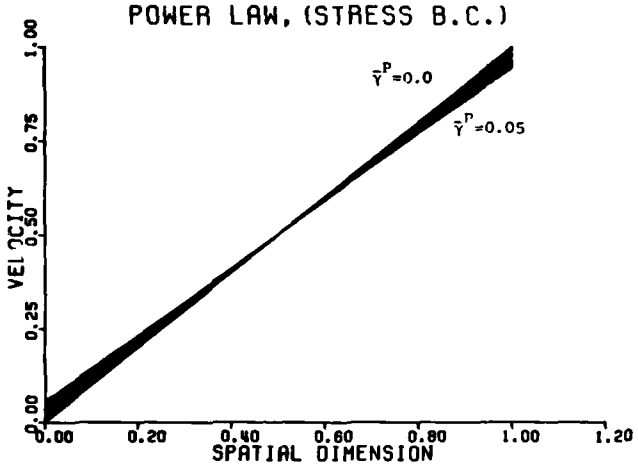

Figure (V.18.a) - Initial temperature perturbation, ε=0.005, stress boundary conditions, v=-0.75, m=0.1, n=1; profiles are obtained for intervals of $\bar{\gamma}^P$=0.005.

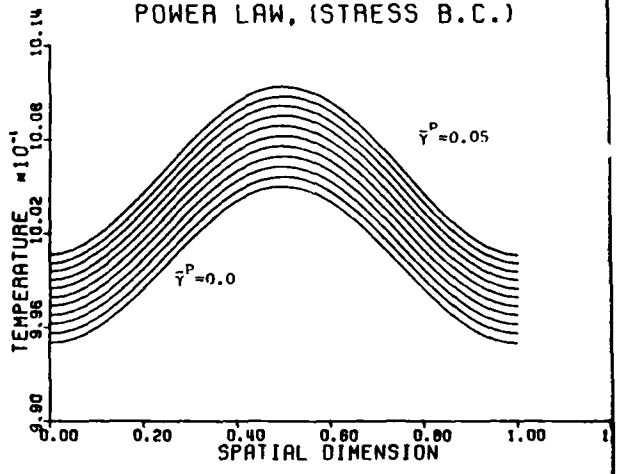

Figure (V.18.b) - Temperature profiles for the problem defined in Fig. (V.18.a).

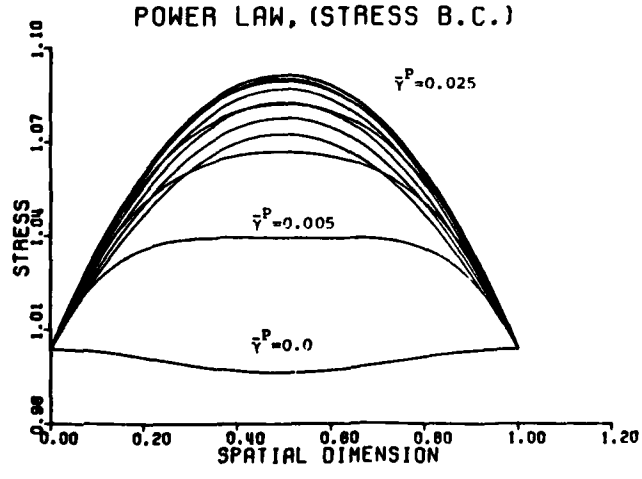

Figure (V.18.c) - stress profiles for the problem defined in Fig. (V.18.a) - stress reaches its maximum at ($\bar{\gamma}^P$=0.025).

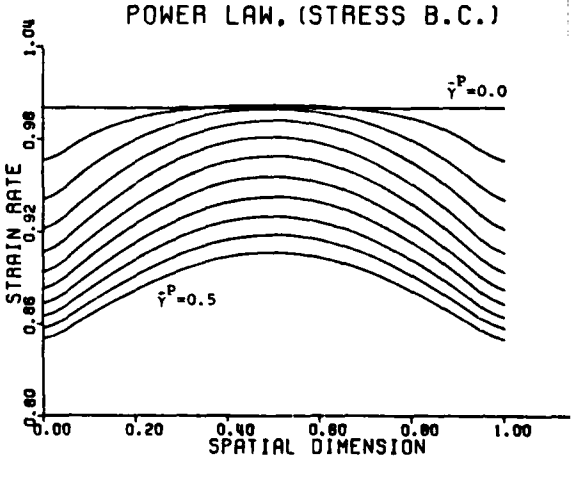

Figure (V.18.d) - strain rate profiles for the problem defined in Fig. (V.18.a).

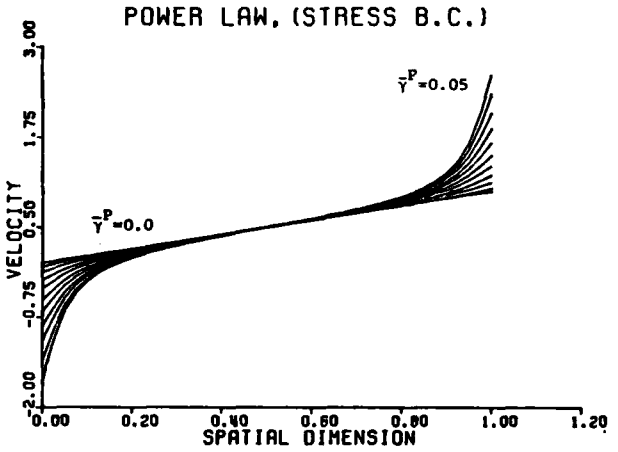

Figure (V.19.a) - Initial temperature perturbation, ϵ=0.005, ν=-0.75, m=-0.95, n=1; stresses are prescribed at the boundaries, Plots are obtained for intervals of $\bar{\gamma}^P$=0.005.

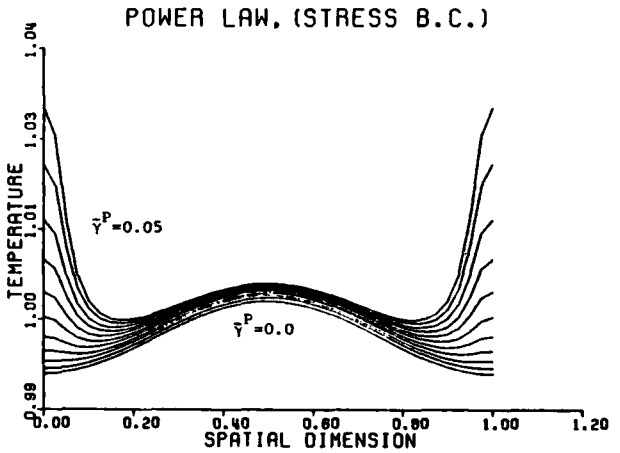

Figure (V.19.b) - Temperature profiles for the problem defined in Fig. (V.19.a).

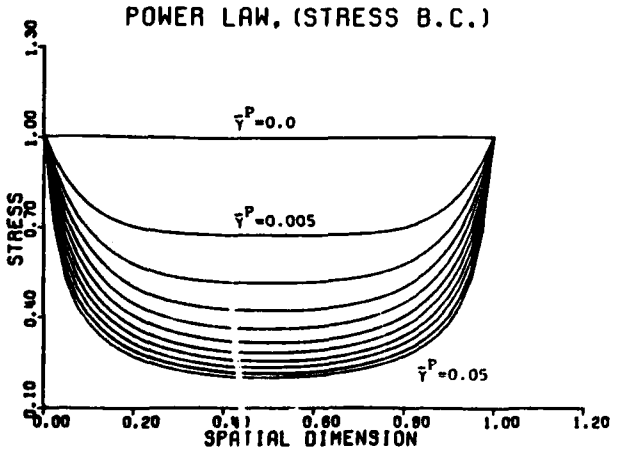

Figure (V.19.c) - stress profiles for the problem defined in Fig. (V.19.a).

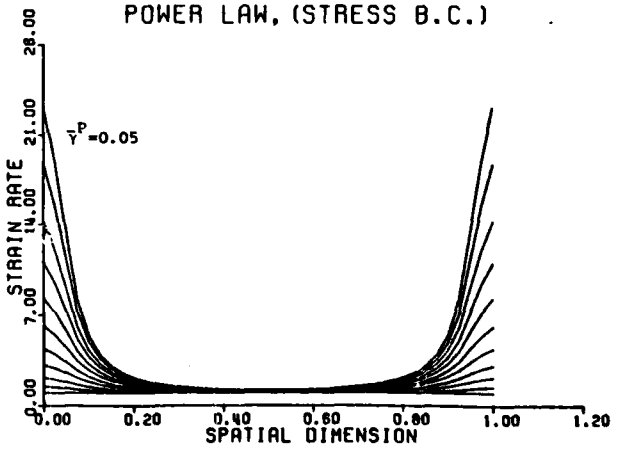

Figure (V.19.d) - strain rate profiles for the problem defined in Fig. (V.19.a). Notice the intense deformation rates near the boundaries.

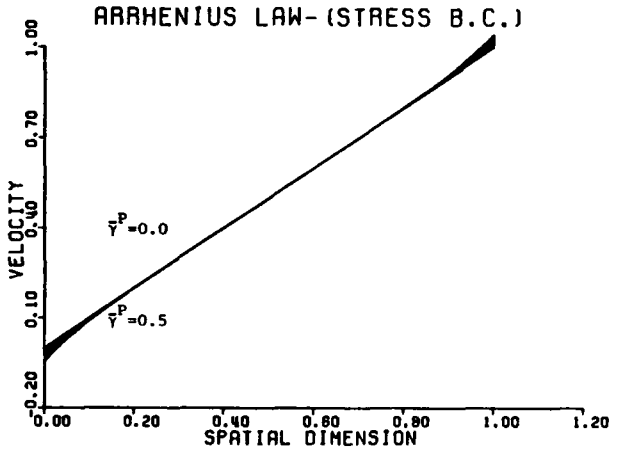

Figure (V.20.a) - Unperturbed initial solution, stress boundary conditions, no hardening considered, plots are obtained for intervals of $\bar{\gamma}^P$=0.05.

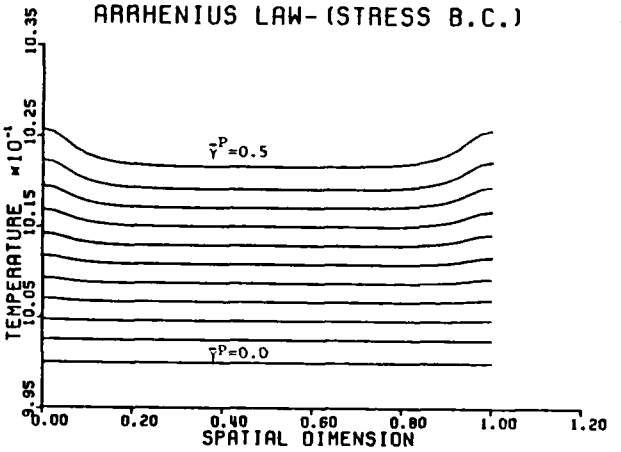

Figure (V.20.b) - Temperature profiles for the problem defined in Fig. (V.20.a).

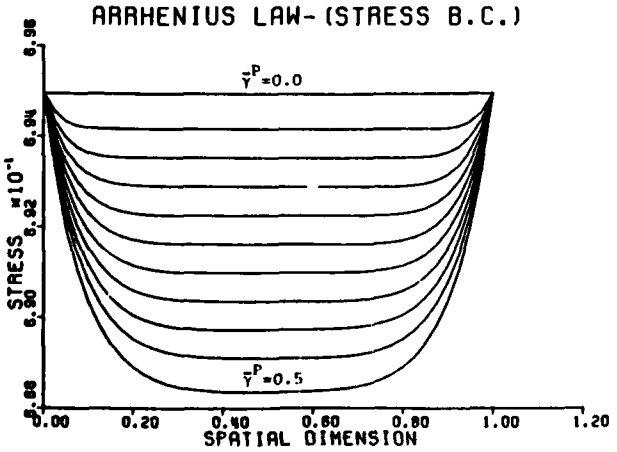

Figure (V.20.c) - Stress profiles for the problem defined in Fig. (V.20.a).

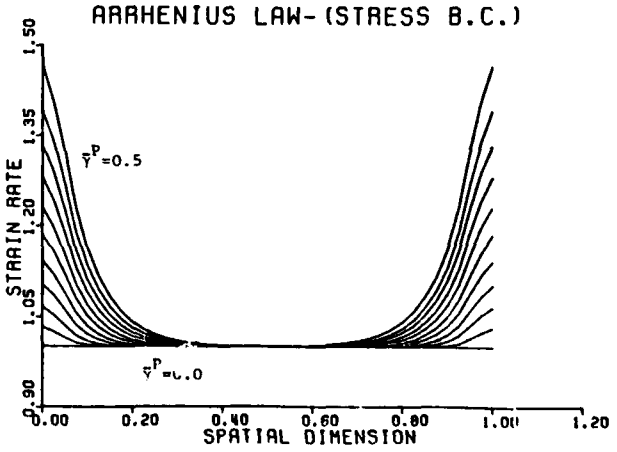

Figure (V.20.d) - Strain-rate profiles for the problem defined in Fig. (V.20.a).

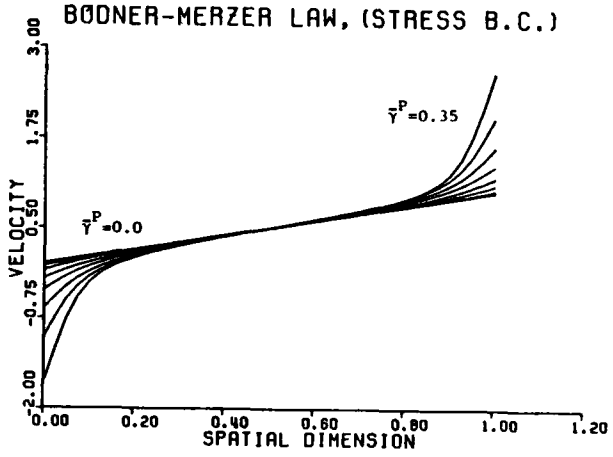

Figure (V.21.a) - Unperturbed initial solution, stress boundary conditions, plots are obtained for intervals of $\bar{\gamma}^P$=0.05.

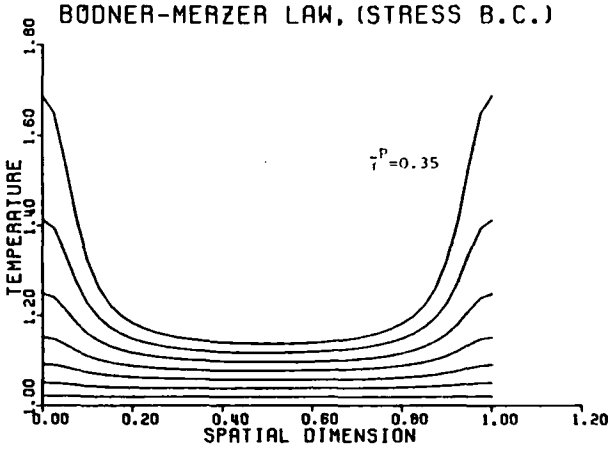

Figure (V.21.b) - Temperature profiles for the problem defined in Fig. (V.21.a), notice that the temperature values at the boundaries reach the limit (IV.46.b)

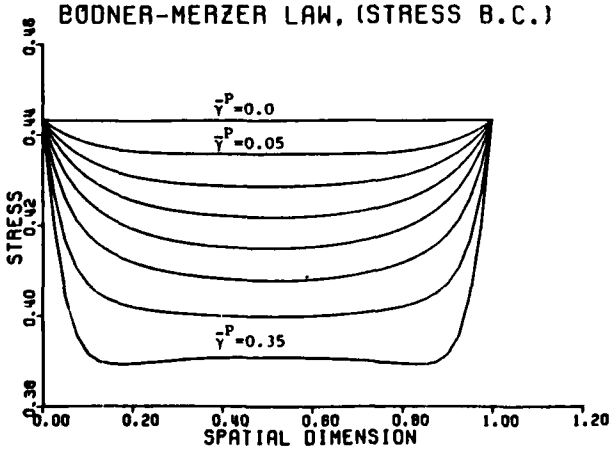

Figure (V.21.c) - Stress profiles for the problem defined in Fig. (V.21.a).

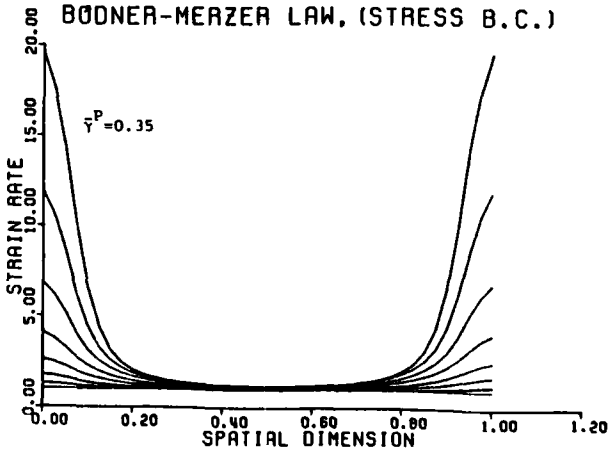

Figure (V.21.d) - Strain-rate profiles for the problem defined in Fig. (V.21.a).

APPENDIX (I)

Closed Form Solution of a Linear, 1st Order, Time-Dependent System of Equations

Consider the system:

$$\dot{\underset{\sim}{F}} = W(t)\underset{\sim}{F} \tag{1}$$

with the initial condition

$$\underset{\sim}{F}(t_0) = \underset{\sim}{F}^o \tag{2}$$

Claim:

If $W(t)$ commutes with $\int_{t_0}^{t} W(\tau)d\tau$,

then

$$\underset{\sim}{F}(t) = \exp\left\{\int_{t_0}^{t} W(\tau)d\tau\right\} \underset{\sim}{F}(t_0) \tag{3}$$

is the unique solution of (1) and (2).

Proof:

Let $K(t)$ be a fundamental matrix of the system (1), i.e.

$$\dot{K}(t) = W(t)\ K(t) \tag{4}$$

and det. $K(t) \neq 0$. Then the solution of (1) and (2) can be written as

$$\underset{\sim}{F}(t) = K(t)\ K^{-1}(t_0)\ \underset{\sim}{F}^o. \tag{5}$$

Introduce the notation

$$\phi(t,t_0) = K(t)\ K^{-1}(t_0) \tag{6}$$

for the fundamental matrix $\phi(t,t_0)$ which is the solution operator of the system (1) and (2).

Assume

$$\phi(t,t_0) = \exp\left\{M(t,t_0)\right\} \tag{7}$$

Where

$$M(t,t_0) = \int_{t_0}^{t} W(\tau)d\tau \tag{8}$$

It is clear that $\phi(t,t_0)$ satisfies (1), i.e.

$$\dot{\phi}(t,t_0) = W(t)\ \phi(t,t_0) \tag{9}$$

We seek a proof that (7) satisfies (9). Moreover, we are guaranteed that this solution is unique, (Haar's uniqueness theorem)*.

$$\exp\{M(t)\} = I + M + \frac{1}{2!} MM + \cdots .$$

Then the R.H.S. of equation (9) becomes

$$\text{R.H.S.} = W + WM + \frac{1}{2!} WMM + \cdots . \tag{10}$$

While the L.H.S. of (9) becomes

$$\begin{aligned}
\text{L.H.S.} &= \frac{d}{dt}\,[\phi(t,t_0)] \\
&= \frac{d}{dt}\,[I + M + \frac{1}{2!} MM + \cdots] \\
&= \dot{M} + \frac{2}{2!} M\dot{M} + \cdots \\
&= W + \frac{2}{2!} MW + \frac{3}{3!} M^2W + \cdots \\
&= W + MW + \frac{1}{2!} MMW + \cdots\cdots . \qquad (11)
\end{aligned}$$

Comparing expressions (10),(11); we conclude that, if $W(t)$ commutes with $M(t)$, i.e.

$$MW = WM$$

then (10) and (11) are identical, and consequently $\phi(t,t_0)$ is the unique solution to (9).

---

*In general, for $\dot{A} = f(A,t)$ if f is "Lipschitz Continuous", there is one and only one solution $A(t)$ satisfying

$$A(t_0) = A_0.$$

From (5) and (6), we find

$$\underset{\sim}{F}(t) = \exp\left\{\int_{t_0}^{t} W(\tau)\,d\tau\right\}\ \underset{\sim}{F}(t_0)$$

which completes the proof.

APPENDIX II

Numerical Solution of Merzer's Problem

The outlines of the numerical algorithm are discussed in (V.4). The governing equations used are

$$\rho_0 \frac{\partial v}{\partial t} = S_1 \frac{\partial^2 v}{\partial y^2} + S_2 \frac{\partial \theta}{\partial y} + S_3 \frac{\partial \gamma^P}{\partial y} \tag{1}$$

$$\frac{\partial \gamma^P}{\partial t} = \frac{\partial v}{\partial y} \tag{2}$$

$$\frac{\partial \theta}{\partial t} = \left(\frac{K}{\rho_0 C}\right) \frac{\partial^2 \theta}{\partial y^2} + \frac{\beta}{\rho_0 C} \tau \frac{\partial \gamma^P}{\partial t} \tag{3}$$

$$\tau = \frac{\tau_1(W^P)}{\sqrt{3}} \cdot \left\{ 2 \ln\left(\frac{2D_0}{\dot{\gamma}^P}\right) \right\}^{[(-1/2)/(a/\theta+b)]} \tag{4}$$

where

$$S_1 \equiv \frac{\partial \tau}{\partial \gamma^P} = \frac{\tau}{n\dot{\gamma}^P \cdot f(\eta)}$$

$$S_2 \equiv \frac{\partial \tau}{\partial \theta} = -a\tau \cdot \ln[f(\eta)]/(2\theta^2 n^2)$$

$$S_3 \equiv \frac{\partial \tau}{\partial \gamma^P} = A\tau/(1-A)$$

where

$$A = m\tau\left(\frac{\tilde{\tau}_1}{\tau_1} - 1\right)$$

and

$$\tau_1(W^P) = \tilde{\tau}_1 - (\tilde{\tau}_1 - \tilde{\tau}_0)e^{-mW^P}$$

$$\tau = \frac{\tau_1(W^P)}{\sqrt{3}} [f(\eta)]^{C(\theta)}$$

$$f(\eta) = 2\ \ell n\ \eta\ ; \qquad \eta = \frac{2D_0}{\dot{\gamma}^P}$$

$$C(\theta) = \frac{-1/2}{n(\theta)} \quad ; \quad n(\theta) = \frac{a}{\theta} + b.$$

Evaluation of velocity at the interface:

The interface velocity, say $\hat{v}$ is obtained by means of equation (V.46), as described in (V.4) assuming that

$$\frac{(\dot{\gamma}^P)^+}{(\dot{\gamma}^P)^-} \approx 1.0$$

From (V.46) we obtain

$$\dot{\gamma}^+ = (2D_0)^{1-\xi(\theta)} (\dot{\gamma}^-)^{\xi(\theta)} \tag{5}$$

where

$$\xi(\theta) = (\lambda)^{\frac{1}{C(\theta)}}; \quad \lambda = A^-/A^+ > 1.$$

We approximate the strain rates by second order one-sided derivatives as follows:

$$\dot{\gamma}^+ = (\frac{-3}{2h})\hat{v} + [\frac{1}{2h}\ (4v_{+1} - v_{+2})] \tag{6}$$

$$\dot{\gamma}^- = (\frac{3}{2h})\hat{v} + [\frac{1}{2h}\ (-4v_{-1} + v_{-2})] \tag{7}$$

substitution of (6) and (7) in (5) gives a nonlinear equation for $\hat{v}$ which is solved by Newton's method. The initial velocity distribution is obtained in a similar manner where the jump in the flow stress is satisfied through an equivalent jump in the strain rate assuming continuous strain and temperature distributions.

Finite-difference formulation

Computational experiments for the considered system of equations, with Merzer's values for the parameters, indicate that the formal explicity scheme is no longer efficient. Therefore, the scheme is improved by using the two-level, explicit, stable Du-Fort and Frankel algorithms, with careful choice of k, h to maintain consistency. The additional initial value is evaluated by the formal explicit, one-level method; the formal method with time step k_1 is used until we reach $t = nk_1 = k_2$; then the calculation is continued by the Du-Fort and Frankel method with a uniform time step $k_2 >> k_1$. The efficiency of the algorithm is strongly improved by this technique. The accuracy is also improved since the Du-Fort method is second order in time and space.

The Du-Fort and Frankel approximation to the standard heat equation

$$\frac{\partial u}{\partial t} = \nu \frac{\partial^2 u}{\partial x^2} \tag{8}$$

is given by

$$\frac{u_j^{n+1} - u_j^{n-1}}{2k} = \frac{u_{j+1}^n - (u_j^{n+1} + u_j^{n-1}) + u_{j-1}^n}{h^2} \tag{9}$$

Our system has variable coefficients and lower order terms; however, computation evidence shows the utility of this algorithm. The algorithm described in (V.4) is applied for this system of equations with the exception that we use Merzer's constitutive equation and the differencing procedure illustrated in (9).

APPENDIX III

On the lack of Homogeneous Solutions for the Case of Stress Boundary Conditions

Consider the momentum and compatability equations (II.9) and (II.10)

$$\rho_o \frac{\partial v}{\partial t} = \frac{\partial \tau}{\partial y} \tag{1}$$

$$\frac{\partial \gamma^P}{\partial t} = \frac{\partial v}{\partial y} - \frac{1}{G}\frac{\partial \tau}{\partial t} \tag{2}$$

Assume there exists a homogeneous solution for the velocity and stress given by

$$v(y, t) = V(t)y \tag{3}$$

$$\tau(y, t) = \hat{\tau}(t) . \tag{4}$$

Substituting solution (3), (4) in (1), (2) we obtain

$$\rho_o \dot{V}(t)y = 0 \rightarrow \dot{V}(t) = 0$$

i.e.

$$V(t) = V_o \quad \text{(Constant)} \tag{5}$$

Moreover, Equation (2) yields

$$\dot{\gamma}^P = V_o - \frac{1}{G}\dot{\hat{\tau}}(t)\Big|_{\text{velocity b.c.}} \tag{6}$$

Now, let us distinguish two cases

A. Velocity boundary Conditions:

In this case, $V(0, t) = 0$, $v(1, t) = V_o$, and Equation (6) is

$$\dot{\gamma}^P = V_o - \frac{1}{G}\dot{\hat{\tau}}(t)\Big|_{\text{velocity b.c.}} \tag{7.A}$$

where the last term is the stress rate obtained for the homogeneous solution corresponding to the velocity boundary conditions.

B. Stress Boundary Conditions:

In this case, $\hat{\tau}(t)$ is prescribed at the boundaries and - in turn - across the specimen since the solution is homogeneous, hence; Equation (6) reads

$$\dot{\gamma}^P = V_o - \frac{1}{G} \dot{\hat{\tau}}(t) \Big|_{\text{prescribed}} \quad . \tag{7.B}$$

Comparison of Equations (7.A) and (7.B) allows us to conclude that the only way by which (7.B) is satisfied becomes

$$\dot{\hat{\tau}}(t) \Big|_{\text{prescribed}} = \dot{\hat{\tau}}(t) \Big|_{\text{velocity b.c.}} \quad .$$

In other words, the unique possible homogeneous solution is the one that corresponds to velocity boundary conditions, otherwise the solution becomes inhomogeneous as deformation proceeds.

APPENDIX IV

The Rate of Growth of the Energy Norm in the Linear Stability Analysis

Consider the system of linearized partial differential equations defined in (IV.7) by

$$L(\underset{\sim}{\omega}) = \underset{\sim}{0} \tag{1}$$

This system can be rewritten as

$$A^{t}\underset{\sim}{\omega}_{,t} = B_2\underset{\sim}{\omega}_{,yy} + B_1\underset{\sim}{\omega}_{,y} + B_0\underset{\sim}{\omega} \tag{2}$$

where

$$B_2 = -A^{yy}, \quad B_1 = -A^{y} \quad \text{and} \quad B_0 = -A$$

Introduce the change of variables

$$\underset{\sim}{\omega} = D\underset{\sim}{z} \tag{3}$$

where

$$D = \begin{pmatrix} \frac{1}{\sqrt{\rho_0}} & 0 & 0 & 0 \\ 0 & \sqrt{G} & 0 & 0 \\ 0 & 0 & 1 & 0 \\ 0 & 0 & 0 & 1 \end{pmatrix} \tag{3a}$$

Then the system of equations (2) becomes

$$\underset{\sim}{z}_{,t} = B_2\underset{\sim}{z}_{,yy} + C_1\underset{\sim}{z}_{,y} + C_0\underset{\sim}{z} \tag{4}$$

where

$$C_1 = DB_1D \quad \text{and} \quad C_0 = DB_0D \tag{5}$$

The matrices B_2 and C_1 are symmetric; B_2 is positive, semi-definite.

Now consider the rate of change of the energy norm of the solution

$$\langle \underset{\sim}{z}, \underset{\sim}{z} \rangle \equiv \int_0^H \underset{\sim}{z} \cdot \underset{\sim}{z} dy \quad . \tag{6}$$

From (4) and

$$\frac{\partial}{\partial t} \langle \underset{\sim}{z}, \underset{\sim}{z} \rangle = \langle \underset{\sim}{z}_{,t}, z \rangle + \langle \underset{\sim}{z}, \underset{\sim}{z}_{,t} \rangle$$

we obtain

$$\frac{\partial}{\partial t} \langle \underset{\sim}{z}, \underset{\sim}{z} \rangle = \langle (B_2\underset{\sim}{z}_{,yy} + C_1\underset{\sim}{z}_{,y} + C_0\underset{\sim}{z}), \underset{\sim}{z} \rangle +$$

$$+ \langle \underset{\sim}{z}, (B_2\underset{\sim}{z}_{,yy} + C_1\underset{\sim}{z}_{,y} + C_0\underset{\sim}{z}) \rangle \tag{7}$$

Integration of the second derivatives by parts gives

$$\langle B_2\underset{\sim}{z}_{,yy}, \underset{\sim}{z} \rangle + \langle \underset{\sim}{z}, B_2\underset{\sim}{z}_{,yy} \rangle = -2\langle B_2\underset{\sim}{z}_{,y}, \underset{\sim}{z}_{,y} \rangle \tag{8}$$

plus boundary terms which vanish for boundary conditions of either prescribed heat flow or prescribed temperature. Since B_2 is positive, semi-definite, the right side of (8) is non-positive. Integration of the first derivatives in (7) by parts gives

$$\langle C_1\underset{\sim}{z}_{,y}, \underset{\sim}{z} \rangle + \langle \underset{\sim}{z}, C_1\underset{\sim}{z}_{,y} \rangle = -\langle C_1\underset{\sim}{z}, \underset{\sim}{z}_{,y} \rangle + \langle \underset{\sim}{z}, C_1\underset{\sim}{z}_{,y} \rangle \tag{9}$$

plus boundary terms which vanish for prescribed velocities or prescribed shear tractions. From the symmetry of C_1, the right side of (9) is zero.

Use of the results (8) and (9) in (7) gives

$$\frac{\partial}{\partial t}\langle \underset{\sim}{z}, \underset{\sim}{z}\rangle \leq 2\langle C_0 \underset{\sim}{z}, \underset{\sim}{z}\rangle \tag{10}$$

or

$$\frac{\partial}{\partial t}\| \underset{\sim}{z}\|_2^2 \leq 2\| C_0\|_2 \| \underset{\sim}{z}\|_2^2 \tag{11}$$

where $\| \underset{\sim}{z}\| \equiv \langle \underset{\sim}{z}, \underset{\sim}{z}\rangle$ and $\|C_0(t)\|_2$ is the L_2-norm of the matrix $C_0(t)$.

Integration of (11) gives

$$||\underset{\sim}{z}(t)||_2^2 \leq \left\{\exp\left[\int_0^t 2||C_0(\eta)||_2 d\eta\right]\right\} ||\underset{\sim}{z}(0)||_2^2 \tag{12}$$

or

$$||\underset{\sim}{z}(t)||_2 \leq \left\{\exp\left[\max_{\eta\in[0,t]} ||C_0(\eta)||_2 t\right]\right\} ||\underset{\sim}{z}(0)||_2 . \tag{13}$$

Using the equivalence of norms for finite-dimensional spaces, we can, for convenience, replace the L_2-norm of C_0 with the maximum norm to obtain

$$||\underset{\sim}{z}(t)||_2 \leq \left\{\exp\left[\alpha \max_{\eta} ||C_0(\eta)||_\infty t\right]\right\} ||\underset{\sim}{z}(0)||_2 \tag{14}$$

The well-posedness of the system (2) is ensured provided that

$$\max_{\eta\in[0,t]} ||C_0(\eta)||_\infty \leq \sigma \tag{15}$$

where σ is a positive constant.

The estimate (15) gives the inequalities (IV.24) obtained from the analysis in Chapter IV for finite wave numbers ξ.